Universitat
de les Illes Balears

DOCTORAL THESIS

2023

COASTAL HAZARDS UNDER CLIMATE CHANGE. THE CASE OF THE BALEARIC ISLANDS.

Miguel Agulles Gámez

Universitat de les Illes Balears

DOCTORAL THESIS

2023

Doctoral Programme in Physics

COASTAL HAZARDS UNDER CLIMATE CHANGE. THE CASE OF THE BALEARIC ISLANDS.

Miguel Agulles Gámez

Thesis Supervisor: Gabriel Jordà Sánchez

Thesis tutor: Alejandro Orfila Förster

Doctor by the Universitat de les Illes Balears

Universitat de les Illes Balears

This thesis has been written by Miguel Agulles Gámez under the supervision of Dr. Gabriel Jordà Sánchez

Mallorca, 18th April 2023

Supervisor: **PhD student:** **Tutor:**

List of publications included in the Doctoral Thesis

Agulles, M., Jordà, G., (2022). Quantification of error sources in wave runup estimates on two Mediterranean sandy beaches. Under review in Coastal Engineering Journal.

Agulles, M., Jordà, G., and Lionello, P. (2021). Flooding of Sandy Beaches in a Changing Climate. The Case of the Balearic Islands (NW Mediterranean). Frontiers in Marine Science 8, 1-15. Doi: 10.3389/fmars.2021.760725. Published in Frontiers in Marine Science.

Agulles, M., Marbà, N., and Jordà, G., (2022). Mediterranean Seagrasses provide valuable coastal protection under climate change. To be submitted

The 2021 quality indices of the journals based on the JCR 2021 Impact Factor where articles are published (or under review) are:

Journal	Impact factor	Category Name	Quartile in Category	State
Coastal Engineering	5.427	Coastal Engineering	Q1	Under review
FMARS	5.247	Global Change and the Future Ocean	Q1	Published
Nature	28.66	Nature climate change	Q1	To be submitted

Universitat de les Illes Balears

Dr Gabriel Jordà, of University of Balearic Islands

I DECLARE:

That the thesis titles *"Coastal hazards under climate change. The case of the Balearic Islands"*, presented by Miguel Agulles Gámez to obtain a doctoral degree, has been completed under my supervision.

For all intents and purposes, I hereby sign this document.

Signature

Palma de Mallorca, 18th April, 2023

A mi familia.

Agradecimientos

Quiero mostrar mi sincero agradecimiento a la vida que se me ha brindado, por darme salud y una familia que siempre me apoya en las decisiones que voy tomando en el camino. Sin estos dos pilares, hubiese sido todo mucho más complicado.

También quisiera dar las gracias a toda la gente que ha estado a mi lado durante estos últimos años en los que me he adentrado en el mundo de la investigación. En especial a mi director de tesis, Biel Jordà, que sin su guía, paciencia y valiosos consejos no hubiese sido posible.

Abstract

Coastal areas are of vital importance for the socio-economic development of coastal regions due to their role in providing food, trade, tourism, transportation, and recreation. In addition, coastal ecosystems are essential for biodiversity, climate regulation, and protection against natural disasters such as storm surges. The coast is particularly vulnerable to the impacts of climate change, especially due to the risks of flooding and erosion resulting from mean sea level rise and the possible increase in frequency and intensity of extreme events.

Obtaining robust projections of coastal flooding is therefore crucial for the effective management of coastal regions. Despite several studies have addressed the generation of future beach flooding projections, there is still a lack of knowledge in several aspects of those projections. Firstly, the uncertainties associated to the modelling of these projections are not yet understood. Secondly, regional scale projections often rely on assumptions that may compromise the quality of the results. Finally, the optimal approach to protect the coastal areas in a context of sea level rise.

The main goal of this thesis is to improve the understanding we have on coastal impacts induced by a changing climate. In particular, the thesis focuses on the impact of marine storms on sandy beaches, which are a key environmental and economic asset for many Mediterranean countries. To reach that goal, a combination of observational data and numerical models are used to address three specific objectives: (1) to quantify the uncertainties associated to state-of-the-art approaches to the modelling of beach flooding, (2) to develop and apply a new methodology able to quantify beach flooding at regional scale and (3) to assess if submerged vegetation (i.e. seagrass meadows) can offer a nature-based solution to reduce coastal impacts. The work has been conducted using the Balearic Islands, located in the Western Mediterranean, as a paradigmatic case study. Three chapters constitute the core of the thesis, each one addressing one of the specific objectives.

In chapter 2, we quantify the uncertainties associated to wave runup computations on sandy beaches. The strategy followed has been to implement different approaches based on numerical models and empirical equations and to compare the results with multi-year wave runup observations on two sandy beaches, Playa de Palma and Cala Millor, located in the South and Northeast of the Mallorca Island, respectively. The results show that depending on the modelling strategy chosen, the uncertainty in the wave runup estimates can range between 12% and 30% of the total value. These results imply that the uncertainty associated with the wave runup calculation is comparable to the uncertainty associated to mean sea level rise projections.

In chapter 3, a cost-efficient and accurate methodology is developed to quantify the flood level along the coasts of the Balearic Islands. Once the methodology is implemented and validated at different locations, it is used to quantify the projected flooding in more than 800 beaches of the Balearic Islands under different climate scenarios. The results show, on average, that more than 50% of beach area will be permanently lost at the end of the century under a high emissions scenario. During storm conditions, the loss of beach area would reach up to 80% under the same scenario.

In chapter 4, a regional assessment of the reduction of coastal impacts induced by the presence of seagrass meadows, particularly *Posidonia Oceanica,* is performed under present and future climate conditions. In order to address this goal, a numerical modelling system able to reproduce the wave-seagrass interactions is first implemented and validated with field observations. Next,

an analysis of the past evolution of seagrass characteristics in the region during the last decades is carried out in order to set up realistic scenarios of future seagrass evolution. Finally, different simulations are performed to quantify the total water level reduction under different scenarios of climate and seagrass evolution. The results show that, under present climate conditions, a complete loss of seagrass would imply an increase in the extreme flood level of 0.7 m, thus highlighting the present role of the seagrass meadows for coastal protection. Under future scenarios, the results show that sea level rise and the expected reduction of seagrass abundance will equally contribute to a large increase in total water level during storm conditions. In particular, under a scenario of large emissions (RCP8.5) and assuming a total loss of seagrass by the end of the century (2080-2100), the extreme flood level would be 1.5 m higher than it is at present.

Resumen

Las zonas costeras son de vital importancia para el desarrollo socioeconómico de las regiones adyacentes por su papel en la alimentación, el comercio, el turismo, el transporte y la recreación. Además, los ecosistemas costeros son esenciales para la biodiversidad, la regulación del clima y la protección contra desastres naturales como las tormentas marinas. La costa es especialmente vulnerable a los impactos del cambio climático debido particularmente por los riesgos de inundación y erosión costera derivados del aumento del nivel medio del mar y el posible aumento de la frecuencia e intensidad de los eventos climáticos extremos.

Obtener, por tanto, proyecciones fiables de inundación costera es crucial para la gestión adecuada de las regiones costeras. A pesar de que varios estudios han abordado la generación de proyecciones futuras de inundaciones costeras, todavía hay una falta de conocimiento en varios aspectos. En primer lugar, todavía hay una falta de conocimiento en las incertidumbres asociadas a la modelización de estas proyecciones. En segundo lugar, las proyecciones a escala regional a menudo se basan en asunciones que pueden comprometer la calidad de los resultados. Por último, es necesario un enfoque óptimo y realista para proteger las áreas costeras en un contexto de aumento del nivel del mar.

El principal objetivo de esta tesis es profundizar en el conocimiento de los impactos costeros inducidos por el cambio climático. Concretamente, la tesis se centra en el impacto de las tormentas marinas sobre las playas de arena, las cuales tienen un valor medioambiental y económico de gran importancia para muchos países del Mediterráneo. Para alcanzar dicho objetivo, se hace uso de observaciones y modelos numéricos con el objeto de abordar tres tareas específicas: (1) cuantificar las incertidumbres asociadas en el cálculo de la modelización de la inundación en playas, (2) desarrollar y aplicar una nueva metodología capaz de cuantificar la inundación en playas a escala regional y (3) evaluar si la vegetación en el fondo marino (por ejemplo, las praderas marinas) ofrece una solución natural para reducir los impactos costeros. El trabajo ha sido llevado a cabo en las Islas Baleares, situadas en el Mediterráneo Occidental, como caso paradigmático. Tres capítulos constituyen el cuerpo principal de la tesis, abordando cada uno de los cuales los objetivos específicos.

En el capítulo 2, cuantificamos las incertidumbres asociadas al cálculo del wave runup en playas. La estrategia seguida ha sido implementar diferentes aproximaciones basadas en modelos numéricos y ecuaciones empíricas y comparar los resultados obtenidos con observaciones multianuales de wave runup en dos playas de arena, Playa de Palma y Cala Millor, situadas en el Sur y Noreste de la isla de Mallorca, respectivamente. Los resultados muestran que, dependiendo de la aproximación considerada, la incertidumbre en el cálculo del wave runup abarca entre el 12 y el 30% del valor total. Estos resultados implican que la incertidumbre asociada a la estimación del wave runup es comparable a la incertidumbre asociada a las proyecciones del nivel medio del mar.

En el capítulo 3, se desarrolla una precisa y eficiente metodología con el objeto de cuantificar el nivel de inundación a lo largo de la costa de las Islas Baleares. Una vez la metodología es implementada y validada en diferentes localizaciones, se usa para cuantificar las proyecciones de inundación en más de 800 playas del archipiélago bajo diferentes escenarios climáticos. Los resultados muestran en promedio que, más del 50% del área de playa se perderá permanentemente a final de siglo bajo un escenario de altas emisiones. En condiciones de tormenta, el área de playa perdida alcanzaría el 80% bajo el mismo escenario.

En el capítulo 4, se cuantifica a escala regional la reducción de los impactos costeros inducidos por la presencia de las praderas marinas, particularmente *Posidonia Oceánica,* en condiciones de clima presente y futuro. Para abordar este objetivo, como primer paso, se implementa un sistema de modelado numérico capaz de reproducir las interacciones del oleaje con la vegetación marina, validado con observaciones. Seguidamente, se caracteriza la evolución de las praderas marinas en la región de estudio durante las últimas décadas con el objeto de definir escenarios realistas de la evolución de las praderas a lo largo del presente siglo. Finalmente, se llevan a cabo diferentes simulaciones para cuantificar la reducción del nivel del mar total bajo diferentes escenarios climáticos y de evolución de las praderas. Los resultados muestran que, bajo condiciones de clima presente, una pérdida completa de las praderas marinas implicaría un incremento en el nivel del mar extremo de 0.7 m, destacando así el papel actual de las praderas marinas en la protección costera. Bajo escenarios futuros, los resultados obtenidos muestran que el incremento del nivel del mar y la reducción de la abundancia de las praderas marinas contribuirán de igual manera en el nivel del mar durante condiciones de tormenta. En particular, bajo un escenario de altas emisiones (RCP8.5) y asumiendo una pérdida total de las praderas marinas para finales de siglo (2080-2100), el nivel de inundación en condiciones extremas sería 1.5 m más alto que en el presente.

Resum

Les zones costaneres són de vital importància per al desenvolupament socioeconòmic de les regions adjacents pel seu paper en l'alimentació, el comerç, el turisme, el transport i la recreació. A més, els ecosistemes costaners són essencials per a la biodiversitat, la regulació del clima i la protecció contra desastres naturals com les tempestes marines. La costa és especialment vulnerable als impactes del canvi climàtic degut particularment pels riscos d'inundació i erosió costanera derivats de l'augment del nivell mitjà del mar i el possible augment de la freqüència i intensitat dels esdeveniments climàtics extrems.

Obtenir, per tant, projeccions fiables d'inundació costera és crucial per a la gestió adequada de les regions costaneres. Malgrat que diversos estudis han abordat la generació de projeccions futures d'inundacions costaneres, encara hi ha una manca de coneixement en diversos aspectes. En primer lloc, encara hi ha una manca de coneixement en les incerteses associades a la modelització d'aquestes projeccions. En segon lloc, les projeccions a escala regional sovint es basen en assumptes que poden comprometre la qualitat dels resultats. Finalment, és necessari un enfocament òptim i realista per protegir les àrees costaneres en un context d'augment del nivell del mar.

L'objectiu principal d'aquesta tesi és aprofundir en el coneixement dels impactes costaners induïts pel canvi climàtic. Concretament, la tesi se centra en l'impacte de les tempestes marines sobre les platges, que tenen un valor mediambiental i econòmic de gran importància per a molts països de la Mediterrània. Per assolir aquest objectiu, es fa ús d'observacions i models numèrics per abordar tres tasques específiques: (1) quantificar les incerteses associades en el càlcul de la modelització de la inundació a platges, (2) desenvolupar i aplicar una nova metodologia capaç de quantificar la inundació en platges a escala regional i (3) avaluar si la vegetació al fons marí (per exemple, les praderies marines) ofereix una solució natural per reduir els impactes costaners. El treball es centra en les Illes Balears, situades a la Mediterrània Occidental, com a cas paradigmàtic. Tres capítols constitueixen el cos principal de la tesi, abordant cadascun dels quals els objectius específics.

Al capítol 2, quantifiquem les incerteses associades al càlcul del wave runup a platges. L'estratègia seguida ha estat implementar diferents aproximacions basades en models numèrics i equacions empíriques i comparar els resultats obtinguts amb observacions multianuals de wave runup a dues platges de sorra, Platja de Palma i Cala Millor, situades al Sud i Nord-est de l'illa de Mallorca , respectivament. Els resultats mostren que, depenent de l'aproximació considerada, la incertesa en el càlcul del wave runup es mou entre el 12 i el 30% del valor total. Aquests resultats impliquen que la incertesa associada a l'estimació del wave runup és comparable a la incertesa associada a les projeccions del nivell mitjà del mar.

Al capítol 3, es desenvolupa una metodologia precisa i eficient per tal de quantificar el nivell d'inundació al llarg de la costa de les Illes Balears. Un cop la metodologia és implementada i validada en diferents localitzacions, es fa servir per quantificar les projeccions d'inundació a més de 800 platges de l'arxipèlag sota diferents escenaris climàtics. Els resultats mostren de mitjana que, més del 50% de l'àrea de platja, es perdrà permanentment a final de segle sota un escenari d'altes emissions. En condicions de tempesta, l'àrea de platja perduda arribaria al 80% sota el mateix escenari.

Al capítol 4, es quantifica a escala regional la reducció dels impactes costaners induïts per la presència de les praderies marines, particularment Posidònia Oceànica, en condicions de clima

present i futur. Per abordar aquest objectiu, primerament, s'implementa un sistema de modelatge numèric capaç de reproduir les interaccions de l'onatge amb la vegetació marina, validat amb observacions. Després, es caracteritza l'evolució de les praderies marines a la regió d'estudi durant les darreres dècades per tal de definir escenaris realistes de l'evolució de les praderies al llarg d'aquest segle. Finalment, es duen a terme diferents simulacions per quantificar la reducció del nivell del mar total sota diferents escenaris climàtics i d'evolució de les praderies. Els resultats mostren que, sota condicions de clima present, una pèrdua completa de les praderies marines implicaria un increment al nivell del mar extrem de 0.7 m, destacant així el paper actual de les praderies marines en la protecció costanera. Sota escenaris futurs, els resultats obtinguts mostren que l'increment del nivell mitjà del mar i la reducció de l'abundància de les praderies marines contribuiran de la mateixa manera al nivell d'inundació durant condicions de tempesta. En particular, sota un escenari d'altes emissions (RCP8.5) i assumint una pèrdua total de les praderies marines per a finals de segle (2080-2100), el nivell d'inundació en condicions extremes seria 1.5 m més alt que en el present.

Contents

Chapter 1

1 General Introduction

1.1 The importance of the coastal zone

The coast can be defined as the strip of land that borders the sea or the contact zone between the marine and the terrestrial environments (Suárez de Vivero, 1999). More generically, the coastal zone is typically composed by very different natural and artificial elements, like beaches, cliffs, ports, estuaries, and salt marshes (Figure 1. 1).

In general, the coastal zone is of great importance for several reasons. Firstly, it is a vital habitat for a wide variety of marine and terrestrial flora and fauna. Many species rely on the coastal zone for their survival and reproduction. Secondly, it provides a large range of ecosystems services, including coastal protection or carbon storage. Besides, the coastal zone is a significant economic source, providing opportunities for fishing, trade, recreation, tourism, etc.

These coastal units have diverse origins and evolution. For instance, natural beaches are generated by the accumulation of sediments from rivers or the seabed for thousands of years. In contrast, ports are artificial structures built by humans in a relatively short time compared to natural beaches. Cliffs suffer from erosion due to the impact of wind and waves although their evolution is usually much slower than the one suffered by beaches. In addition, those elements can interact among them, since the construction of an artificial structure (i.e., ports) can modify the currents and the sedimentary balance of adjacent locations. Therefore, the coastal zone is a complex area where many processes interact at different spatial and temporal scales.

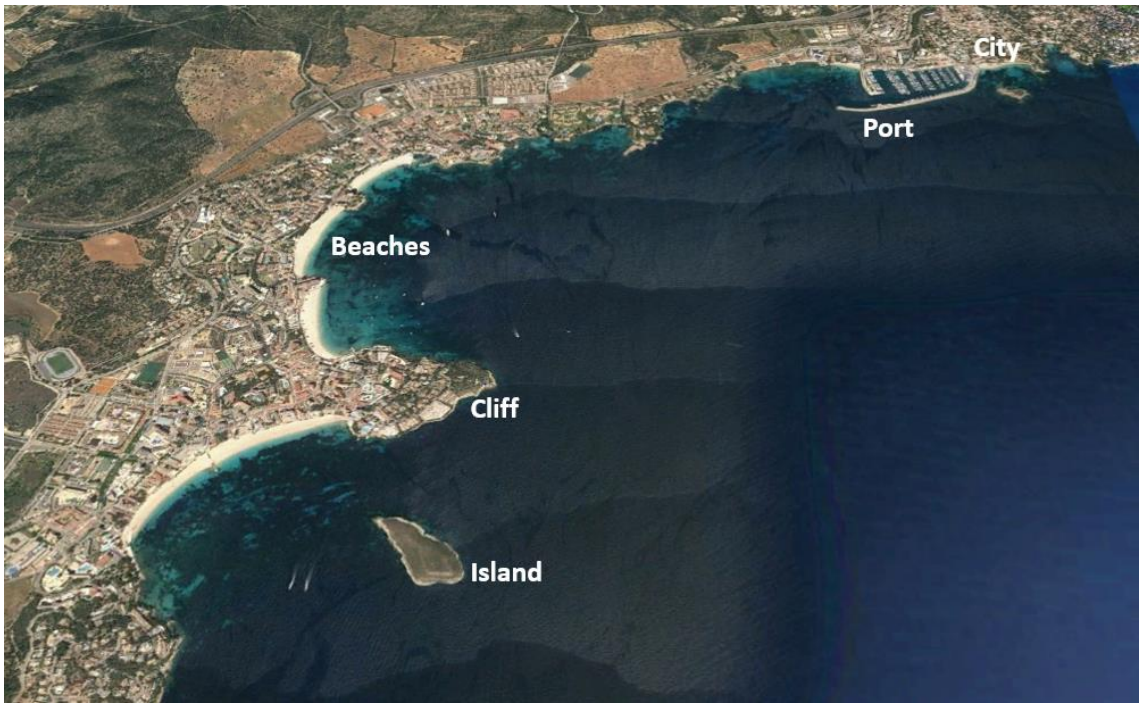

Figure 1. 1 Example of a coastal zone that shows different units.

Further exploring the importance of the coastal zone, it is also an important element of the biosphere where diverse natural systems and resources are located. It houses more than 45% of the human population and is where 75 % of those cities with more than 10 million inhabitants

are located (Crossland et al., 2005). This is also true for the Mediterranean coasts as many major cities and ports and a big share of the industrial and touristic development are located along them (Vogiatzakis et al., 2005). As an example, it is estimated that 50-70 % of the population in Mediterranean countries live within 60 km of the coast and this proportion is increasing (Caffyn et al., 2002).

The coastal zone also provides benefits like a favorable environment for fishing, recreation and tourism, oil and gas production, marine transport and waste disposal (Turner and Bower, 1999). Another well-known benefit is that spending time by the beach is good for both mental and physical health. It enhances the feel of calm from hearing the ocean and relaxation of the nervous system due to a reduction of city noise and technology, (Medvedev et al., 2015; Garrett et al., 2019) . One of the most important benefits according to coastal management is that the shore zone provides significant coastal protection: Coral reefs, seagrasses, mangroves and beaches work as wave energy sinks and natural barriers against coastal storms (Morton and Sallenger, 2003; Ondiviela et al., 2014; Beck et al., 2018; Menéndez et al., 2020).

Coastal zones usually encompass a combination of high human population density, overlapping sectors with different interests and an intensive use of space and natural resources. They also promote economic benefits for the region landward. Regarding that, the paradigmatic example is the beaches, which create a high tourism demand. Tourism is a major global economic sector that has undergone tremendous growth over the last decades (UNWTO, 2018) with an increasing impact on the global economy. The World Travel and Tourism Council (WTTC) estimates the sectorial contribution to global economy in 2015 was US$7.2 trillion (9.8% of the global GDP) and 284 million jobs (9.1% of jobs worldwide) (Wttc, 2016). In this context, the western Mediterranean is one of the favorites sun and beach tourism destinations (Rovira Soto and Anton Clavé, 2017) and the tourism activity has a great impact in the economy of the region (Coccossis and Koutsopoulou, 2020). The ports are another example of the economic importance of the coastal zone, as most of the goods are distributed worldwide by sea. Thus, ports located in strategic zones generally offer a huge economic and social benefits to the nearby region (Rodrigue and Notteboom, 2020).

1.2 Parts of the coastal zone

Some general concepts about the coastal zone have also to be clarified. First, defining the concept of “coastline” is important. The coastline can be defined as the imaginary line that defines the intersection between land and sea. Often this concept can be a bit ambiguous as sea level, and therefore the intersection between land and sea, are always changing over time, so a reference “zero” level is necessary to identify the coastline variations along time. Here several reference levels are normally used as the lowest tide throughout the year, the mean sea level or the zero’s port where tide gauge is installed. Second, it is also necessary to delimit the different zones that play a role shaping the characteristics of wind waves. The offshore region is relatively far from the coast and is where waves are generated and from where they travel up to the coast. The nearshore region is defined as the zone where waves start to interact with the seabed (Figure 1. 2). In turn, the region closest to the coastline can be separated in three zones, i) the shoaling zone, where waves change in shape and behavior as they enter into waters of decreasing depth, ii) the breaking zone, where waves break and iii) the swash zone, where waves bore run up and run down the beach (Figure 1. 2).

Figure 1. 2 Delimitation zones of wave's behavior in the beach

It should be noted that beaches, as a fundamental part of the coast, are a complex and dynamic system. From a physical perspective, beaches are influenced by factors such as wave action, currents, tides, as well as the geology and topography of the coastline. In order to reflect the complexity of the system, there are several types of beaches based on their morphodynamic, mainly classified by 1) reflective beaches, that have a steep slope and are characterized by large waves that break close to the shoreline. They are typically composed of coarse sand and gravel and are found on exposed coasts with high wave energy. 2) Dissipative beaches, which have gentle slopes and are characterized by small waves that break far from the shoreline. They are typically composed of fine-grained sand. 3) Intermediate beaches, which have a moderate slope and are characterized by waves that break closer to the shoreline.

Understanding the morphodynamics of beaches is important for coastal management and conservation efforts, as it can help to predict how they will respond to natural and human-induced changes.

1.3 Marine storms and coastal impacts

Marine storms can be defined as a severe weather event that occurs in coastal areas, characterized by strong winds, heavy precipitation, high waves, and storm surges. These atmospheric phenomena can be caused by a variety factors, including the collision of different air masses, the interaction of weather systems with ocean currents, and the influence of tropical storms or hurricanes (Molinari and Mestas-Nunez, 2003). Marine storms can cause significant damage to coastal infrastructure, property and a threat to human life.

One of the most impact due to a marine storm is the coastal flooding, which can be defined as an inundation that happens when land that is usually dry, is flooded with seawater that spills landward due to abrupt sea level changes. Coastal flood assessment is not an easy task due to the large number of physical processes that can be involved with the joint action of ocean and atmospheric dynamics. Many natural phenomena can cause the sea to rise, such as wind drag, air pressure drop, astronomical tides, earthquakes, etc. The sea level changes have different periods depending on the physical mechanism that generates them. For instance, wind waves have a period of several seconds, long waves of few minutes, storm surges about hours to days or tides about hours to months.

In order to estimate the coastal flood in any kind of coastal typology at a given moment, we must consider different contributors. The first one is the astronomical tide (AT), which is entirely predictable and is caused by the relative rotation of the sun and the moon around the Earth (Van der Meer et al., 2018). The second one is the meteorological tide, commonly called storm surge (SS), that refers to the water level variations caused by the atmospheric mechanical forcing exerted by the atmospheric pressure and winds. Another contributor is the wave runup (WR). Over the tide level, the swell generated by the wind in deep waters travels in groups of waves until they reach the coast. Its interaction with the seabed and the coastline modifies the wave parameters by the effect of refraction, diffraction, white-capping, bottom friction and breaking, among others (Roland and Ardhuin, 2014). Upon reaching the coast, the waves break and experience an ascent-descent movement over the littoral called wave runup. By convention, it is measured vertically from the still water line and is defined as the level which is exceeded by 2% of the number of incident waves (Stockdon et al., 2006). The WR component has two main contributors. From one side, when waves break nearshore, a sea level rise is produced near the coastline, called wave setup. From this level, individual waves rise and fall on the beach, generating instantaneous flooding, called swash. Depending on the shape of wave spectrum reaching the coast and the coastal slope, the infragravity component of swash (associated to waves with long periods), could be very important. Other mechanisms can also contribute to sea level variations at the coast. For instance, seiches in bays and harbors can induce fast variations of sea level, as meteotsunamis (Monserrat et al., 2006), while changes in the density of the water column or mass displacements also induce low frequency variations of the coastal sea level (Gomis et al., 2012). Nevertheless, it is usually assumed that the dominant mechanisms driving the coastal sea level are the tidal forcing, storm surge and wave runup. Therefore, in this thesis we well define the total water level (TWL) as the result of the combination of those three components:

$$TWL = AT + SS + WR \quad (1)$$

If a marine storm, mainly generated by low atmospheric pressures leading to strong coastward winds and high wind waves, coincide in time with high astronomical tidal levels, the TWL reach the maximum values causing serious coastal damages (i.e., physical, and biological damages, loss of human lives, etc.). In the last decade, several severe storms hit the coast at different worldwide locations (Bidlot, 2017) attracting public attention to the importance of extreme events in the coastal area. For instance, in August 2005, Hurricane Katrina caused a large number of life losses (1.833) and more than 800.000 housing units were destroyed or damaged by the storm, with estimated cost over $81 billion (Figure 1. 3, left). In the Mediterranean Sea, in January 2020, the storm Gloria left many coastal sectors flooded, destroyed coastal infrastructures, and induced strong erosion in sedimentary coasts, causing losses of several millions of euros (Figure 1. 3, right).

Figure 1. 3 Left: Coastal flooding during Hurricane Katrina in the southeastern United States in late August 2005 (source: elpais.com). Right: Storm Gloria in Xàbia in January 2020 (source: lamarinaplaza.com).

1.4 Simulation of coastal impacts

Different strategies for modeling coastal impacts can be found in the literature, depending on the methodology considered and the objectives to be addressed. In this context, some approaches could be adopted to simulate the physical effects of waves reaching the coast and their consequence impacts.

To simulate offshore waves there are numerical models that generates wave spectrum from wind and atmospheric pressure forcing. Some examples are SCHISM (Zhang et al., 2016), WWIII (Tolman, 1989), WAM (Hasselmann et al., 1988) , Etc.,. They are called spectral models because the energy balance equation is resolved in the frequency dimension. Those models are better suited to generate global or regional wave fields while they are typically not used for applications near the coast. From other side, wave fields are propagated from offshore up to the coast by using numerical models with higher spatial resolution and relatively low computational cost (i.e., SWAN, DELFT 3D (Booij and Holthuijsen, 1987; Kernkamp et al., 2011)). Those models are typically implemented in small areas at a spatial resolution that allows to solve the coastline characteristics. They take the wave conditions at the open boundaries from buoy observations or from the outputs of large-scale models.

In order to quantify coastal flooding, two different approaches can be used, direct numerical simulation or empirical equations. The numerical models used for this require more computational cost than the above-mentioned models since they resolve the sea level surface and the wave phase in a transitory way. According to those transitory phase-resolved models, they can be separated into two categories depending on the level of realism. The most sophisticated ones solve the 3D Navier-Stokes equations (i.e., OPENFOAM, (Chen et al., 2014)). They are capable of simulating the physical processes involved in wave propagations in a very realistic way, but with a high computational cost. Other type of numerical models solves the phase-averaged coupled 2D horizontal equations for wave propagation, with a relatively low computational effort, like XBEACH (Roelvink et al., 2015) or SWASH (Zijlema et al., 2011). If the goal is estimate the wave runup on beaches, a different approach is to use empirical equations for wave runup fed by information on the characteristics of the incident sea state and the coastal slope (Stockdon et al., 2006; Gomes da Silva et al., 2020). This approach is fast but assumes some simplifications as they do not explicitly solve the physical processes involved.

The quality of the simulated coastal flooding will thus depend on the modelling choice, but not only. The spatiotemporal scales of the numerical model, the quality of the information introduced through the boundary conditions (e.g., from buoys or from models), as well as the

accuracy of the topography used will also determine the level of accuracy of the estimated coastal inundation.

In this context, the coastal impacts can be assessed at different spatial scales. In the last decade, several methodologies have been implemented to quantify the coastline retreat at local scale (Villatoro et al., 2014; Enríquez et al., 2019; Serafin et al., 2019). These works are based on the use of high-resolution wave numerical models and sea level databases along with detailed information on local bathymetry, providing accurate results. However, these approaches require a huge computational effort. Consequently, they are limited to a few locations for a short period of time and cannot be used to get an overview of at regional scale. Conversely, other methodologies have been developed to measure the shoreline evolution and to project its future evolution at a global scale (Vousdoukas et al., 2020). However, those approaches are dangerous as some crucial information related to local features is missed leading to oversimplified description of the coastal processes.

Another important aspect to consider in the modelling of the coastal flooding is the presence of submerged vegetation. The most important transformation of wave characteristics occurs in the shoaling and swash zone, where diffraction, shoaling and breaking highly reduce the waves energy (Lin and Liu, 1998). Moreover, in this critical zone, the bottom friction plays a paramount role in the energy wave dissipation, especially over vegetated grounds (Duarte et al., 2013; Beck et al., 2018; Menéndez et al., 2020). Some numerical models like XBEACH, can simulate the wave damping and breaking over the vegetation fields at variable depths (Mendez and Losada, 2004; van Rooijen et al., 2015). This kind of tool could be very useful to count on the attenuation of incoming waves reaching the coast thanks to the seabed vegetation.

1.5 Climate change in coastal zone

Increasing greenhouse gases (GHG) concentrations and the consequent global warming are already affecting inhabited regions all across the globe and it has been proved that human influence is responsible of many observed changes in weather and climate extremes (Shukla et al., 2019a). According to the sixth assessment report of the IPCC (Shukla et al., 2019b), the global surface temperature has increased by 0.99 ºC from 1850-1900 to the first two decades of the 21st century (2001-2020). Compared to 1850-1900, the average global surface temperature over the period 2081-2100 is very likely to be 1ºC-1.8ºC higher assuming a low CO2 emissions scenario (SSP1-1.9) and between 3.3ºC to 5.7ºC higher in case of a high CO2 emissions scenario (SSP5-8.5).

Global warming will have consequences on the marine environment. For instance, it will lead to changes in the characteristics of Marine Heat Waves (MHWs). The projected MHWs exhibit a significant increase in their intensity and duration with the largest changes projected to occur in the tropics, North Pacific, and North Atlantic (Qiu et al., 2021). Furthermore, the heating of the climate system has caused global mean sea level rise (GMSLR) in the last decades, and it is projected to continue rising throughout all the 21st century. Projections of future mean sea level including all the factors that play a role at a global scale (mass variations linked to the addition or removal of water from the ocean and thermal expansion due to ocean warming) and at regional scale (gravitational fingerprint of changes in the ocean mass, changes in the circulation patterns, mass redistribution by atmospheric pressure and wind and land motion) show worrying results Relatively to 1995-2014, the likely GMSLR by 2100, will be 0.44-0.76 m, under the intermediate GHG emissions scenario (SSP2-4.5) and 0.63-1.1 m under the business as usual

scenario (SSP5-8.5), (Zhongming et al., 2021). That rise in the mean sea level will increase the frequency and intensity of coastal floods and erosion. Also, the resulting inundation from rising seas will heavily impact low-lying areas; at least 100 million persons live within one meter of mean sea level and are at increased risk in the coming decades (Zhang et al., 2004). Future changes in global storm surges and ocean waves are also expected, but the results are not completely robust. The spatial pattern in the trend of annual maximum sea surface heights and wave heights is predominantly driven by changes in tropical cyclones (TC). Although highly intense TC are expected to be enhanced in a warmer climate, it is not clear yet what will be the response of the very extreme storm surges and wave heights (Shimura et al., 2022).

In the Mediterranean, during the 21st century, the basin mean sea surface temperature is expected to increase by 1.1ºC to 2.1ºC and 2.7ºC to 3.8ºC under the RPC4.5 and RPC8.5 scenarios, respectively, (Soto-Navarro et al., 2020), threating the future of the Mediterranean seagrass meadows. Salinity is also expected to increase in the basin, although the evolution of surface salinity is not yet clear, (Soto-Navarro et al., 2020). Regarding to the mean sea level, it is projected to rise throughout the 21st century, reaching by 2100 around 37-90cm, depending on the scenario (Cramer et al., 2020).

The combination of sea level rise and sea warming will imply a large increase in extreme events in terms of flooding and erosion. These events that historically occurred once per century are projected to occur at least yearly in most parts of the world during the 21st century (Loarca et al., 2020). Consequently, there is an urgent need to carry out coastal adaptation planning according to the projected changes in frequency and magnitude of the coastal impacts (Oppenheimer et al., 2019). In this context, the protection of coasts from flooding and erosion is traditionally approached from an engineering perspective with “hard solutions” (e.g., seawalls, dikes). However, these solutions provide protection to a limited coastal extent and most of them lead to local and long-term environmental impacts. Conversely, the preservation or incorporation of ecosystem services into coastal protection against the likely increase of coastal damages in the coming decades is a new field that has gained strong interest over the last decade (Borsje et al., 2011). Although nature-based solutions may not always provide the required defense against marine storms, combining engineering and nature-based options seems a promising way toward innovative coastal protection solutions (Bouma et al., 2014). In this sense, the presence of submerged vegetation can be an effective element to minimize the impacts of coastal marine storms, although it has not been quantified yet at regional scales.

1.6 Objectives and structure of the thesis

The main goal of this thesis is to contribute to the research on coastal impacts induced by global warming. In particular, the thesis aims at producing robust and actionable knowledge on the impacts associated to the sea level rise and the expected increase of beach flooding. In order to achieve this goal this manuscript tries to solve some open questions:

- Which strategy is the most appropriate to quantify coastal flooding on beaches and what are the sources of uncertainty associated to that quantification?
- Is it possible to provide reliable results of coastal flooding at a regional scale to be used for coastal management purposes?
- Is the presence of seagrass meadows a suitable solution to reduce the expected coastal flooding associated to global warming?

This thesis focuses on the coasts of the Balearic Islands. The archipelago is in the western part of the Mediterranean Sea and is composed by 4 different islands (Mallorca, Menorca, Ibiza and Formentera). The Balearic Islands have a large coast with a huge marine diversity and more than 800 beaches that are an essential touristic asset. However, the increase in anthropogenic pressure on the coastline has led to an accelerated coastal deterioration with an increase of eutrophication and coastal erosion, a reduction of water clarity and the loss of habitat and biodiversity (Marbà et al., 2014). In addition, global warming may increase the risk of flooding and coastal erosion due to two main threats. On the one hand, mean sea level rise has caused an increase in the coastal impacts due to marine storms (Dangendorf et al., 2017; Krestenitis et al., 2017) and will accelerated in the coming decades. On the other hand, the increase in marine heat waves endanger the survival of seagrass meadows, with the consequent loss of habitat and the natural protection they offer to the coast against marine storms (Mendez and Losada, 2004; Marbà and Duarte, 2010). Then, the region is particularly vulnerable to eventual reduction in beach availability and degradation of marine diversity. Furthermore, there is a social awareness developed in recent years on the risks associated to climate change. For instance, a recent research reveals that tourists and residents in this region would support the implementation of adaptation policies aimed at counteracting climate-induced environmental changes, (Enríquez and Bujosa Bestard, 2020). In consequence, the Balearic Islands are a good case study to investigate the impacts of global warming on coastal areas.

The manuscript has been organized in three chapters addressing each one of the above-mentioned open questions.

In the first part of the thesis (chapter 2), we study the uncertainties associated with wave runup calculations using different modelling strategies. In particular, the floodable area of two beaches of the Balearic Island is quantified both for present climate and under different future climate scenarios. These beaches are Playa de Palma and Cala Millor, located in the South and East of Mallorca, respectively. They are chosen because they are well monitored (Tintoré et al., 2013) and are representative of two contrasting marine conditions. The strategy has been to implement different modelling chains using several models and forcing conditions and to validate their results against wave runup observations. This has allowed us to identify the major sources of uncertainty in the modelling of beach flooding.

Afterwards this knowledge is applied to develop a new and robust methodology that allows the massive analysis of flooding for a large number of beaches (chapter 3). The methodology is used to quantify the beach surface loss under different climate scenarios and different wave conditions for all the beaches in the Balearic Islands.

Once the future scenarios of beach loss have been defined, the role of seagrass meadows in the coastal protection is assessed (chapter 4). In particular, a careful calibration of the modelling system in presence of seagrass meadows is carried out first. Then, the system is applied to all the Balearic Islands coasts under different scenarios of global warming and of seagrass evolution. The results are analysed to provide a quantification of the benefits that seagrasses provide for the mitigation of coastal impacts.

Finally, an overview of the main results of this thesis is presented in chapter 5. At the end of the thesis, we include an annex with information of other studies carried out during the last years but that are not directly related to the topic of this thesis.

This thesis has been developed in the Centre Oceanogràfic de Balears (CN-IEO/CSIC) and the Institut Mediterrani d'Estudis Avançats (IMEDEA, UIB/CSIC) in the framework of two contracts

funded by the TEMPERSEA project (funded by the Kaust University) and the MOCLI project (funded by the CN-IEO/CSIC). Additionally, I have contributed to the H2020 SOCLIMPACT project, the Spanish VENOM project and the JPI-ERANET AXIS UNCHAIN project. Those contributions have resulted in the publications listed in the annex.

Chapter 2

2 Quantification of error sources in wave runup estimates on two Mediterranean sandy beaches.

This paper is under review as:

Agulles, M., Jordà, G., (2022). Quantification of error sources in wave runup estimates on two Mediterranean sandy beaches. Coastal Engineering.

Chapter summary

Projected future sea level rise and marine storminess is a serious threat for beaches as they induce beach flooding and erosion. Among other factors, wave runup plays an important role in beach evolution and must be robustly assessed. However, little attention has been paid to the uncertainties associated with its characterization and how do they compare to other sources of uncertainty. As a first step towards this goal, we have quantified the impact of several sources of error in the estimation of wave runup on sandy beaches. Understanding what factors are more influential in the quality of the results will help to determine the main sources of uncertainty in beach flooding projections. To reach that goal, a calibrated state-of-the-art numerical modelling system has been set up for two beaches in the Mallorca islands (NW Mediterranean). The system has been forced with the best available information of nearshore incoming waves and has been validated against observations to define the benchmark quality. To determine the key factors affecting the quality of the system's results, different systems configurations have been tested with different degrees of complexity.

Our results show that using the most sophisticated modelling system with the best information on boundary conditions, bottom bathymetry, and submerged vegetation leads to a swash RMSE comparable to the standard deviation of the observed swash. We have also found that the choice of lateral boundary conditions (i.e., source of information for the incoming waves) can double the RMSE and induce large biases. Our results also show that using a simple empirical approach usually underestimates the wave runup. However, in locations with vegetated seabed there is a compensation error, and the empirical approach can lead to acceptable results if forced by nearshore waves. In addition, we have compared the error estimates obtained with uncertainties associated with projected sea level rise. Our findings suggest that the uncertainty associated with wave runup modelling should be considered in the assessment of the total uncertainty of future beach flooding, since the analysis performed indicates that this uncertainty can account for between 16% to 60% of the uncertainties linked to mean sea level projections.

2.1 Introduction

Sandy beaches provide a natural barrier for coastal protection against marine storms. Also, they are a key asset for coastal tourism and socioeconomic system of many countries (Di Luccio et al., 2018). Particularly, the Mediterranean coastal zone is severely impacted by extreme climatic events (e.g., storm surges and high waves) coupled with human-induced pressures (e.g., uncontrolled coastal urbanization), resulting in a growing vulnerability (Satta et al., 2017; Mejjad et al., 2022). In consequence, assessing how climate change, and in particular, the projected changes of sea level and wind waves can affect the sandy beaches is of paramount importance.

The magnitude of beach flooding depends on the total water level at the coast. In turn, this depends on the astronomical tidal level, changes in the mean sea level, the storm surge and the wave runup (Holman and Guza, 1984). Regarding the later, as waves approach the coast, part of the energy dissipates due to wave-breaking in the surf zone and the remaining energy reaches the beach and drives oscillations of the water edge over the foreshore (Gomes da Silva et al., 2018). The vertical value of this oscillations is called runup, composed of a steady super elevation called setup, and a fluctuating component called swash (Holman and Guza, 1984; Stockdon et al., 2006). In regions with small tidal range and relatively mild storm surges, like the Mediterranean Sea (Tsimplis et al., 1995; Marcos and Tsimplis, 2007; Amores et al., 2020), the wave runup can represent the main contributor of the total water level under extreme wave conditions (Agulles et al., 2021).

In the last decades, great efforts have been done to develop wave runup empirical equations based on field observations (Gomes da Silva et al., 2020). Among them, Stockdon et al. (2006) have developed an empirical formulation that has become a standard in runup computations. Based on the work of Holman, (1986) and gathering the information obtained in ten field experiments, Stockdon et al. (2006; hereinafter S2006) fitted runup observations from video cameras to beach slope and incident wave parameters. They have obtained a formulation for the setup and swash that has been widely used with reliable results in many different contexts (e.g: Atkinson et al., 2017; Di Luccio et al., 2018). A foreseen problem with this formulation is that it does not take into account the modification of wave parameters by refraction, diffraction, bottom friction and breaking, among other effects, that take place when the waves approach the coast. Alternatively, the use of wave phase-resolving numerical models capable to simulate the wave runup in the swash zone has increased in the last years thanks to the increase of computational power (Zijlema et al., 2011; Roelvink et al., 2018; Enríquez et al., 2019). While numerical models offer greater flexibility and are capable of simulating complex coastlines and bathymetries, they entail a much higher computational cost compared to using empirical equations. Additionally, the calibration of numerical models requires suitable data, which can add to the complexity and cost of their implementation. Both approaches, the empirical and the numerical, have been applied to a broad variety of situations. In particular, projections of future beach flooding due to global warming have been implemented using empirical approaches (Didier et al., 2015; Vousdoukas et al., 2020), numerical ones (Enríquez et al., 2019; Orejarena-Rondón et al., 2019; Agulles et al., 2021) or mixed ones (Stockdon et al., 2014).

Uncertainties associated to climate projections are an important information that must be provided to stakeholders (Cobb et al., 2021). Those uncertainties come from several sources like future greenhouse gas emissions (GHG), natural variability or model limitations (Hawkins and Sutton, 2009; Giorgi, 2010; Horton et al., 2020; Oddo et al., 2020). The first two sources are

commonly addressed by running ensembles of model simulations under different GHG scenarios (Hawkins and Sutton, 2009). The third one, however, requires specific studies that consider the particularities of the modelling system, defined hereinafter as the model itself, as well as its particular configuration and the boundary conditions used to force it. In the case of beach flooding some studies have quantified the quality of the model results during short periods of time corresponding to field experiments on a specific beach (Di Luccio et al., 2018; Gomes da Silva et al., 2018; Xie et al., 2019). However, up to our knowledge there has not been a detailed comparison on how different elements of the modelling system impact on the accuracy of the wave runup estimates for an extended period of time.

The goal of this paper is to quantify the errors associated with estimates of wave runup on sandy beaches, and to assess how these errors vary depending on the choices adopted in the modelling setup. The strategy followed has been to implement several modelling approaches based on empirical and numerical models with different degrees of complexity (1D and 2D) and to compare their results with a long time series of observations in two different sandy beaches which are representative of Mediterranean beach typology. This quantification of the error sources can help to assess the relative impact of model limitations in the uncertainties associated to projections of future wave runup.

The work is organized as follows. In Section 2, data and site description are presented along with the methodology of the experimental protocol proposed to obtain the wave runup uncertainties. Results of the different methodologies proposed are shown in section 3. To conclude, discussion and conclusions are presented in sections 4 and 5.

2.2 Data and methods

2.2.1 Study sites

In this work we analyse two microtidal sandy beaches located in the Mallorca Island (Western Mediterranean Sea, see Figure 2. 1). These beaches can be considered representative of a large fraction of Mediterranean sandy beaches. Specifically, the Playa de Palma beach (hereinafter, PDP) located on the South of the island and Cala Millor beach (hereinafter, CLM) located on the East. PDP is a large beach of ~4.5 km alongshore by ~30-50 m wide with fine grain size (0.20-0.25mm of D50) and relatively low slope of ~0.027 with dissipative conditions (Figure 2. 1A). CLM is ~1.7 km alongshore by 35-40 m wide, with a mixed rock and sand bed and a small cliff at the southernmost sector of the beach. It has a medium grain size (0.35-0.40mm of D50) with a mean beach slope ~0.044 and slightly reflective conditions (Figure 2. 1B). The two beaches are included in the beach monitoring program of the Balearic Islands Coastal Observing and Forecasting System (SOCIB) since 2011. This program includes periodic topography and bathymetry surveys, continuous video monitoring of the shoreline position and in situ measurements of nearshore waves and currents, among others (Tintoré et al., 2013).

The wave conditions in both sites are shown in Figure 2. 2. The mean conditions of the two locations are similar with significant wave height (Hs) around 0.5-1.0 m and a peak period (Tp) of around 5-6 s. PDP is exposed to offshore wave conditions from the SSW to SW (dominant direction ~200º) and this dominant direction is kept as the waves refract and approach the shoaling zone (Figure 2. 2a). In contrast, in CLM there are large differences between offshore

and onshore wave conditions, both for the mean and extreme waves (Figure 2. 2b). The offshore waves arrive from NNE to SSE (directions from ~30º to 150º) while the nearshore mean direction is around E (~100 º) due to diffraction.

An important characteristic of Mediterranean coasts is the presence of vegetation in seabed. Seagrass meadows are commonly present at shallow depths in the whole basin and therefore along the coast in our study region (Cebrián et al., 1996; Ruiz et al., 2015; Telesca et al., 2015). In particular, the presence of seagrass is constant from depths between 5 and 40 m both in PDP and CLM (Figure 2. 3). This fact determines the magnitude of the bottom friction and has been carefully considered in the model configuration (see section 2.6.2).

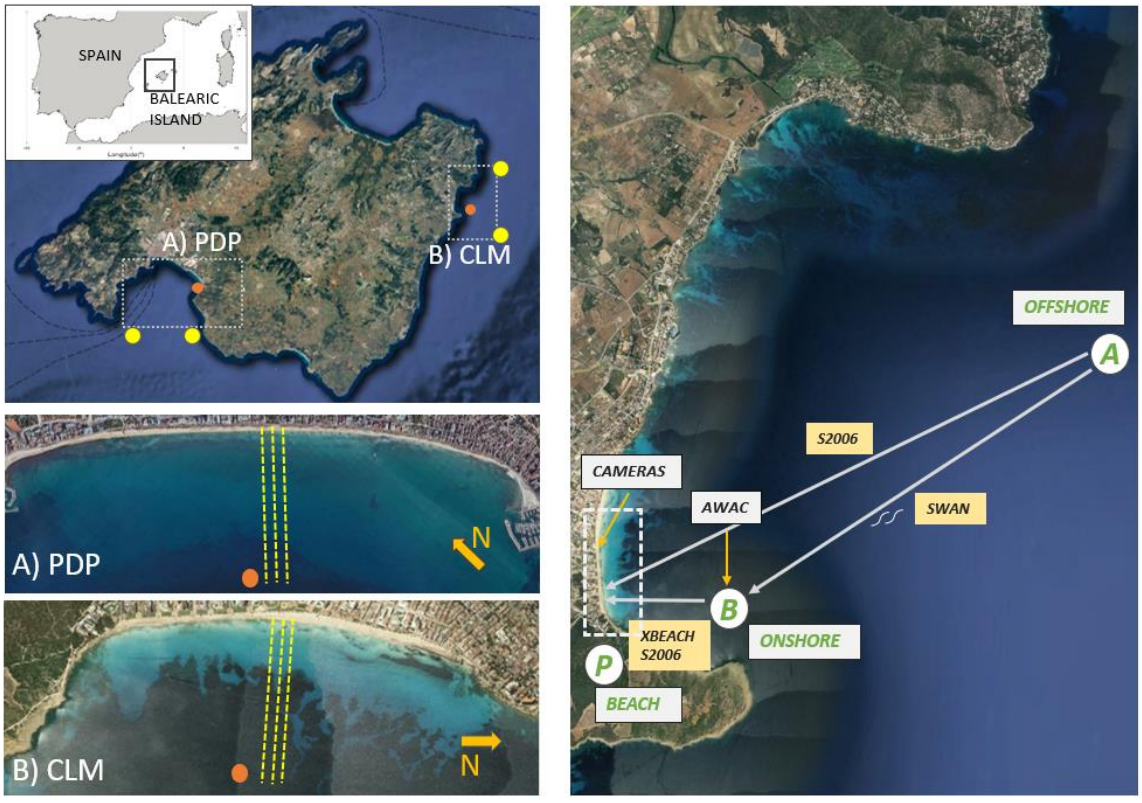

Figure 2. 1 Left panel, location of the study sites with the position of the onshore wave observations (orange dots), SIMAR points (yellow dots) and SWAN grids (gray dashed rectangles). (a) Detailed view of Playa de Palma beach (PDP) with the transects considered to obtain a representative beach profile (yellow dashed lines), (b) the same for Cala Millor Beach (CLM). A sketch of the modelling approach is presented in the right panel.

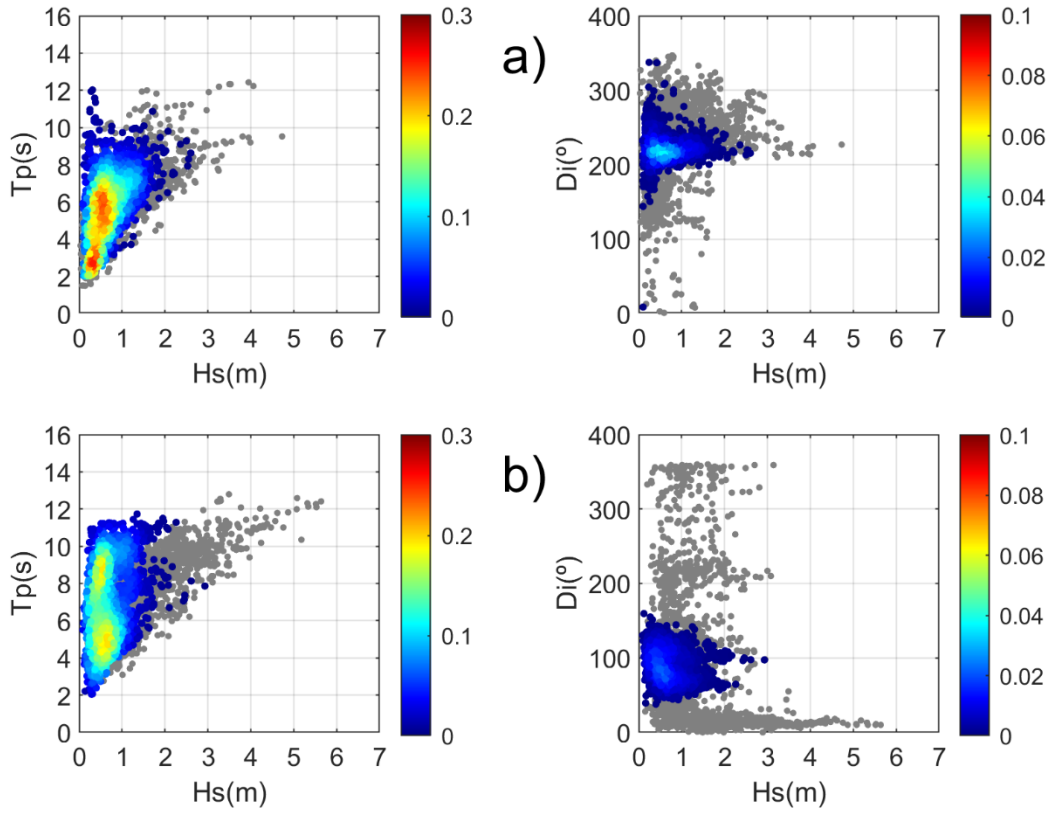

Figure 2. 2 Wave maritime climate for (a) Playa de Palma Beach and (b) Cala Millor Beach. The panels represent a scatter plot of Hs (in m) vs Tp (s), left column, and Hs (m) vs Direction (º), right column. The offshore conditions are represented by the grey dots while the observed nearshore conditions are represented by the colored dots, with the color representing the frequency of occurrence.

2.2.2 Topo-bathymetric surveys

Bathymetry surveys were conducted by SOCIB (Tintoré et al., 2013), using a single-beam echo sounder, BioSonics DT/DE Series Digital Echosounder, in the CLM beach and a multi-beam echo sounder, R2Sonic2020, in PDP. The final spatial resolution is 1 m x 1 m. These measurements were complemented with topographies of the aerial beach obtained using a survey-grade RTK-GPS (Real Time Kinematic Global Position System). The surveys were conducted under calm conditions and more information can be found in https://medclic.es/en/instrumentos/monitorizacion-de-playas/.

The characteristic cross-shore profile of each beach is obtained by averaging the transects located in the middle of the beach (area limited by yellow dashed lines in Figure 2. 3A and B). Winter and summer profile are available for CLM while only summer profile is available for PDP (Figure 2. 3). The beach slope (β_f) is calculated as the average slope over the swash zone. This zone has been delimited from the observed horizontal swash variability (see video imagery section). Those beaches have seagrass meadows from 5 meters depth, as you can see in green patches in Figure 2. 3.

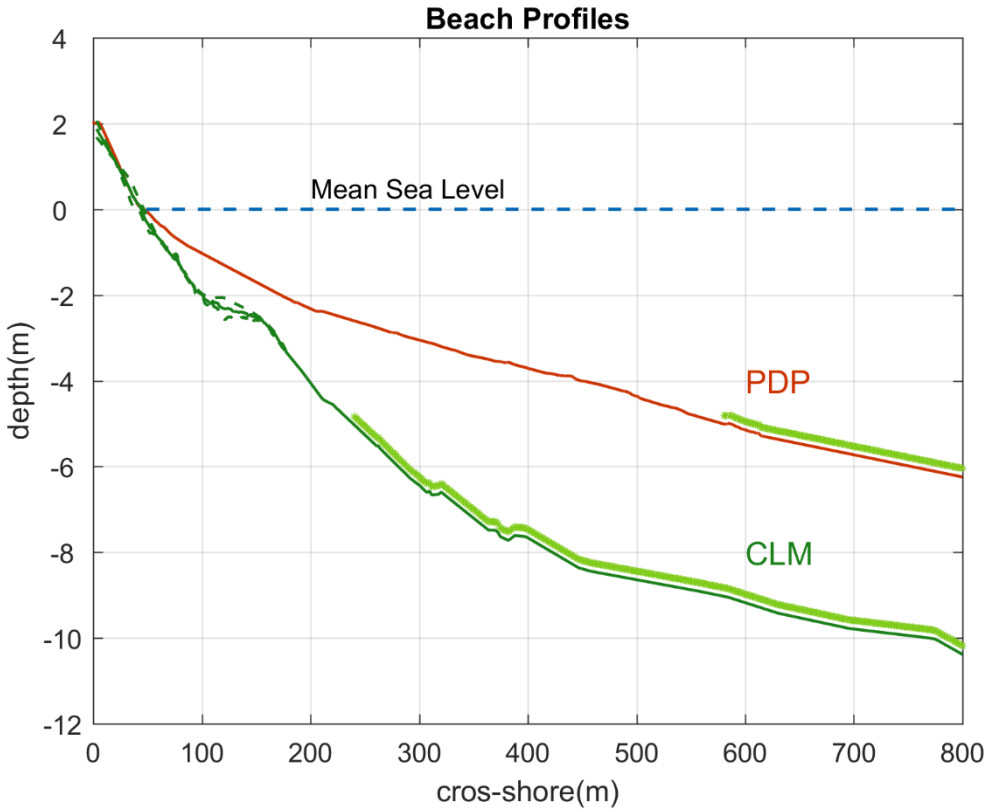

Figure 2. 3 Beach profile at PDP (red) and CLM (green). Seasonal profiles (dashed lines) and annual mean profile (continuous lines). Green patches represent the presence of seagrass meadows.

2.2.3 Wave data

Nearshore waves observations at hourly resolution are obtained from directional Acoustic Waves and Currents (AWACs) sensors located at ~20 m water depth at the two studied beaches (Figure 2. 1, orange dots), covering a period from 2012 to 2017 at PDP beach and from 2011 to 2019 at CLM beach. Data have been downloaded from http://thredds.socib.es/thredds/catalog.html, and the wave parameters for each beach are presented in Figure 2. 2.

Offshore waves conditions were retrieved from the SIMAR database developed and maintained by Puertos del Estado (Pilar et al., 2008). SIMAR is a 62-year wave reanalysis generated with the WAM model (Hasselmann et al., 1988) from 1958 to 2020. It covers part of the Atlantic Ocean and the Western Mediterranean (Longitude -12º to 8º and Latitude 34º to 48º) with a spatial resolution of ~3 Km and hourly temporal resolution (see yellow dots Figure 2. 1 for locations, and in Figure 2. 2). Data can be obtained throughout the Puertos del Estado dataserver at https://www.puertos.es/es-es/oceanografia/Paginas/portus.aspx.

2.2.4 Video Imagery

Timestack images cover the period from 2012 to 2017 in PDP and from 2011 to 2018 in CLM. Those images has been provided by the SOCIB beach monitoring facility (Alvarez-Ellacuria et al., 2011). Timestack shows a cross-shore transects of pixel intensity sampled at 7.5 Hz over 10 minutes every hour (Simarro et al., 2017). This created timestack of pixel intensity, on which

wave runup and rundown are showed as a black edge moving back and forth in the swash zone (Figure 2. 4). A quality control was applied to keep only those images clear enough to extract information on the wave runup. As a result, 2015 images were kept for PDP and 1909 images for CLM.

The wave runup is composed by a steady super elevation called setup ($< \eta >$) and a fluctuating component called swash (S) (Holman and Guza, 1984). In order to extract the setup from images, it would be necessary to know where exactly the coastline in calm conditions is located for each of the timestack. Unfortunately, this is challenging because the coastline has been modified either by natural causes or by human intervention (e.g., beach nourishment) during the time covered by the images (i.e., 5 years at PDP and almost 8 years at CLM). Consequently, direct observations of wave setup were unavailable to validate the model results. Nevertheless, in order to have an idea about how crucial that could be for the goal of this work, we have compared the relative importance of setup and swash contributions to the total wave runup (see Figure S2. 1). The setup component has been computed using the S2006 formulation and XBEACH simulations fed with nearshore waves from AWACs, while the swash has been infered from the images. The results show that setup is ~25-30% of the wave runup, so eventual unaccuracies in their estimates may be considered of second order of importance with regard to the goal of this study.

Therefore, we have decided to remove the mean value of the runup computed from each timestack, and thus obtaining only observations of the swash. In particular, the swash component is estimated as the 98% quantile of the water/land transition time series (Figure 2. 4 yellow line, bottom panel) respect to the mean value (Figure 2. 4 white dashed line, bottom panel). Thereby the swash 2% is retrieved from each timestack. Once the swash observations are obtained, it is necessary to transfer the horizontal swash to the vertical component using the beach slope (, β_f). Following previous works (Stockdon et al., 2006; Vousdoukas et al., 2012) , β_f is defined as the average slope over a region ±2*STD around the swash zone, where STD is the standard deviation of the horizontal swash variability. Thus for PDP β_f is 0.027 and for CLM is 0.044. The standard deviation of the resulting vertical swash in PDP is 0.06 m and 0.12 m in CLM.

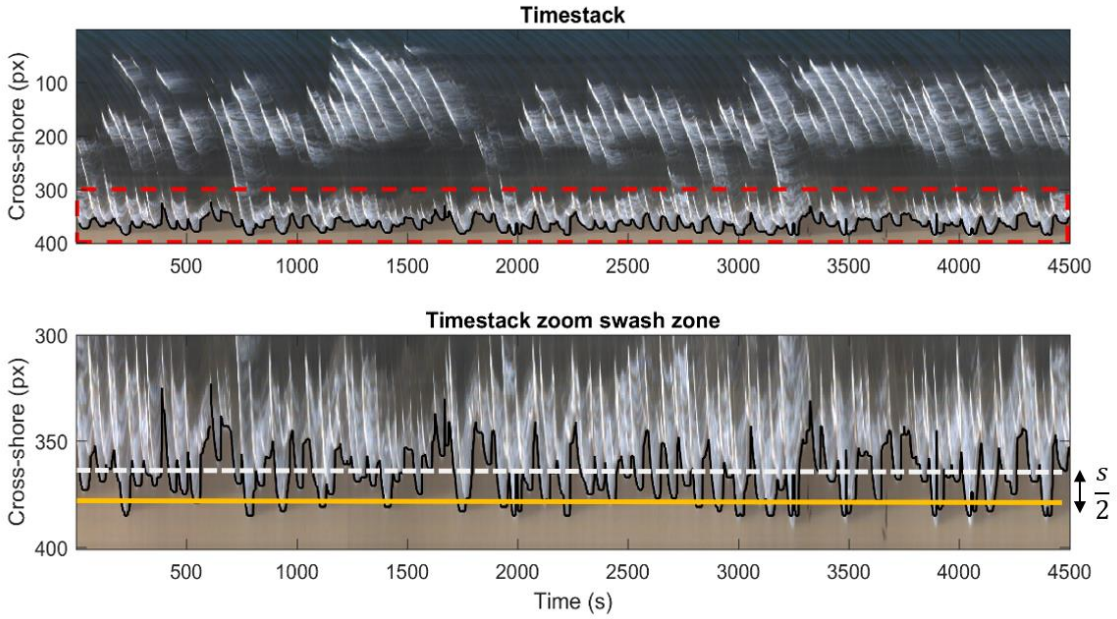

Figure 2. 4 Runup timestack generated with the time sequence of cross-shore pixels for day 7th of January 2016 (top panel). Zoom of the swash zone (bottom panel). Runup and rundown is showed as a black edge moving back and forth in the swash zone. The 98% quantile of the swash (yellow line) and swash mean value (white dashed line) are also plotted.

2.2.5 Empirical runup estimates

In this work we use the S2006 formulation as it is one of the most widespread empirical approaches to estimate wave runup. The expression for R_2 (i.e.: the runup elevation which is exceeded by 2%) is composed by two terms, the setup ($< \eta >$) and the swash (S):

$$R_2 = 1.1(< \eta > + \frac{S}{2}) \quad (1)$$

$$< \eta > = 0.35\beta_f (H_O L_O)^{\frac{1}{2}} \quad (2)$$

$$S = S_{inc} + S_{IG} \quad (3)$$

where β_f represent the beach slope at the swash zone and $H_O L_O$ are the significant wave height and the wavelength, respectively. The swash component (S) is represented by the sum of two different processes, the incident swash ($S_{inc} = 0.75\beta_f (H_O L_O)^{\frac{1}{2}}$) and the infragravity swash ($S_{IG} = 0.06(H_O L_O)^{\frac{1}{2}}$). On dynamically different beaches, energy in the incident and infragravity frequency band will contribute varying amounts to total swash (Stockdon et al., 2006).

2.2.6 Numerical approach

2.2.6.1 Nearshore wave climate

The SWAN numerical model (Booij and Holthuijsen, 1987) is used to propagate the offshore maritime climate up to the coast. SWAN is a third-generation wave model that solves the spectral action balance equation for the propagation of wave spectra

(http://swanmodel.sourceforge.net/). This model allows an accurate and computationally feasible simulation of waves in relatively large areas (Camus et al., 2013; Enríquez et al., 2017; Orejarena-Rondón et al., 2019). SWAN simulations are performed in a stationary mode over a regular 200 x 200 m grid (see gray dashed rectangles in Figure 2. 1). The boundary conditions to drive the model have been extracted from the closest SIMAR point located in deep waters (Figure 2. 1, yellow dots). The propagated sea states have been the same as those occurring in the period covered by the observations (Fig. SI2 black dots). The model outputs in terms of Hs, Tp and mean direction have been extracted from the simulations at the same depths where AWACs are installed (~20 m depth). A comparison between the modelled nearshore waves and the waves recorded by the AWACs in PDP and CLM is shown in Figure S2. 3. A high agreement is found between observed and modelled nearshore waves with a root mean square error (RMSE) of 0.24 m and 0.22 m and a correlation of 0.86 and 0.86 for PDP and CLM, respectively.

2.2.6.2 Wave Runup

The wave propagation until the swash zone and the wave runup on the beach are simulated using the XBEACH model (Roelvink et al., 2015). XBEACH is an open-source numerical model which originally was developed to simulate hydrodynamic and morphodynamic processes and impacts on sandy beaches. The model solves the phase-averaged coupled equations for cross-shore and longshore hydrodynamics and morphodynamics. XBEACH has been implemented and validated in many situations (e.g: Harley et al., 2011; Roelvink et al., 2018) becoming a standard faithfully tool for runup computations provided the model parameters were previously calibrated. The model is forced by observed or simulated nearshore waves (Figure 2. 1, orange dots) and has been implemented in 1D and 2D modes. The 1D runs were carried out without directonal spreading and assuming the waves to be perpendicular to the coastline orientation, with a cross-shore spatial resolution (dx) of 1 m and 20 minutes of Jonswap espectra mode. The 2D runs were implemented with a spatial resolution of 2 m in the cross-shore direction and 10m in the alongshore direction with the same set up of the 1D simulations.

The most important transformation in the wave characteristics occurs in the shoaling and breaking zones where the energy is considerably reduced. Moreover, in this critical zone, the bottom friction plays a paramount role in the wave dissipation, specially over vegetation grounds (Duarte et al., 2013; Beck et al., 2018; Menéndez et al., 2020). As we pointed out in section 2.1, the seagrass meadows are commonly present at shallow depths along the Mediterranean coasts and therefore in our study region (Cebrián et al., 1996; Ruiz et al., 2015; Telesca et al., 2015). In particular, the presence of seagrass is almost constant from depths between 5 and 40 m both in PDP and CLM (Figure 2. 3). Consequently, the vegetation module in XBEACH has been activated in the simulations. This module includes wave damping and wave breaking over vegetation fields at variable depths. Based on nonlinear formulation of the drag force, either irregular or monochromatic waves can be modelled considering geometric and physical characteristics of the vegetation field (Mendez and Losada, 2004; van Rooijen et al., 2015). In particular, the vegetation stem diameter (Bv), the mean shoot length (Ah), the vegetation density (N) and the drag coefficient (C_D) are parameters affecting the wave evolution and are included in the vegetation module. The first three parameters were set to the observed values in the region (Bv= 0.02 m, Ah = 0.35 m and N= 615 shoots/m^2 , de los Santos et al., 2019; Infantes et al., 2012).

In order to calibrate the drag coefficient, wave observations from another field experiment (Infantes et al., 2012) have been used. In that experiment, the wave height was measured along

a cross-shore transect in CLM beach during the period from 7 to 23 July 2009 (see Figure S2. 4). In that beach, seagrass was present up to a depth of 6 m and the nearshore wave height observed during the experiment ranged from 0.3 to 1.2 m when a moderate storm hit the area. The wave propagation during the same period was simulated using XBEACH testing different values for the drag coefficient. The optimal value found was to use C_D = 0.05, leading to a good agreement between the modelled and observed cross-shore wave transformation (see Fig SI4).

Simulating with XBEACH all the sea states corresponding to the available timestack observations (3924 cases in total for PDP and CLM) would require a highly computational effort. To overcome this, a clustering technique has been used to select a statistically representative set of sea states following two steps. First, sea states with directions out of ±30º with respect to the cross-shore direction and periods shorter than 4s have been discarded. Then, among the remaining ones, 100 sea states were selected using the k-means algorithm (Fig. SI2 green dots). Those 100 states have been simulated to obtain the corresponding wave runup. Finally, the complete time series of wave runup has been reconstructed through the analogues identification method (see Camus et al., (2011) for the details of the methodology).

2.2.7 Experimental protocol

In this study we aim at assessing the relative importance of different sources of error in the swash and setup computation. To do so, a series of complementary simulations have been performed with different configurations of the models (Table 2. 1). First, the calibrated XBEACH model is run in its 2D version and forced with observed bathymetry, seagrass coverage and nearshore waves from the AWAC. This simulation NUM2D-OBS will be considered as the benchmark run. Then, several simplifications of the system are considered. First, XBEACH is run with the same forcing but in its 1D version (NUM1D-OBS run). Next, the empirical formulation is utilized, based on the observed bathymetric slope and forced with nearshore waves, (EMP-OBS run). Then, instead of using observed nearshore waves, the empirical formulation is forced with simulated nearshore waves (EMP-ON run). Finally, the simplest approach is to use the empirical formulation using offshore waves from SIMAR (EMP-OFF run). This is the easiest most common approach since information on open sea waves is usually available from wave hindcasts.

Complementary, a set of sensitivity experiments have been also performed to estimate the impact of uncertainties in the bathymetric characteristics. In particular, the EMP-OBS experiment is repeated but varying the slope of the bathymetry (β_f) from 0.025 to 0.075 to have a broader view of how the selected slope may affect the results (BATHY runs). In addition, the NUM1D-OBS experiment has been repeated using several bottom drag coefficients representative of the potential uncertainties associated to the representation of vegetation (FRIC runs). In particular the wave-seagrass bottom friction (Cd) has been set to 0.05 (like in NUM1D-OBS), 0.1, 0.2 and 0 (absence of vegetation). Finally, the sensitivity of the wave setup characterization has been estimated by comparing the setup component from runs EMP-OFF, EMP-ON, EMP-OBS and NUM1D-OBS.

All the simulations have been run for the two beaches and for the whole period when observations were available in each beach. Then, the quality of the model outputs have been assessed in terms of the RMS error, the bias and the correlation with respect to the observations.

RUN	MODEL	WAVE FORCING	BATHYMETRY
1. EMP-OFF	Empirical – S2006	Offshore Modelled (SIMAR)	Observed Slope
2. EMP-ON	Empirical – S2006	Onshore Modelled (SWAN)	Observed Slope
3. EMP-OBS	Empirical – S2006	Onshore observations (AWAC)	Observed Slope
4.NUM1D-OBS	Numerical XBEACH-1D	Onshore observations (AWAC)	Observed Profile
5.NUM2D-OBS	Numerical XBEACH-2D	Onshore observations (AWAC)	Observed 2D bathymetry
6. BATHY	Empirical – S2006	Onshore observations (AWAC)	Varying Slope
7. FRIC	Numerical XBEACH-1D	Onshore observations (AWAC)	Varying vegetation

Table 2. 1 List of simulations performed with the model, bathymetry and the wave forcing used.

2.3 Results

2.3.1 Impact of the representation of the incoming waves

The comparison of the EMP-OFF, EMP-ON and EMP-OBS simulations shows that the source of information used to feed the empirical formulation has a significant impact on the swash results (Figure 2. 5 and Table 2. 2). Using observed nearshore waves, the RMSE is 0.07 m and 0.11 m for PDP and CLM, respectively. Using modelled nearshore waves, the RMSE increases to 0.09 m in PDP and 0.13 m in CLM. When offshore waves are considered the RMSE reaches a maximum value of 0.13 m in PDP and 0.25 m in CLM. Moreover, the representation of the incoming waves also affects the bias (Table 2. 2). Using observed nearshore waves (either observed or modelled), the bias is almost negligible in both locations. However, if offshore waves are used there is an overestimation of the swash (i.e., the bias reaches 0.07 m in PDP and 0.16 m in CLM).

The RMSE and bias obtained in PDP are lower than those from CLM since PDP is located within an embedded bay, so the offshore and onshore waves are restricted to a range of directions and wave heights which implies smaller swash variability. In contrast, CLM is more exposed to

offshore waves coming from different wave directions, so the range of observed swash values increases, and in consequence the RMSE and bias.

A complementary view can be obtained by looking at the quantile-quantile plots (see Figure 2. 6). In general, the empirical formulation provides higher values than the observations for all the quantiles with a clear overestimation of the extreme swash values. This is more noticeable in PDP than in CLM.

	PDP		CLM	
	RMSE (m)	**BIAS (m)**	**RMSD (m)**	**BIAS (m)**
EMP-OFF	0.13	0.07	0.25	0.16
EMP-ON	0.09	0.00	0.13	0.03
EMP-OBS	0.07	0.01	0.11	0.00
NUM1D-OBS	0.09	-0.06	0.14	-0.07
NUM2D-OBS	0.07	-0.06	0.12	-0.04

Table 2. 2 Validation of the swash obtained from different simulations against observations in terms of RMSE (in m) and bias (in m) for PDP and CLM.

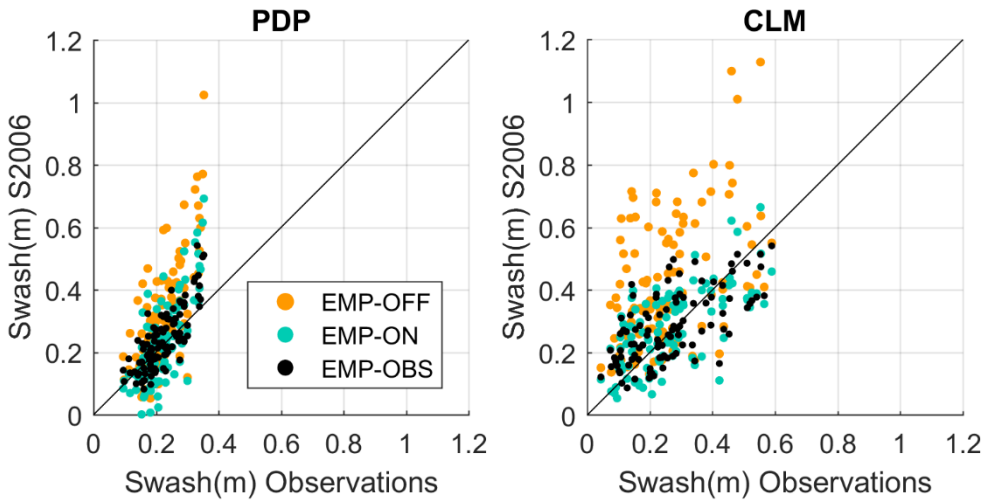

Figure 2. 5 Scatter of swash observations versus swash estimated using the S2006 formulation with different wave forcing in the Playa de Palma (left) and Cala Millor (right). The offshore waves (EMP-OFF run, yellow dots), nearshore modelled waves (EMP-ON run, green dots) and nearshore observed waves (EMP-OBS run, black dots) have been used.

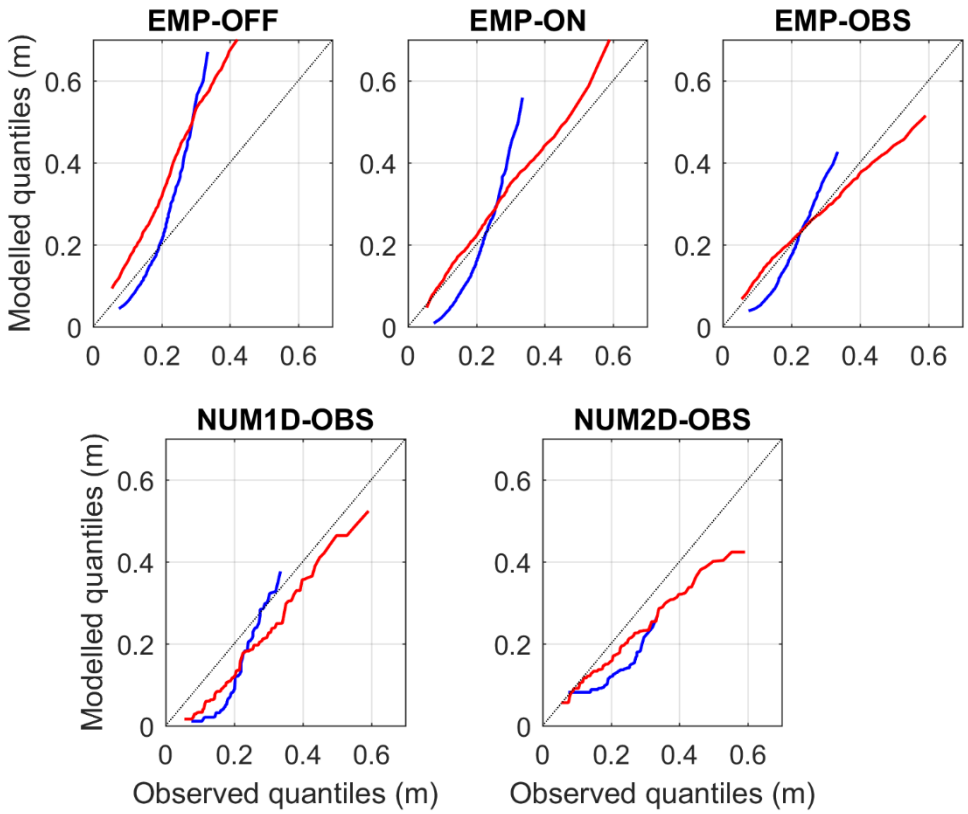

Figure 2. 6 Comparison of observed and modelled quantiles for different simulations. Each subplot depicts the results of PDP (blue) and CLM (red).

2.3.2 Empirical versus numerical approaches

The results obtained using the S2006 formulation fed by observed nearshore waves are similar to those obtained using XBEACH in the 1D or 2D configuration. In PDP, the RMSE are 0.07 m, 0.09 m and 0.07 m, respectively, while in CLM the RMSE are 0.11 m, 0.14 m and 0.12 m (see Figure 2. 7 and Table 2. 2). Moreover, the numerical solutions show a negative bias (i.e., underestimates the swash) with values of -0.06 m for both runs in PDP and -0.07 m and -0.04 m for the 1D and 2D runs in CLM, respectively. The results suggest that the numerical approach exhibits similar skills to the simpler empirical formulation. However as discussed later, there is a compensating error in the use of S2006 due to the presence of vegetation. Regarding the quantile-quantile plots (Figure 2. 6), the results are somehow different in both locations. In PDP, the 1D modelling underestimates the observed swash except for the extreme values, which are correctly represented. Conversely, the 2D modelling also underestimates them. In CLM, the underestimation of the 1D modelling is almost constant and linked to the above-mentioned bias. The 2D modelling, instead, underestimates more the extreme values (about 30%).

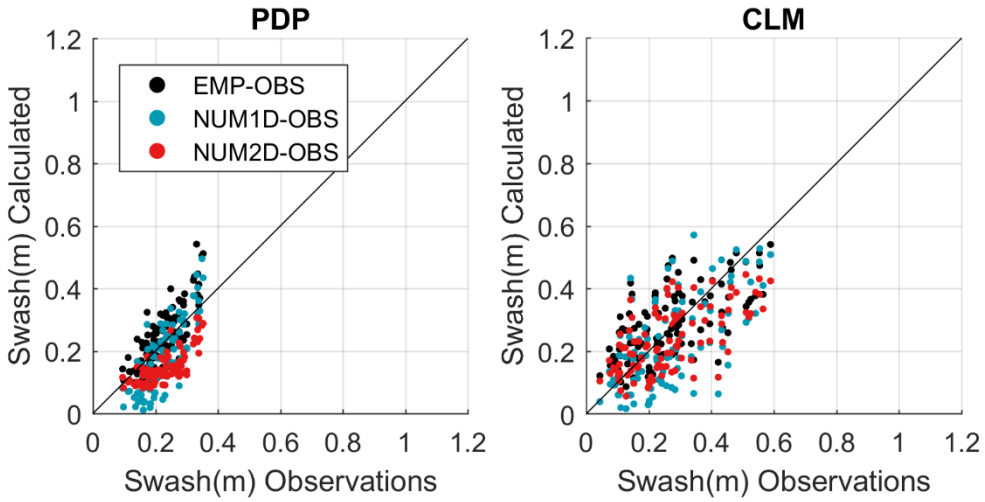

Figure 2. 7 Scatter of swash observations versus swash estimated using the S2006 formulation (black), XBEACH1D (blue) and XBEACH-2D (red) in the Playa de Palma (left) and Cala Millor (right). In all cases observed nearshore waves have been used to force the models.

2.3.3 Sensitivity to errors in the bathymetry slope

The beach slope has a significant impact on the wave runup estimation (Lange et al., 2022). Aiming at assessing what is the sensitivity of the swash calculation to the bathymetry , we have estimated the range of swash RMSE we obtain using S2006 forced by observed nearshore waves and perturbing the bottom slope from 0.025 to 0.075 (Figure 2. 8), covering all range of slopes for sandy beaches in the region (Agulles et al., 2021). The results for PDP, where the observed bottom slope is 0.027, show how RMSE would range from 0.06 m to almost double, 0.11 m. In CLM, where the observed bottom slope is 0.044, the RMSE would increase when using larger slopes, going from 0.11 m to 0.13 m. Compared to the simulation run with the observed slope (EMP-OBS), we see that the RMSE only increases a maximum of 0.02 m. In other words, using an incorrect slope in CLM would result in an increase of less than 20% of the RMSE.

Inaccuracies in the bottom slope would also have an impact on the extreme values (Figure 2. 9). Namely, using larger slopes lead to larger extreme values in wave runup estimates (equations 1-3). In PDP, this would imply that the extreme values would be even more overestimated, between 20 % and 40%. In CLM the extreme values are underestimated between -25% using a slope of 0.025 to almost 0% using a slope of 0.075 (Figure 2. 9).

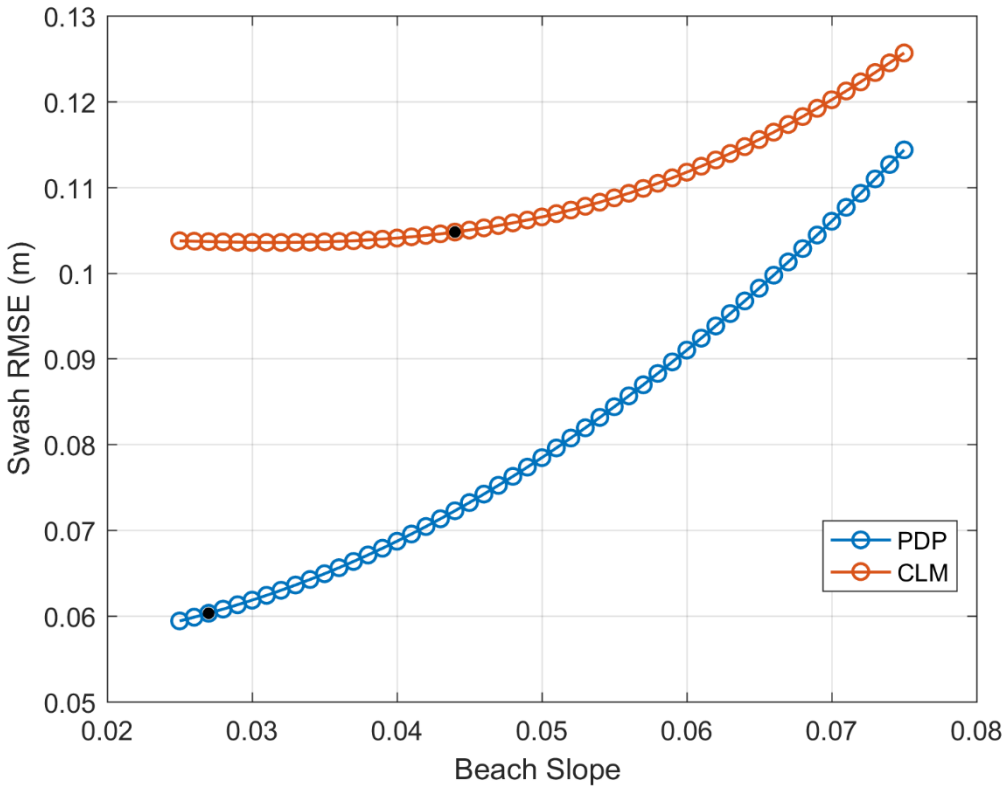

Figure 2. 8 Swash RMSE (in m) using S2006 formulation with a range of values for the beach slope for PDP (blue) and CLM (red). The black cercles indicate the RMSE corresponding to the observed slopes.

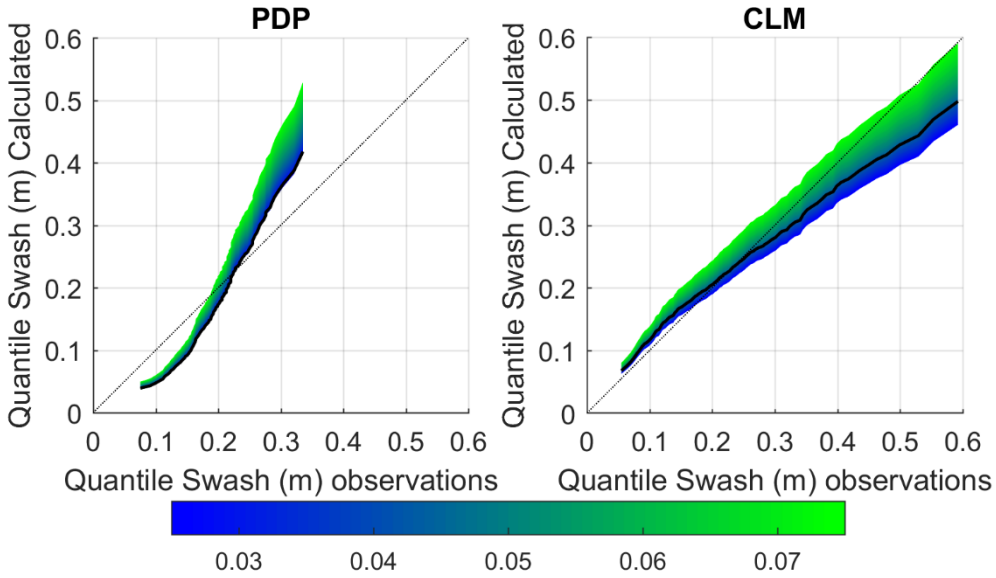

Figure 2. 9 Comparison of observed and modelled quantiles using S2006 formulation with a range of values for the beach slope for PDP (left) and CLM (right). The black line indicates the results obtained with the observed beach slope.

2.3.4 Sensitivity to errors in the bottom friction

Several sensitivity runs have been performed forcing the 1D version of Xbeach with observed nearshore waves and changing the bottom drag coefficient due to wave-seagrass interactions

(see Table 2. 3 and Fig. SI5). The inclusion of the vegetation module improves the results in both beaches. Without vegetation (FRIC 1), the RMSE is 0.19 m (0.15 m) for PDP (CLM). With the optimal drag coefficient (NUM1D-OBS), the RMSE is reduced to 0.08 m (0.13 m). For the other intermediate cases the results lie in the middle. Using vegetation with Cd= 0.20 the RMSE was 0.13 m (0.17 m) and with Cd=0.10, the RMSE was 0.10 m (0.13 m). Therefore, not considering the submerged vegetation in PDP would more than double the RMSE, while in CLM would represent only a 13% of error increase. Conversely, if the presence of vegetation is considered but the characteristics of the vegetation are unknown, and thus the bottom friction is not properly tuned, the resulting RMSE could increase up to 0.05 m in PDP and 0.04 m in CLM.

Tests	Ah (m)	Bv (m)	N (shoots/m2)	Cd	RMSE (m)	
					PDP	CLM
FRIC 1	-	-	-	-	0.19	0.15
FRIC 2	0.35	0.02	615	0.20	0.13	0.17
FRIC 3	0.35	0.02	615	0.10	0.10	0.13
NUM1D-OBS	0.35	0.02	615	0.05	0.08	0.13

Table 2. 3 Parameters used in the sensitivity tests for the drag coefficient calibration and results of the validation in terms of RMSE (in m). The parameters considered are the mean shoot length (Ah), stem width (Bv), vegetation density (N) and drag coefficient (Cd). The symbol (-) indicates that no vegetation module has been included in the XBEACH simulations.

2.3.5 Sensitivity analysis of the wave setup

As mentioned above, we assume that the wave setup extracted from video imagery is unreliable due to some unquantified processes that could happen on a beach modifying its width (i.e., abrupt erosion under an extreme event, gradually losing or gaining sand or human nourishment). Consequently, here we can only assess the sensitivity of the setup estimation to different configurations. Particularly, we compare the setup provided by the simulations based on S2006 (EMP-OFF, EMP-ON and EMP-OBS) with the results from the numerical simulation (NUM2D-OBS, see Figure 2. 10 and Table 2. 4). The RMS difference between the numerical and empirical approaches for PDP are 0.03 m, 0.02 m and 0.02 m, respectively. This represents around 20 % of the RMSE of the swash estimates (Table 2. 2). In CLM, the RMS difference is 0.10 m, 0.05 m and 0.04 m (~30 % of the RMSE of the swash estimates). As expected, the primary source of discrepancies in the setup estimation is the data source for the waves, as happened for the swash (see section 3.1). Namely, using offshore waves induces a large positive bias. Since the setup component has less influence than the swash component on the total runup, the absolute contribution to runup uncertainties remains relatively low.

	PDP		CLM	
	RMSD (m)	BIAS (m)	RMSD (m)	BIAS (m)
EMP-OFF	0.03	0.02	0.10	0.08
EMP-ON	0.02	0.00	0.05	0.02
EMP-OBS	0.02	0.01	0.04	0.01

Table 2. 4 Comparison of the setup obtained from the empirical approaches with the one provided by NUM1D-OBS in terms of RMS difference (in m) and bias (in m).

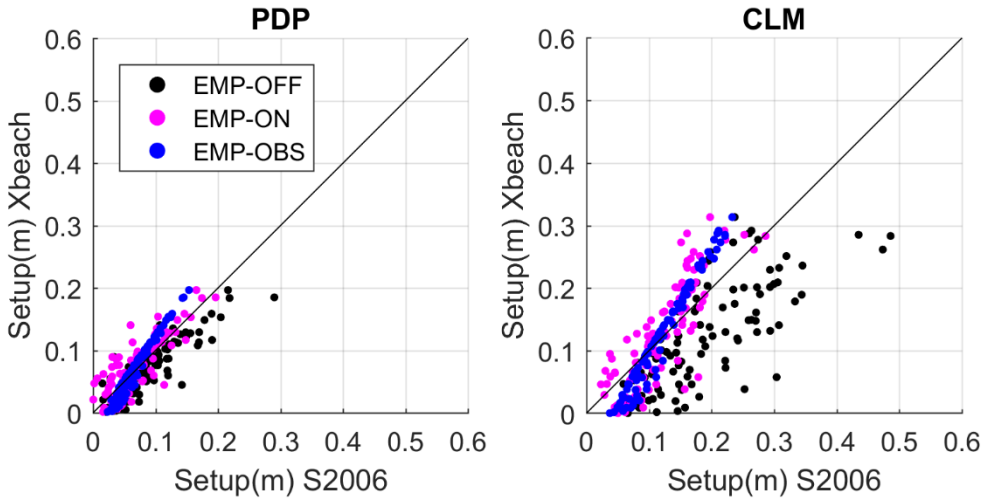

Figure 2. 10 Comparison of wave setup between XBEACH (NUM1D-OBS run) and the empirical approach fed by offshore waves (black dots), modelled nearshore waves (magenta dots) and observed nearshore waves (blue dots) in PDP (left) and CLM (right).

2.4 Discussion

The quantification of beach flooding requires the implementation of a modelling system able to propagate the information from open sea waves up to the beach. This can be done using cost-effective empirical approaches or using more sophisticated strategies based on numerical modelling that allows us to cope with local specificities. If the runup estimates are needed for a large number of beaches (e.g., in regional assessments), then the second approach is unfeasible. And that is not only because of the computational cost, but also due to the lack of detailed information on nearshore bathymetries and bottom type (e.g., vegetation, sand, rock, etc), which determines the wave damping.

Under some circumstances, using an empirical approach can lead to results comparable to what is obtained with a calibrated numerical model. However, it is worth noting that there may be error compensation. For instance, in our case, the results have shown that the S2006 empirical approach forced with nearshore waves provides similar results than the most sophisticated numerical configuration. At the same time, this approach does not consider the role of vegetation in wave damping. Therefore, it can be expected that in a location without submerged vegetation close to the shore, the same approach would lead to an underestimation of the observed wave runup. These results are consistent with (Stockdon et al., 2014) in which some modifications to the S2006 formulation were done to improve the wave runup estimates under extreme events.

The quantification of the error sources conducted in this study can help to establish the relative importance of different sources of uncertainty in projections of beach flooding. Those projections will be inherently uncertain for several reasons. Leaving aside that the future evolution of greenhouse gases (GHG) is uncertain and assuming a certain GHG scenario, two other main sources of uncertainty can be identified. These are the natural variability in the forcings and the inaccuracies of the modelling system (Hawkins and Sutton, 2009). In the case

of beach flooding, the later can be roughly approximated from the error estimates we have carried out in this study.

For illustrative purposes, we estimate the uncertainties associated to wave runup computation in a realistic study of beach flooding associated to climate change. For doing that, the baseline is the flood distance projections in the Balearic Islands developed by (Agulles et al., 2021), where projections of mean sea level, storm surges and wave runup evolution are computed along the coast of the archipelago to obtain the flood distance on sandy beaches under different wave conditions and climate scenarios. Based on the results of that work, under the greenhouse gas (GHG) emission scenario RCP8.5, the flood distance under extreme conditions in 2100 in PDP and CLM is projected to be 24.5 m and 23.6 m, respectively (see Table 1 in Supplementary Material of Agulles et al., 2021). These values can be compared to the uncertainty associated with the wave runup modelling.

The total uncertainties associated to the modelled wave runup could be computed from the uncertainties associated to the swash and the setup. Assuming those are independent and provided that runup is the result of the addition of swash and setup, the wave runup uncertainty (e_{runup}) can be estimated as the quadratic sum of the uncertainties in each component (Kirchner, 2001; Ranftl et al., 2021), which results in:

$$e_{runup} = \sqrt{e_{swash}^2 + e_{setup}^2} \quad (4)$$

The uncertainties linked to the modelling of the swash can be estimated from the errors quantified above. Regarding the uncertainties in the setup, we can use the RMS difference of the sensitivity study shown in section 3.5. Both uncertainties would depend on the modelling approach. In the case where the 2D numerical approach is implemented with observed 2D bathymetry and vegetation and forced with observed nearshore waves (NUM2D-OBS), the swash results would have an uncertainty similar to the baseline swash error (0.07 m for PDP), and the setup results would have an uncertainty similar to the baseline setup error (0.02 m, for PDP; here we use the minimum RMSD of Table 2. 4). Thus, from (4), the uncertainty in the vertical runup in PDP would be 0.07 m. Considering that the PDP beach slope is 0.027, this value corresponds to an uncertainty of 2.70 m for the horizontal displacement. The same configuration for CLM would have an uncertainty in the wave swash and setup of 0.12 m and 0.04 m, respectively. This leads to uncertainty in the wave runup of 0.13 m and 2.95 m in the flood distance assuming a beach slope of 0.044 (Table 2. 5). Thus, the uncertainties associated to the wave runup modelling correspond to a 11% and 12% of the total flood distance estimated by Agulles et al (2021) (green patch in Figure 2. 11) for PDP and CLM, respectively.

A second example would be the case of most regional studies, where wave run up is estimated from the empirical formulation of S2006 with offshore waves and little knowledge on bathymetry or vegetation. In this case, we should add the uncertainty in the swash and setup due to the use of offshore waves with the empirical formulation, the unknown bathymetry and the unknown bottom friction. Once again, we can assume that the distinct sources of uncertainty are independent, and we can combine them as a quadratic sum. For PDP, we assume that the uncertainty linked to the first can be approximated by the estimated error of EMP-OFF run in Table 2. 2 (0.13 m in PDP and 0.25 m in CLM). The uncertainty due to the unknown bathymetry can be approximated from the results of the sensitivity experiments (section 3.3).

There, we have seen that using a wrong bathymetric slope would lead to an increase of 0.02 m in both beaches. For the uncertainty linked to the vegetation, we can use an average value from the results of sensitivity experiments in section 3.4 and assume an uncertainty of 0.08 m in PDP and 0.02 in CLM. Finally, we use again the results of the comparison of wave setup results from section 3.5 for the uncertainty linked to the wave setup (0.03 m for PDP and 0.10 m for CLM). Merging all sources of uncertainty leads to total uncertainty in the vertical displacement of 0.16 m for PDP and 0.27 m for CLM. The corresponding uncertainty in the horizontal displacement would be 5.80 m and 6.15 m, respectively (see Table 2. 5). Thus, the uncertainties associated to the modelling of wave runup using the simplest configuration (EMP-OFF) correspond to a 23% and 26% of the total flood distance estimated by Agulles et al (2021) (green patch in Figure 2. 11) for PDP and CLM, respectively.

	Configuration 1 (NUM2D-OBS)		Configuration 2 (EMP-OFF)	
	PDP(β=0.027)	CLM(β=0.044)	PDP(β=0.027)	CLM(β=0.044)
Vertical uncertainties				
Swash (m)	0.07	0.12	0.15	0.25
Setup (m)	0.02	0.04	0.03	0.10
Runup (m)	0.07	0.13	0.16	0.27
Horizontal uncertainties				
Uncertainty in the horizontal coastline displacement (in m)	2.70	4.95	5.80	6.12

Table 2. 5 Total uncertainties in the vertical swash, setup, wave runup and the horizontal coastline displacement. In Configuration 1, a 2D numerical system with good knowledge on bathymetry and vegetation and forced by observed waves has been considered. In Configuration 2 an empirical formulation with poor knowledge on the bathymetry or vegetation and forced by offshore modelled waves has been considered.

It is also worthwhile to compare the uncertainties associated to the modelling of wave runup with the other sources of uncertainty for beach flooding projections. In particular, in the Mediterranean, most of the uncertainties linked to beach flooding projections are associated to the representation of changes in the mean sea level, as storm surge and open sea waves are well modelled and projected to suffer minor changes (Agulles et al., 2021). Previous studies have quantified the uncertainties in mean sea level projections associated to the scenario or the modelling system. They suggest mean sea level will rise between 0.20 and 1.10 m at the end of the century (Cherif et al., 2020; Zhongming et al., 2021). Thus, the uncertainty in mean sea level projections would be ~0.45 m. Our results suggest that uncertainties associated to the modelling of wave runup would be between 0.07 m and 0.27 m depending on the beach studied and the modelling choices, which represents between a 16 % and 60 % of the uncertainties linked to the mean sea level projections (see Figure 2. 12). This means that uncertainties associated to the wave runup modelling are important and thus should not be neglected when estimating total uncertainties of the beach flooding projections.

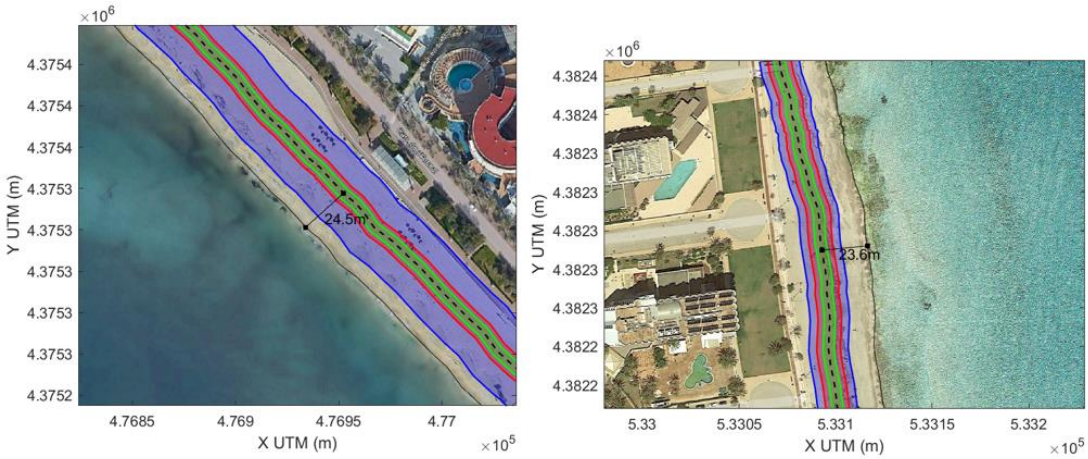

Figure 2. 11 Example of coastal retreat projected for PDP (left panel) and CLM (right panel). Current line coast (black). The projected retreat at the end of the century under scenario RCP4.5 is plotted in blue line (see text for details). The uncertainty associated to the wave runup estimate is plotted in red for the configuration 1 and in green for the configuration 2 (see Table 2. 5).

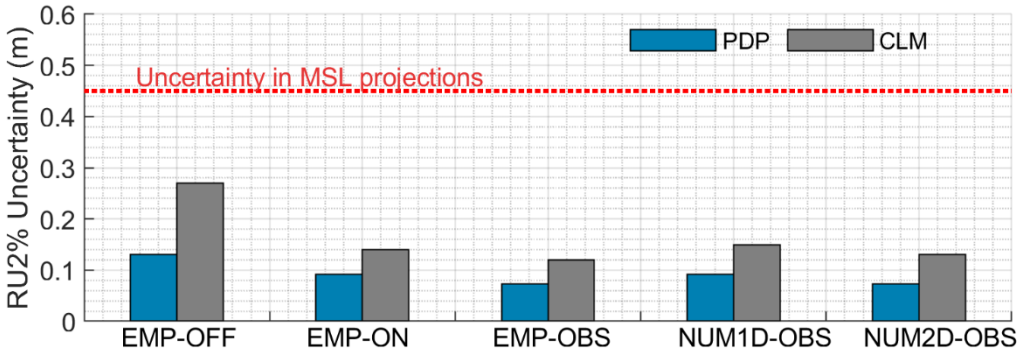

Figure 2. 12 RU2 uncertainties according to the different approximations considered, for both PDP (blue bars) and CLM (grey bars) and uncertainty in Mean Sea Level projections (in red dashed line).

2.5 Conclusions

In this paper, we have quantified the impact of several sources of error in the estimation of wave runup in sandy beaches to assess what factors have a greater influence on the quality of the results. To reach that goal, a calibrated state-of-the-art numerical modelling system has been setup for two beaches in the Mallorca islands (NW Mediterranean), which are representative of most Mediterranean sandy beaches. The system has been forced with the best available information of nearshore incoming waves and has been validated against swash observations to define the benchmark quality. Then different system configurations have been tested with different degrees of complexity.

Our results show that using the most sophisticated modelling system with the best information on boundary conditions, bottom bathymetry, and submerged vegetation leads to a swash RMSE comparable to the standard deviation of the observed swash. We have also found that the choice of lateral boundary conditions (i.e., source of information for the incoming waves) is the most influential factor and can double the RMSE and induce large biases. The second factor in

importance is if submerged vegetation is properly considered or not as it modifies the nearshore wave damping. The comparison between different modelling approaches also demonstrates that employing a simple empirical approach typically underestimates wave runup. Nevertheless, in areas with vegetated seabed, there is an error compensation, and the empirical approach can yield acceptable outcomes if forced by nearshore waves.

The quantification of the sources of error for wave runup estimates can also help to assess the relative importance of the uncertainty associated with the wave runup modelling when projecting future evolution of total water level at beaches. To illustrate this, the projections of beach flooding under scenario RCP8.5 have been used as an example. Assuming that the uncertainties of modelling wave runup can be approximated by the error estimates presented above, those would range between 0.07 m and 0.27 m depending on the beach studied and the modelling choices. Those uncertainties in wave runup represent between 16 % and 60% of the uncertainties associated to the mean sea level rise projections in the region. Therefore, uncertainties associated with wave runup modelling should be considered when assessing the uncertainties associated to beach flooding projections. These outcomes can be extrapolated to other Mediterranean beaches with similar morphodynamical characteristics.

Supporting information for chapter 2

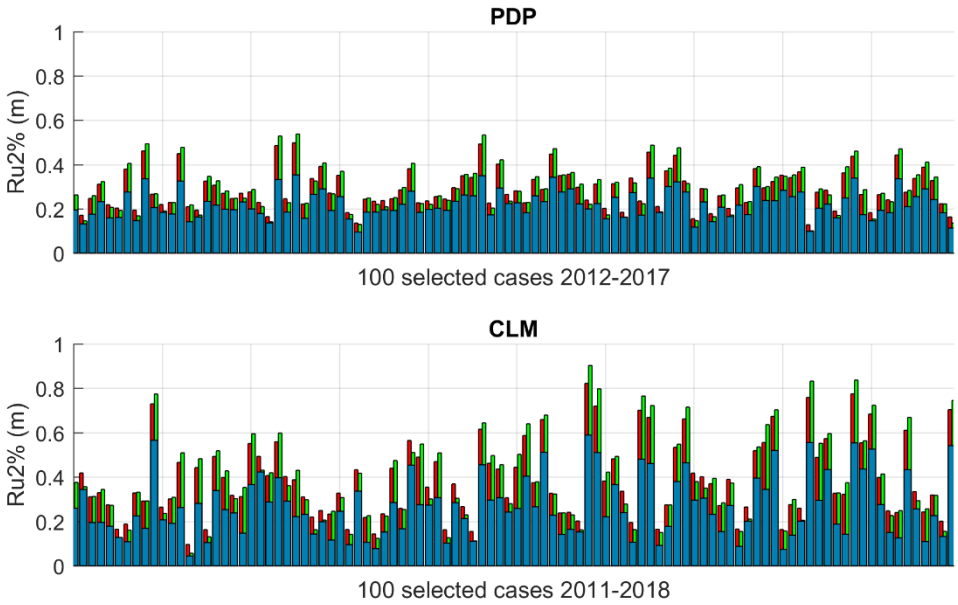

Figure S2. 1 Swash observations extracted from timestack images (blue bars). Setup from S2006 formulation (red bars) and XBEACH (green bars), both for PDP (top) and CLM (bottom panel). The sum of both components represents the wave runup (in m).

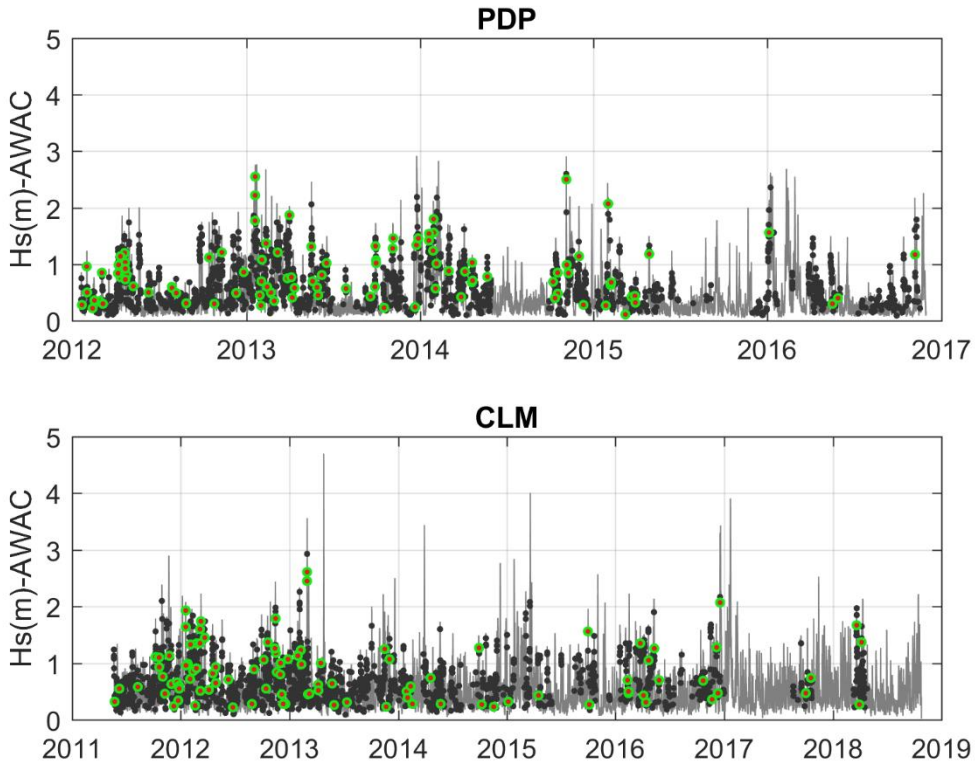

Figure S2. 2 Time series of nearshore waves recorded by the AWACS (gray) and the selected cases modelled by XBEACH (green and red dots). The black dots indicate the periods when timestack images were available.

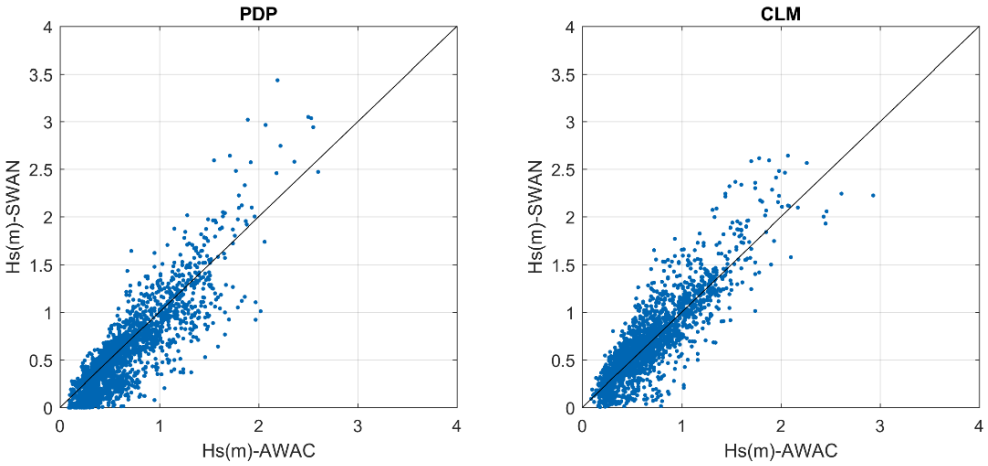

Figure S2. 3 Scatter plot of modelled Hs (m) with SWAN vs observations in PDP (left panel) and CLM (right panel).

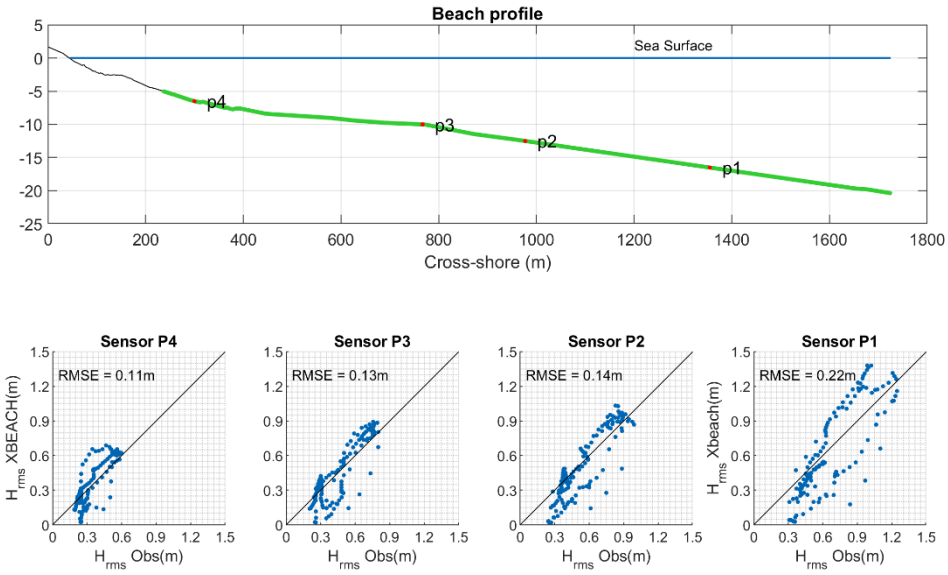

Figure S2. 4 Validation of the XBEACH model outputs in Cala Millor along a cross-shore transect of wave observations by Infantes et al., (2012). The location of the wave observations is indicated by the red dots (P1 to P4) in the upper panel. The lower panels show the comparison of observed and modelled Hrms (in m) for the four observation points. The corresponding RMSE (in m) is included in the insets for the simulation with the calibrated vegetation module (R).

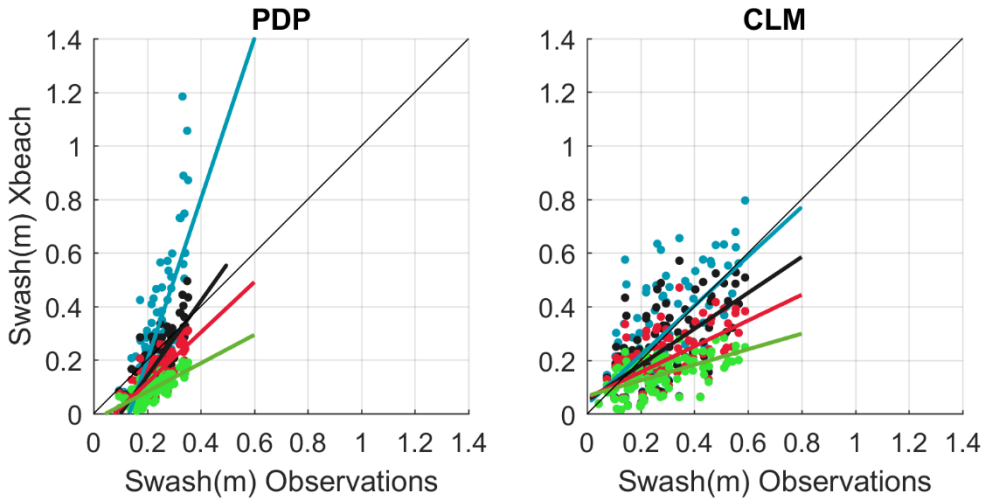

Figure S2. 5 Calibration of XBEACH vegetation module for PDP (left panel) and SNB (right panel). Observed and modelled swash are compared in the absence of seagrass (blue), considering Cd=0.20 (green), Cd=0.10 (red) and Cd=0.05 (black).

Chapter 3

3 Flooding of sandy beaches in a changing climate. The case of the Balearic Islands (NW Mediterranean).

This paper has been published as:

Agulles, M., Jordà, G., and Lionello, P. (2021). Flooding of Sandy Beaches in a Changing Climate. The Case of the Balearic Islands (NW Mediterranean). Frontiers in Marine Science 8, 1–15. doi:10.3389/fmars.2021.760725.

Chapter summary

The fate of the beaches around the world has a paramount importance as they are one the main assets for touristic activities and act as a natural barrier for coastal protection in front of marine storms. Climate change could put them at risk as sea level rise and changes in the wave characteristics may dramatically modify their shape.

In this work, a new methodology has been developed to determine the flooding of sandy beaches due to changes in sea level and waves. The methodology allows a cost-effective and yet accurate estimation of the wave runup for a wide range of beach equilibrium profiles and for different seagrass coverage. This, combined with regional projections of sea level and wave evolution, has allowed a quantification of the future total water level and coastline retreat for 869 beaches across the Balearic Islands for the next decades as a function greenhouse gases emission scenario.

The most pessimistic scenario (RCP8.5) at the end of the century yields an averaged percentage of flooded area of 66 % under mean conditions which increases up to 86 % under extreme conditions. Moreover, 72 of the 869 beaches of the region would permanently disappear while 314 would be completely flooded during storm episodes. Under a moderate scenario of emissions (RCP4.5), 37 beaches would permanently disappear while 254 would disappear only during storm episodes. In both cases, the average permanent loss of beach surface at the end of the century would be larger than 50 % rising over 80 % during storm conditions. The results obtained for the Balearic Islands can be extrapolated to the rest of the Mediterranean as the beaches in all the region have similar characteristics and will be affected by similar changes in sea level and wave climate. These projections indicate that adaptation plans for beach areas should be put in place as soon as possible.

3.1 Introduction

The 20th century has witnessed an unprecedented population expansion and a revolution in the ways of life and work, which together have enhanced and renewed the uses of coastal areas (Galofré et al., 2001). Sea level rise and its acceleration in recent decades (Dangendorf et al., 2017) along with storm events (Krestenitis et al., 2017), constitute a significant hazard in coastal regions, triggering geomorphological changes and threatening harbor facilities, coastal tourism infrastructures, houses, and even human lives, through storm-surge flooding and wave attack (Vousdoukas et al., 2012b). In this context, sandy beaches become a relevant asset, as they occupy more than one-third of the global coastline (Luijendijk et al., 2018) and play a key role to protect the coastal zones against storm events as a natural barrier. Moreover, sandy beaches are a big attractive for coastal tourism and the associate socioeconomic activities (Orams, 2003).

Changes in the beach shape can be induced by modifications of the sediment transport dynamics or by the flooding caused by changes in the total water level (due to variations in the sea level and/or waves). Regarding the former, the morphodynamical balance may be affected both in longitudinal and transversal transport by anthropogenic actions on the coast (e.g. construction of dikes, ports,…) or by changes in the wave climate, leading to a gradual accumulation of sand in some areas and coastal erosion in others (Kudale, 2010; Ballesteros et al., 2018). However, at regional scale it is usually considered that the total surface of the beaches would not significantly change. I.e., there would be a redistribution of sand, but not a significative change in the net balance. On the other hand, flooding can induce a dramatic change on the beaches either during short-term events or from a long-term perspective. Flooding will reduce the usable area of the beach as well as their capacity to act as a natural barrier. In consequence, understanding the coastal response to environmental forcing is a relevant topic as it is the first step for an appropriate long-term management of the coastal zone. In this context, the EU funded project SOCLIMPACT (https://soclimpact.net/), aims at assessing climate change effects and their socioeconomic impacts in European islands for 2030-2100. In particular, a special focus has been put on the Balearic Islands (North-western Mediterranean). The Balearic Islands base a large part of their economic income (25.8% of GDP) on tourism (https://ibestat.caib.es/ibestat/page?p=px_tablas&nodeId=1d75ac96-e3fa-4d60-b45d-33e45a1a0792&path=economia%2FTURISMO%2F13%20CSTIB). Thus, the region is particularly vulnerable to eventual changes on the beach availability. Moreover, recent research reveals that tourists in Balearic Islands support the implementation of adaptation policies aimed at counteracting the climate-induced environmental changes (Enríquez and Bujosa Bestard, 2020). Therefore, this region is a good case study to analyse potential impacts of climate change on beach availability and the derived socioeconomic impacts.

To measure shoreline evolution and to predict its future evolution, several tools based on satellite imagery are available (Vos et al., 2019a, 2019b). This type of data has a huge potential as it may be useful to roughly quantify the coastline retreat at global scale. However, its usefulness for detailed studies at local scale is reduced as far as to delimit the land-water transition with reasonable accuracy as a smaller pixel size, better time coverage and smaller observational errors would be required (Vos et al., 2019b). In the last decade, other methodologies have been implemented to quantify the coastline retreat at local scale. One of these are based on the use of numerical models and high-resolution wave and sea level databases along with topo-bathymetry and coastal flood observations, (Villatoro et al., 2014; Enríquez et al., 2017, 2019; Barnard et al., 2019). This approach is more accurate, but huge

computational effort is required to properly simulate all the nonlinear interactions that occur in the swash zone when the waves are propagated up to the beach. In consequence, up to now this approach has been limited to a few locations at a time. Another technical way for support coastal management is the use of video monitoring stations, which can provide accurate estimates of coastal evolution at high temporal resolution (e.g.: Simarro et al., 2017; Chust et al., 2022). However, its local character makes it difficult to use it for regional studies. A recent attempt to compute coastal retreat at global scale has been made possible thanks to the cross-shore profile database developed by (Athanasiou et al., 2019) using available topographic and bathymetric information. With this database it has been possible to infer the effects of the sea level rise and wave runup on sandy beaches at global scale (Vousdoukas et al., 2020). However, it is not yet clear how accurate this approach is as to faithfully quantify beach loss it is necessary to consider realistic beach slopes and nearshore marine climate (Orejarena-Rondón et al., 2019).

In this framework, the first goal of this paper is to develop a cost-efficient but accurate methodology to obtain present and future high resolution flood levels all along the coasts of the Balearic Island. We focus on the flood level since we consider it the most important driver for the changes in the beach shape. Once the methodology is implemented, we quantify the coastal flooding and the percentage of beach area loss under different scenarios in all the beaches of the archipelago. In particular, we have used information of the beach characteristics (present shape and granulometry) along the four Balearic Islands, in combination with historical runs and projections of regional wave and sea level. This has allowed generating projections of beach reduction for all the sandy beaches of the archipelago under different greenhouse gases (GHG) emission scenarios.

This work is organized as follows. In Section 3.2, the different datasets used are presented while Section 3.3 describes the methodology proposed to obtain the flood level at the coast. Results of the beach reduction obtained for two climate change scenarios are shown in section 3.4. In section 3.5 we discuss the results and the limitations of our approach while the conclusions are presented in section 6.

3.2 Data

3.2.1 Study site and beach characterization

The Balearic Islands are located in the western part of the Mediterranean Sea. Regarding the marine climate in the area, the most energetic waves (maximum wave height (Hs) of ~7 m and periods (Tp) of ~12 s) come from the north of the archipelago due to the action of intense northly winds in the Gulf of Lions (Figure 3. 1, left wave rose). The southern coasts of the islands are exposed to two different regimes, 1) waves from the southwest with maximum Hs of ~ 6 m and 2) waves from the southeast with maximum Hs of 3 m (Figure 3. 1, right wave rose). Under mean conditions, typically occurring from April to September, the coast exposure is low with mean Hs ~0.5 m and Tp ~6 s. The astronomical tide in the region is practically negligible respect to the total flood level at coast with values around 10 – 20 cm (Bonaduce et al., 2016). The storm surge reaches 25-30 cm at coast (Figure 3. 1).

Bathymetric information is obtained primarily from the GEBCO datasets (General Bathymetric Charts of Ocean, http://www.gebco.net). Data is provided globally in a 30 arc-second grid. In order to increase the spatial resolution in shallow waters, the bathymetric information is

supplemented with higher resolution data provided by the coastal authority from the shoreline to 40 meters depth (MITECO, https://www.miteco.gob.es/es/costas/temas/proteccion-costa/actuaciones-proteccion-costa/illes-balears/default.aspx).

Information about the beaches of the Balearic Islands has been provided also by MITECO. Here we have gathered detailed information of 869 beaches located around the archipelago coasts. The database contains, among other indicators, the coordinates of the beach contour and a coarse estimate of the granulometry. This granulometry classifies each beach from fine to very coarse sand. In order to work with a representative value of the grain size of each beach, a D50mm parameter has been assigned to each beach (i.e., particle size corresponding to the median of a given sample). To do so, we use the Udden-Wentworth grain-size scale (Blair & McPherson, 1999). This results in a range of D50 that goes from 0.15 mm, representative of fine grain sand, to 1 mm, very coarse grain size, (Figure S3. 1). The size of the beaches is very heterogeneous in the region, ranging from 100 m2 on the small beaches to 40.000 m2 in the largest ones.

The seagrass coverage in each beach has also been considered as it plays a key role on the energy dissipation and thus the intensity of wave runup under storm conditions (see Section 3.3.3). The information has been obtained from the seagrass atlas for the Mediterranean sea (Álvarez et al., 2015), see Figure S3. 2.

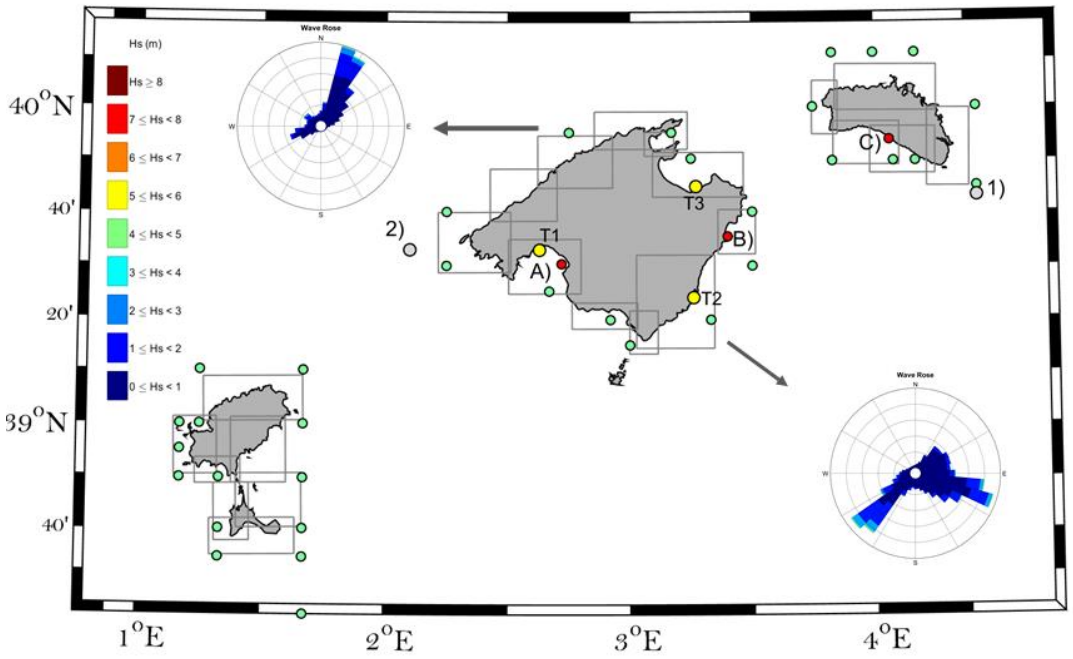

Figure 3. 1 Study area and data availability: Offshore wave buoys, grey dots, 1) Mahon Buoy and 2) Sa Dragonera buoy, coastal AWACS, red dots, A) Playa de Palma, B) Cala Millor and C) Son Bou and tide gauges, yellow dots, T1) Palma, T2) Portocolom and T3) Colonia de San Pere. The SWAN model grids are represented by the gray rectangles while the offshore waves from the climate simulations used to force SWAN are represented by a green dot. Two waves' roses represent the offshore maritime climate given in the North (top left rose) and the South (bottom right rose). Note that the Hs values are represented by a colorbar at the left of the figure.

3.2.2 Observations

3.2.2.1 Sea level

Hourly sea level data from tide gauge at three different sites have been used to validate sea level simulations: Palma, Colonia de Sant Pere and Portocolom (see Figure 3. 1, yellow dots). The Palma tide gauge belongs to the Spanish Harbor Authority, Puertos del Estado (http://www.puertos.es/es-es/oceanografia) and provides hourly sea level data from 2009 to present. The tide gauges in Colonia de Sant Pere and Portocolom belongs to the Balearic Islands Coastal Observing and Forecasting System, SOCIB (Tintoré et al., 2013) and provide hourly sea level from 2015 and 2016 to present, respectively.

3.2.2.2 Waves

For model validation purposes, hourly wave data from two offshore buoys managed by Puertos del Estado (http://www.puertos.es/es-es/oceanografia/Paginas/portus.aspx) have been used. The selected buoys (see Figure 3. 1, grey dots) are the Mahon buoy (1970-1993, 300 m depth) and Sa Dragonera buoy (2006-2020, 135 m depth). At shallow waters, nearshore wave data is obtained from three directional Acoustic Waves and Currents sensors (AWACs) managed by SOCIB, (Tintoré et al., 2013). These sensors are located in front of the Playa de Palma (hereafter PDP), Cala Millor (CLM) and Son Bou (SNB) beaches (see Figure 3. 1, red dots). The sensors are installed at ~15/20 m depth covering the period of 2012-2018 for PDP and 2011-2018 for CLM and SNB (http://thredds.socib.es/thredds/catalog.html).

3.2.3 Hindcast

3.2.3.1 Sea level

The characterization of extreme sea level in present climate has been done using an ensemble of three storm surge simulations run with the shallow water HYPSE model, Hydrostatic Padua Surface Elevation model, (Lionello et al., 2005). The model configuration is the same used by (Lionello et al., 2017), covering the whole Mediterranean with a spatial resolution of 1/5º. Six hourly sea level pressure and wind fields for regional climate simulations are used to force HYPSE. In particular, the atmospheric fields are provided by the CIRCE-HIPOCAS hindcast, with a spatial resolution of 50 km and covering the period 1958-2001 (Ratsimandresy et al., 2008), the COSMO-ERAINT (50 km resolution covering from 1979 to 2013) and the COSMO-ERAINT011 (12 km resolution covering from 1979 to 2013). Storm surge simulations have been validated comparing the model outputs with tide gauge data at three different sites (Palma, Colonia de San Pere and Portocolom, see section 3.2.2.1). The validation shows that the three hindcasts provide good results for the region (see Figure S3. 3). The RMSE of hourly sea level at Palma, Colonia de Sant Pere and Portocolom are, respectively, 3.8 cm, 1.6 cm and 1.6 cm for CIRCE-HIPOCAS, 4.3 cm, 2.1 cm and 2.4 cm for COSMO-ERAINT and 4.4 cm, 2.0 cm and 2.3 cm for CIRCE-ERAINT011.

3.2.3.2 Waves

Two historical hindcasts have been used in this work. On the one hand, offshore waves conditions were retrieved from the SIMAR database (Pilar et al., 2008) which covers a 61-year wave hindcast generated with the spectral wave model WAM (Hasselmann et al., 1988) at 1/6º resolution and forced with winds from the ECMWF (European Center for Medium-Range Weather Forecasts) for the period 1958 to 2019. On the other hand, we also use the outputs of another WAM simulation forced by the winds from COSMO-ERAINT11 for the period 1979-2013, see (Lionello et al., 2017) for a description of the model. The wave database has been validated

using the data from the offshore buoys described in section 3.2.2.2. For the buoys of Dragonera and Mahón, the RMSE of hourly significant wave height of SIMAR database is 0.14 and 0.21 m, respectively, while for the COSMO-ERAINT011 hindcast are 0.25 m and 0.20 m, respectively (see Figure S3. 4).

3.2.4 Projections

3.2.4.1 Sea level

Mean sea level rise has been modelled including all the factors that play a role. On a global scale, first, mass variations linked to the addition/removal of water from the ocean can be induced by land-based ice melting or by changes in the groundwater due to, basically, human activities. Second, thermal expansion due to ocean warming would also induce a rise of global mean sea level. Furthermore, regional changes are also expected and could induce a major contribution to total sea level rise at coastal scale. These are linked to the gravitational fingerprint of changes in the ocean mass, to changes in the circulation patterns (which in turn are related to the steric/density variations), to mass redistribution by atmospheric pressure and wind, and to land motion. All those factors cannot be modelled at the same time as they involve very different processes, so the typical approach is to use different models to cope with the different contributions. In this work we have used the projections described in (Cherif et al., 2020). Those are mainly based on the results of (Slangen et al., 2014) that include the global and regional signals of the changes in the mass component as well as the dynamic contribution in the Atlantic. Additionally, the regional description of the dynamic component are based on the results of regional ocean models (Cherif et al., 2020).

Extreme sea level has been characterized by the storm surge model described and validated above. The forcing fields come from an ensemble of atmospheric simulations run in the framework of the MedCORDEX initiative (Ruti et al., 2016). In particular, HYPSE has been driven by 6-hourly sea level pressure and wind fields produced by 6 regional climate models (CMCC, CNRM, GUF, ITUbats, ITUclm and LMD, see www.medcordex.eu for more details on those simulations). The model has run under scenarios RCP4.5 and RCP8.5 for the period 2005-2100. The 99th percentile of simulated sea level has been computed for each simulation and the ensemble average has been used in the following.

3.2.4.2 Waves

Offshore waves projections around the Balearic Island have been retrieved from an ensemble of 4 simulations performed using the same configuration of the COSMO-ERAINT wave hindcast described and validated above. The wave model has been forced by 6-hourly wind fields produced by 4 regional climate models from the MedCORDEX initiative (CNRM, CMCC, GUF and LMD) for the period 2005-2100 under scenarios RCP4.5 and RCP8.5. The 99th percentile of simulated significant wave height has been computed for each simulation and the ensemble average has been used in the following.

3.3 Methods

Variations of the total water level (FL, equation 1) at the coast are mainly the result of the combined effect of astronomical tides, changes in mass and thermosteric components, the atmospherical mechanical forcing through wind and atmospheric pressure effects, changes in the ocean circulation and wave runup. From the perspective of a study on climate variability,

astronomical tides can be neglected as they are not expected to significantly change in the Mediterranean Sea (Pickering et al., 2017). Furthermore, the other components can be grouped in changes in the mean sea level (SLR) due to global changes in the mass and thermosteric components and to regional mass redistribution, changes in the extreme sea level (i.e. storm surge, SS), and changes in the wave runup (RU), see Figure 3. 2:

$$FL = RU + SLR + SS \quad (1)$$

In this work, the different terms of (1) are computed using a combination of numerical and empirical models for present and future conditions. In particular, we use climate simulations of sea level rise, storm surge and deep-water waves, as described in Section 2. In order to get a better approximation of the wave effects on the coast we use a two-level strategy. First, we propagate deep-water waves to the nearshore. Second, we compute the wave runup using a transfer matrix that provides the wave runup for a given set of conditions: 1) nearshore wave conditions (significant wave height, Hs and peak period, Tp), 2) beach profile and 3) bottom vegetation. This approach allows a cost-effective but accurate computation of wave runup for a large ensemble of locations. The details on the methodology are presented in the following.

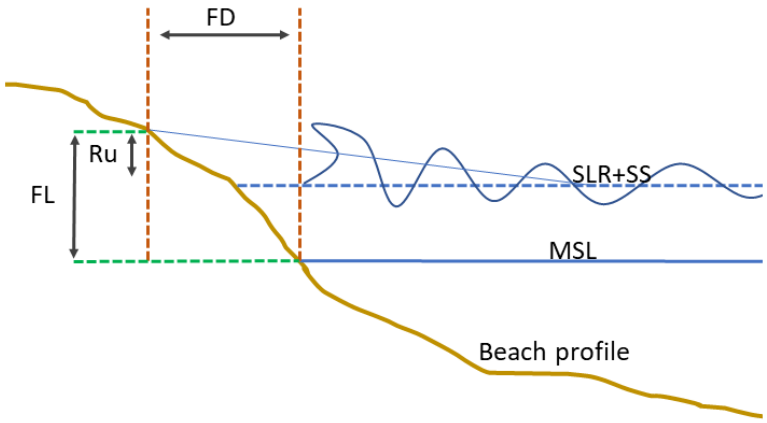

Figure 3. 2 Sketch of Flood Level (FL) at coast, as a combination of sea level rise (SLR), storm surge (SS) and wave runup (Ru). The flood distance, denoted in the figure as FD, is indirectly obtained with FL and the beach slope.

3.3.1 Nearshore sea level changes

For present climate, mean sea level is considered to be zero, while for the future evolution we use the results projections described in section 3.2.4.1. We assume that mean sea level changes in the open sea will be directly transferred to the coast, which is a reasonable assumption for long time scales. Regarding the storm surge, which is affected by short time scales (i.e., on the order of days), we use the results of the storm surge model described before (section 3.2.4.1).

3.3.2 Nearshore wave climate

The swell generated by the wind in deep waters travels in groups of waves until reaching the coast. In the transition to shallower waters, the physical parameters that define the waves are modified by the effect of refraction, diffraction, white-capping, bottom friction and breaking, among other effects. Consequently, the wave energy is decreased as it approaches the coast (Roland & Ardhuin, 2014). Therefore, the wave fields simulated in deep waters (see 3.2.3.2 and

3.2.4.2) need to be transferred up to the nearshore. In this work, we use the SWAN model to propagate the waves from deep waters to shallow waters. SWAN is a third-generation shallow water wave model, which solves the discrete spectral action balance equation (Booij and Holthuijsen, 1987).

A direct simulation of the propagation of the whole time series of offshore waves would require a huge computational effort. Therefore, a high-resolution hybrid downscaling method has been implemented to reduce the computational burden. First, we perform a cluster analysis of the offshore sea states (i.e. sea state is defined as the combination of Hs, Tp and wave direction) using the MAXDISS algorithm (Camus et al., 2011b). This cluster analysis allows to identify the most characteristic and frequent sea states at each offshore location. In the second step, the selected sea states are propagated with SWAN in a stationary mode to get the propagation coefficients for each sea state. Finally, the nearshore wave time series are reconstructed using those coefficients. A sensitivity analysis comparing the results for the present climate reconstructed at the coast with observations at nearshore buoys suggests that 100 clusters are an adequate cost-effective number of sea states to obtain a reliable nearshore wave climate (see Figure S3. 5 and Figure S3. 6). For the significant wave height, we obtain correlations ranging between 0.78 (CLM) and 0.88 (PDP) and RMSE ranging between 0.22 m (PDP) and 0.3 m (CLM and SNB).

This procedure has been applied for 23 domains around the Balearic Islands (Figure 3. 1, gray squares). As a result, we have obtained the nearshore hourly wave record for the period 1958-2019 with a spatial resolution of 200 m along the coast (see blue dots in Figure 3. 3).

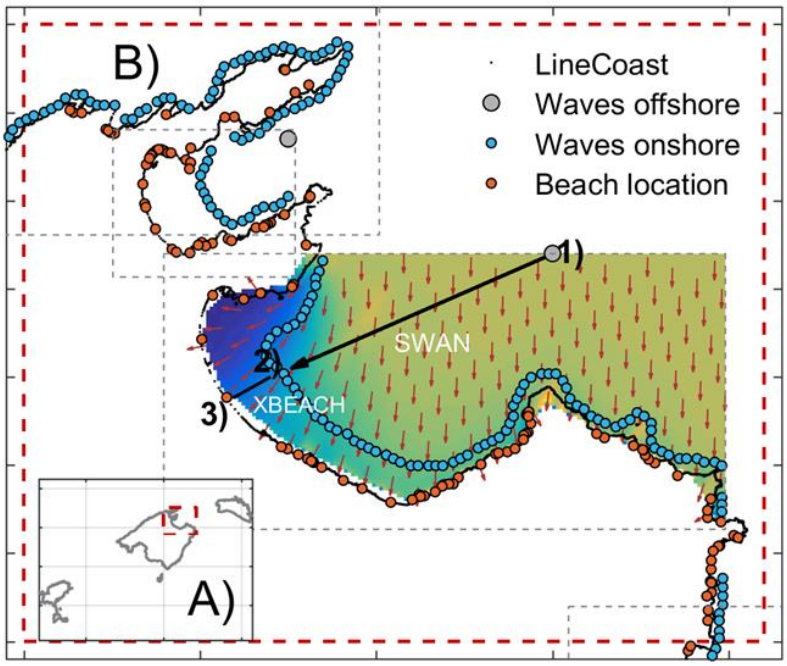

Figure 3. 3 Sketch of the strategy followed for obtaining the wave runup on the beaches from offshore wave climate model outputs. The deep-water model output at the closest grid point (1, grey dot) is propagated to shallow waters (2, blue dots) using SWAN. Then, the XBEACH model is forced with these data to produce the wave runup at beach locations (3, red dots).

3.3.3 Runup Estimation

Wave runup (Ru2%) corresponds to the characteristic value of 2% exceeding probability of individual waves reaching the swash zone during a sea state (Stockdon et al., 2006). At the shoaling and breaking zone, the waves experiment an abrupt change in their characteristics, with a large decrease of energy. In this critical zone, the bottom friction also plays a paramount role in waves dissipation, specially over vegetable fields (Duarte et al., 2013; Beck et al., 2018; Menéndez et al., 2020). In order to accurately simulate all those processes, once waves are propagated to shallow waters, the XBEACH model (Roelvink et al., 2015) is run to explicitly model the wave runup. XBEACH is an open-source numerical model which originally was developed to simulate morpho dynamic processes on sandy coasts. The model solves phase-averaged coupled 2D horizontal equations for wave propagation, flow, sediment transport and bottom changes, that allows, among others parameters, to obtain the runup at the swash zone.

Besides the nearshore sea state, XBEACH requires information on the beach profile and the type of bottom. Regarding the former, there is no accurate information for most of the beaches in the region. Therefore, we use the equilibrium profile, which is defined as the configuration to which the shape of the beach tends to under a stationary situation of hydrodynamic conditions (Rodríguez, 1995). This "ideal" concept allows an approximate but yet accurate representation of the morphology of the beach, (Galofré et al., 2001). Here we use the Bernabeu formulation to define the equilibrium profiles (Bernabeu Tello et al., 2001). The formulation considers two sections: a shoaling and a breaking zone and is based on the physical evidence that the wave propagating towards the coast varies its height due to the shoaling process, until reaching a critical value from which it becomes unstable and breaks, dissipating the excess of energy (Figure 3. 4). Both cross-shore sections are defined throughout a parabolic expression:

$$h_{bz} = A * x^{\frac{2}{3}} \qquad 2)$$

$$h_{sz} = C * x^{\frac{2}{3}} \qquad 3)$$

Where h_{bz} and h_{sz} are the depth in the breaking zone and the shoaling zone, respectively. The shape parameters A and C are defined as:

$$A = 0.15 - 0.009 * \Omega \qquad 4)$$

$$C = 0.03 + 0.03 * \Omega \qquad 5)$$

Ω is the Dean parameter and relates the characteristic grain size of the beach with the maritime climate:

$$\Omega = \frac{H}{wT} \qquad 6)$$

where H is the wave height under mean conditions, T is the associated wave period, and w is the sedimentation speed, which depends on the mean grain size (D50) as $w = 273 * D50^{1.1}$.

Following (Bernabeu Tello et al., 2001), the transition depth between the shoaling and breaking zone can be estimated as $h_r \sim 1 * H$, while the limit of the shoaling zone can be estimated as $h_a \sim 3 * H$, (Figure 3. 4A).

In order to represent the diversity of beach profiles in the Balearic Islands, we have considered 11 equilibrium profiles corresponding to different granulometries of sand beaches, with D50 grain sizes ranging from 0.15 mm to 1 mm. This range of grain sizes is based on the information of the MITECO database. The resulting profiles are presented in Figure 3. 4B, and a comparison with observed profiles in three beaches are presented in the SI (see Figure S3. 7).

In the Balearic Islands, the nearshore bottom are often covered by seagrass meadows (Cebrián et al., 1996; Ruiz et al., 2015). In order to consider the wave attenuation due to the interaction of the near-bottom flow and seagrass, we use the bottom friction parameterization proposed by Mendez and Losada, 2004. For that, we consider typical values of seagrass characteristics (mean shoot length of 0.35 m, a stem width of 0.02 m, a vegetation density of 615 shoots/m2 and a drag coefficient of 0.05) and the coverage identified in the seagrass atlas (see section 3.2.1 and Figure S3. 2).

Running XBEACH at each beach and the whole period of interest is unfeasible, so a cost-effective methodology has been developed to obtain a high-resolution wave runup along the coast. In particular, XBEACH has been used to propagate 39 sea states (i.e., pairs of wave height- wave period) that encompasses the whole range of nearshore sea states simulated by SWAN (wave height from 0.5 to 7.0 m and wave periods between 3 and 12 s). These 39 sea states have been propagated using each one of the 11 beach equilibrium profiles defined previously. Moreover, as the seagrass meadows could appears from shoreline to more than 7 m depth, according to the seagrass atlas, we define 5 scenarios for seagrass coverage in each beach profile: 1) no seagrass and 2 to 5) seagrass starting from shoreline, 2 m depth, 5 m depth and 7 m depth, respectively. In conclusion, we have performed 2145 (39 x 11 x 5) simulations of XBEACH with all the possible combinations of sea states, beach profiles and seagrass coverage.

Each sea state (pair of height-period values) has been simulated for 1 hour using the JONSWAP spectrum. Then, the wave runup has been characterized using the Ru2% parameter defined previously. As a result, we have constructed a transfer matrix that allows to quickly obtain time series of wave runup in each beach from the time series of nearshore wave height/period. This has been done for each one of the 869 beaches of the Balearic Islands (orange dots in Figure 3. 3) and a sketch of the whole procedure is presented in Figure 3. 5.

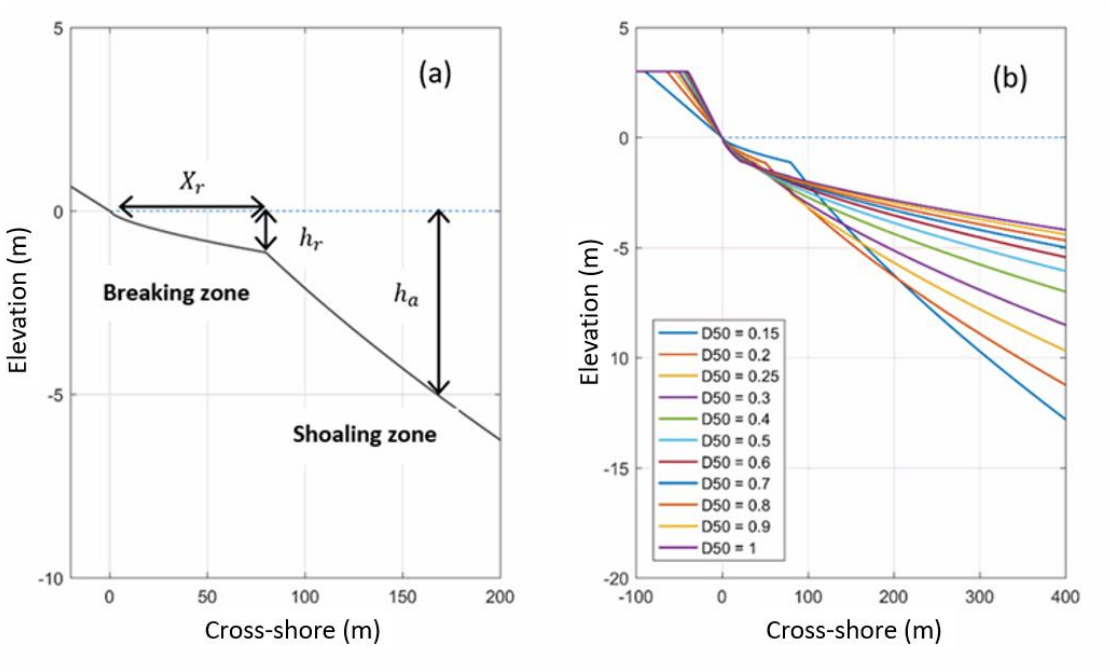

Figure 3. 4 Two-section model profile following the Bernabeu formulation, (a): X_r is the horizontal distance between the coastline and the beginning of the breaking zone, h_r is the depth that defines the beginning of the breaking zone, and h_a is the limit depth of the shoaling zone. The equilibrium profiles considered for different values of the grain size, from D50=0.15 mm to D50 = 1.0 mm, (b).

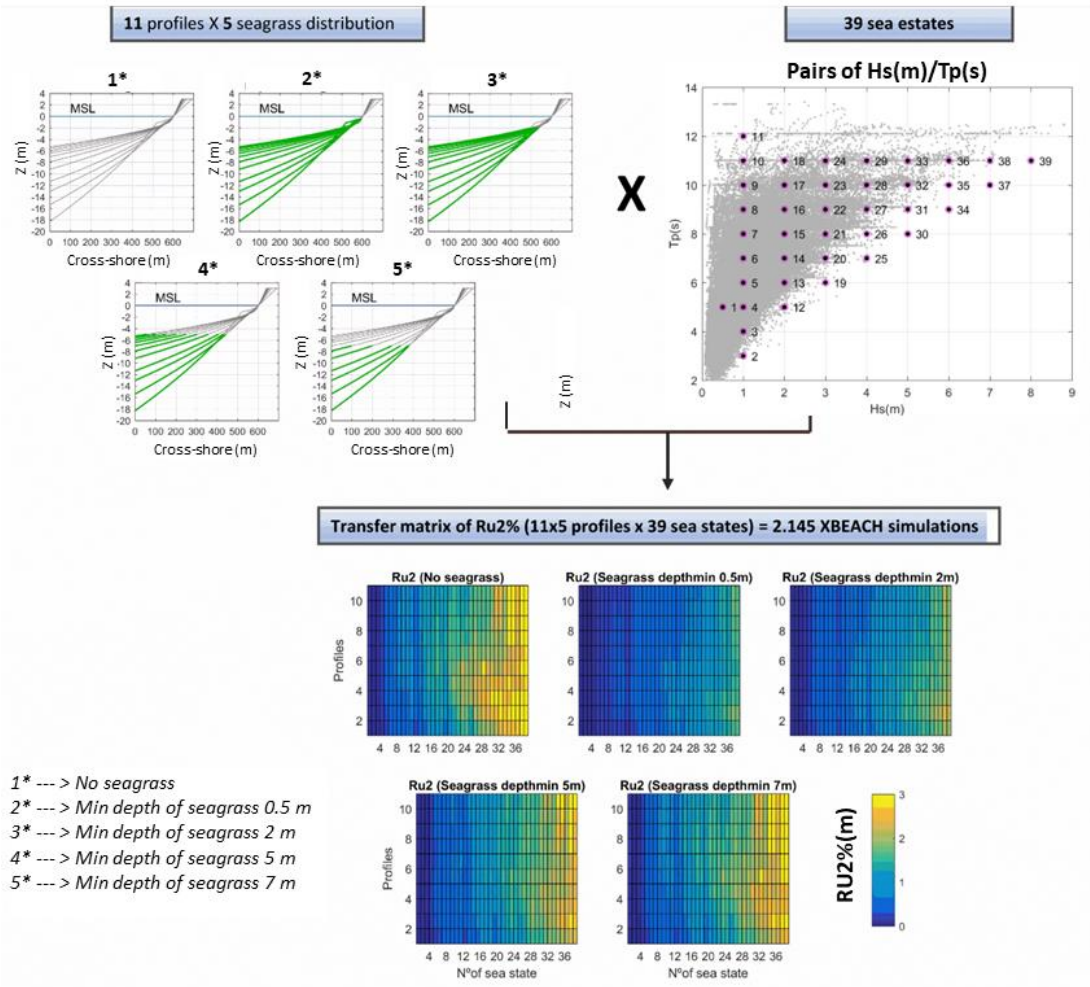

Figure 3. 5 Sketch of the methodology followed to obtain the transfer matrix of wave Runup (bottom) as a function of beach equilibrium profiles and seagrass distribution (top left) and nearshore wave conditions, pairs of Hs (m)/Tp (s) considered in XBEACH propagations scattered with black dots and the values are explicitly showed in an auxiliary table (auxiliary information Figure 5).

3.3.4 Estimation of beach losses under different GHG scenarios

The total sea water level (FL) in a particular beach is obtained as the sum of the mean sea level, storm surge and the wave runup (equation 1). Then, the flood distance (FD) is computed by using the average beach slope ($tg(\alpha)$):

$$FD = \frac{FL}{tg(\alpha)} \qquad (7)$$

The beach slope is computed from the equilibrium profiles described in the previous section (Bernabeu Tello et al., 2001). Therefore, our approach is similar to the one proposed by the Bruun's Rule (Bruun, 1962) and its adaptation by (Dean and Dalrymple, 1991) being the only difference the way the beach slope is defined. Recent studies show that the use of the Dean approach overestimates the coastline retreat considerably, compared to more realistic approximations (Enríquez et al., 2019). The beach slopes estimated here are higher than those

resulting from the Dean approach, and thus produce a more realistic coastline retreat (see Discussion section).

To calculate the new area of the dry beach once we know the FD (equation 7), we would ideally need a detailed topography of each beach. As it is usually not available, a simple but effective approach has been followed. First, we define the orientation of the coastline section corresponding to the analysed beach (Figure 3. 6, grey line). Then, the contour of the beach is moved back by a distance FD in the direction perpendicular to the mean orientation of the beach. The future contour of the beach is defined between the projected shoreline and the current inner boundary beach (Figure 3. 6, orange or green area, for mean and extreme conditions, respectively).

This procedure has been done for the present conditions and two future scenarios of greenhouse gases (GHG) emissions: the RCP4.5 (assuming a moderate reduction of GHG emissions), and the RCP8.5 (which assumes business-as-usual emissions). For each scenario, the mean of the ensemble of simulations described in section 2.4 will be presented for the near future (2030-2050) and the far future (2080-2100).

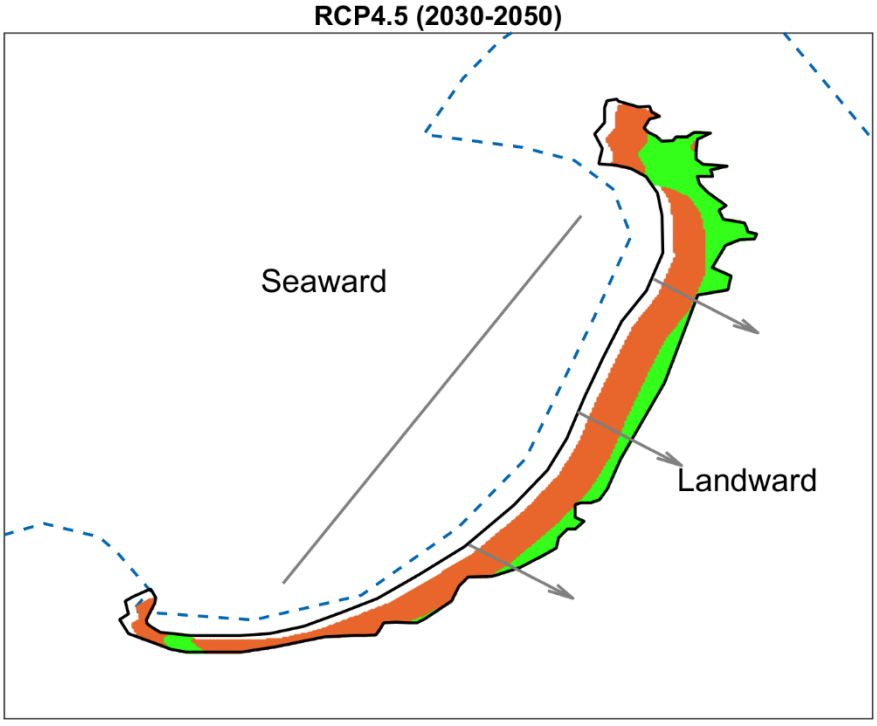

Figure 3. 6 Example of the beach area calculation under future conditions. The coastline is represented (blue dashed line) along with the mean coastline orientation (grey line). The arrows indicate the direction towards which the coastline retreats. The dry beach area is plotted for present conditions (black contour), under future mean conditions (orange area) and under future extreme conditions (green area).

3.4 Results

3.4.1 Projections of the nearshore marine climate

The present and future values of each driver contributing to the total water level on the Balearic beaches are presented in Figure 3. 7. For clarity, the mean sea level is considered to be zero for the present climate (1979-2013). Under both scenarios, it will rise during the century, reaching an averaged value of 0.50 m and 0.67 m for the period 2080-2100 under scenarios RCP4.5 and RCP8.5, respectively (Figure 3. 7b, c). The sea level rise is projected to be very homogeneous in the region with almost negligible differences among sites. Extreme sea level values related to storm surges in present climate are over 0.15 m in the whole archipelago (Figure 3. 7d). The storm surge projections show small changes at the end of the century, with zero changes under scenario RCP4.5 and a slight decrease of 0.02 m under scenario RCP8.5 (Figure 3. 7e, f). In this case, the changes are again projected to be very homogeneous in the region.

The present wave conditions show mean Hs ranging from 0.2 m in the southeast of Mallorca and Ibiza to 0.60 m in the north of Menorca (Figure 3. 7g). In general, the areas exposed to the northerlies show higher wave heights, while the southern areas are sheltered to those dominant winds resulting in a milder mean wave climate. Projected changes for the end of the century in the values of mean Hs are small for both scenarios, with a slight increase of 0.02 m in the eastern coast and a decrease of 0.04 m elsewhere (Figure 3. 7h, i). Concerning the extreme values of waves in present climate, they range from 1.80 m in the southern part of Mallorca and Ibiza to 4.20 m in the north of Menorca, which is very exposed to the intense storms from the north (Figure 3. 7j). The projections show a generalized decrease in the magnitude of the extreme events, with an averaged decrease in the 99th percentile of the wave intensity of ~0.10 m under scenario RCP4.5 and ~0.15 m under scenario RCP8.5 (Figure 3. 7k, l). In this case there is a large heterogeneity in the distribution of the projected changes due to the sheltering effect of the coastline. Those changes in the wave conditions would directly translate into changes in the wave runup. In practice, as the projected extreme wave intensity would remain almost unaltered (~0.10 m change in front of a total value of 2-4 m), the wave runup would remain almost the same.

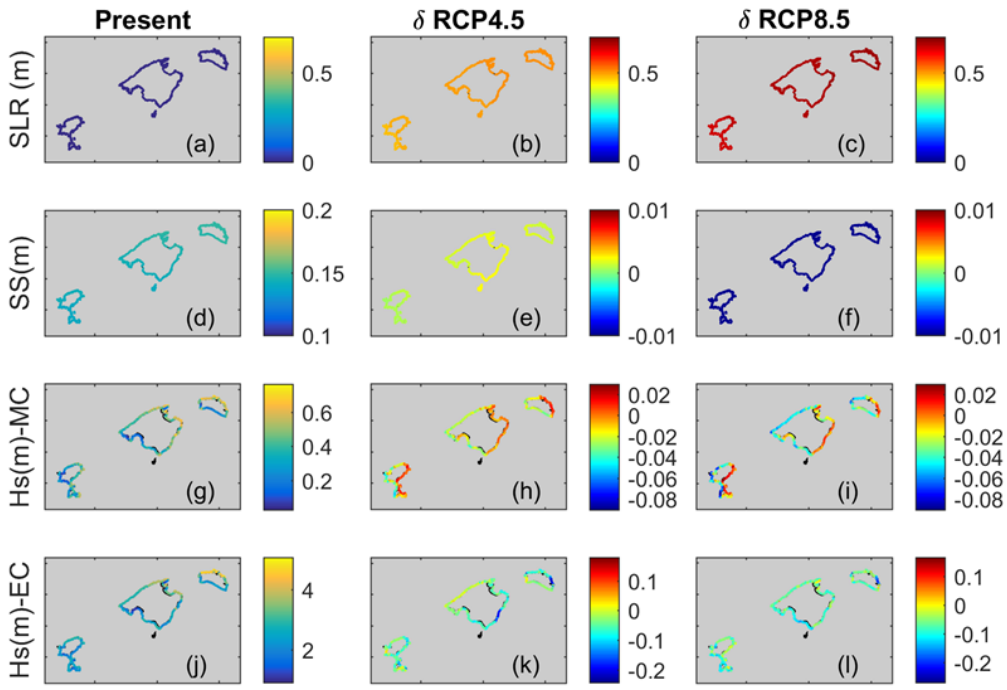

Figure 3. 7 Changes in Sea level (a-c), in storm surge (d-f), Hs mean under mean conditions (g-i) and under extreme conditions (j-l). RCP 4.5 scenario (middle column) and RCP 8.5 scenario (right column) at the end of the century (2080-2100), respect to the current conditions (1979-2013; left column). By definition, the mean sea level in the present climate is set to zero. Units in meters.

3.4.2 Beach reduction

The combined effect of all the components presented in the previous section would translate into a flooding of the beaches (see Table S3.1, for the results at beach level). At the end of the century, under scenario RCP8.5, the coastline retreat at the beach locations under mean conditions ranges between 9.0 m and 15.4 m with a mean value of 11.7 m (Table 3. 1 and Figure S3. 8). Under scenario RCP4.5 the retreat would be lower, ranging between 6.91 m and 12.69 m, with a mean value of 9.19 m (Table 3. 1). Under mean conditions the retreat is mainly due to the mean sea level rise although particular conditions like beach orientation and slope also play a role modulating the effects of mean wave height. Under extreme conditions, the results are quite different. At the end of the century, under scenario RCP8.5, the projected coastline retreat in storm conditions goes from 12.6 m in the sheltered zones to up to 58.2 m in those zones where the exposure to the waves is higher, especially in the North of Mallorca and Menorca (Table 3. 1 and Figure S3. 9). Under scenario RCP4.5 the spatial patterns are similar, and the projected coastline retreat in storm conditions is slightly lower, ranging from 10.9 to 55.6 m (Table 3. 1). The reason for the similarity between both scenarios is because the flood in storm conditions is largely dominated by the wave runup, which is projected to be similar in both scenarios.

Another quantity that is of key importance for the coastal activities is the projected change in the beach area. The loss of area would depend not only on the coastline retreat but also on the beach shape. At the end of the century, the average loss of beach area will be 65.5% and 55.9% in mean conditions, and 86.3% and 83.5% in storm conditions under scenarios RCP8.5 and RCP4.5 respectively (Table 3. 1). However, there is a large heterogeneity among beaches with

values of area loss ranging from as little as 10% to 100% (totally flooded). Both in mean (Figure S3. 10) and extreme conditions (Figure 3. 8), at the end of the century and scenario RCP8.5, in almost all locations more than 80% of the beach area will be flooded.

Regarding the completely flooded beaches (white dots in Figure 3. 8), from the 869 beaches in the Islands, at the end of the century and under scenario RCP4.5, 37 beaches would be completely flooded in mean conditions, basically due to the increase of the mean sea level (Table 3. 1). This value would rise to 254 beaches under extreme conditions. Under the RCP8.5 scenario, 72 beaches would be completely flooded in mean conditions and 314 during storm events (Table 3. 1). In general, the North of Menorca and the Northeast of Mallorca will be the most affected zones, due to the high energy of the waves that reach the coast there.

Near Future (2030-2050)						
	RCP4.5			RCP8.5		
Diagnostics	Min.	Mean	Max.	Min.	Mean	Max.
Coastal Retreat (m) -MC	3.77	5.22	9.30	4.82	6.47	9.74
Coastal Retreat (m) - EC	7.63	17.11	49.98	8.70	18.28	51.49
Beach Loss (%) - MC	10.03	36.60	100	10.16	43.28	100
Beach Loss (%) - EC	17.25	76.34	100	18.78	78.82	100
Beaches completely flooded - MC	8			13		
Beaches completely flooded - EC	173			197		
Far Future (2080-2100)						
	RCP4.5			RCP8.5		
Diagnostics	Min.	Mean	Max.	Min.	Mean	Max.
Coastal Retreat (m) -MC	6.91	9.19	12.69	9	11.74	15.37
Coastal Retreat (m) - EC	10.86	21.07	55.56	12.65	23.36	58.20
Beach Loss (%) - MC	10.28	55.96	100	12.12	65.53	100
Beach Loss (%) - EC	21.07	83.51	100	22.72	86.37	100
Beaches completely flooded - MC	37			72		
Beaches completely flooded - EC	254			314		

Table 3. 1 Summary of the coastal retreat (in m) and beach area loss for all the beaches in the Balearic Islands. Also, the number of beaches totally flooded is presented (total number of beaches in the region= 869). Results are presented under Mean Conditions (MC) and Extreme Conditions (EC) for RCP4.5 and RCP8.5 scenarios.

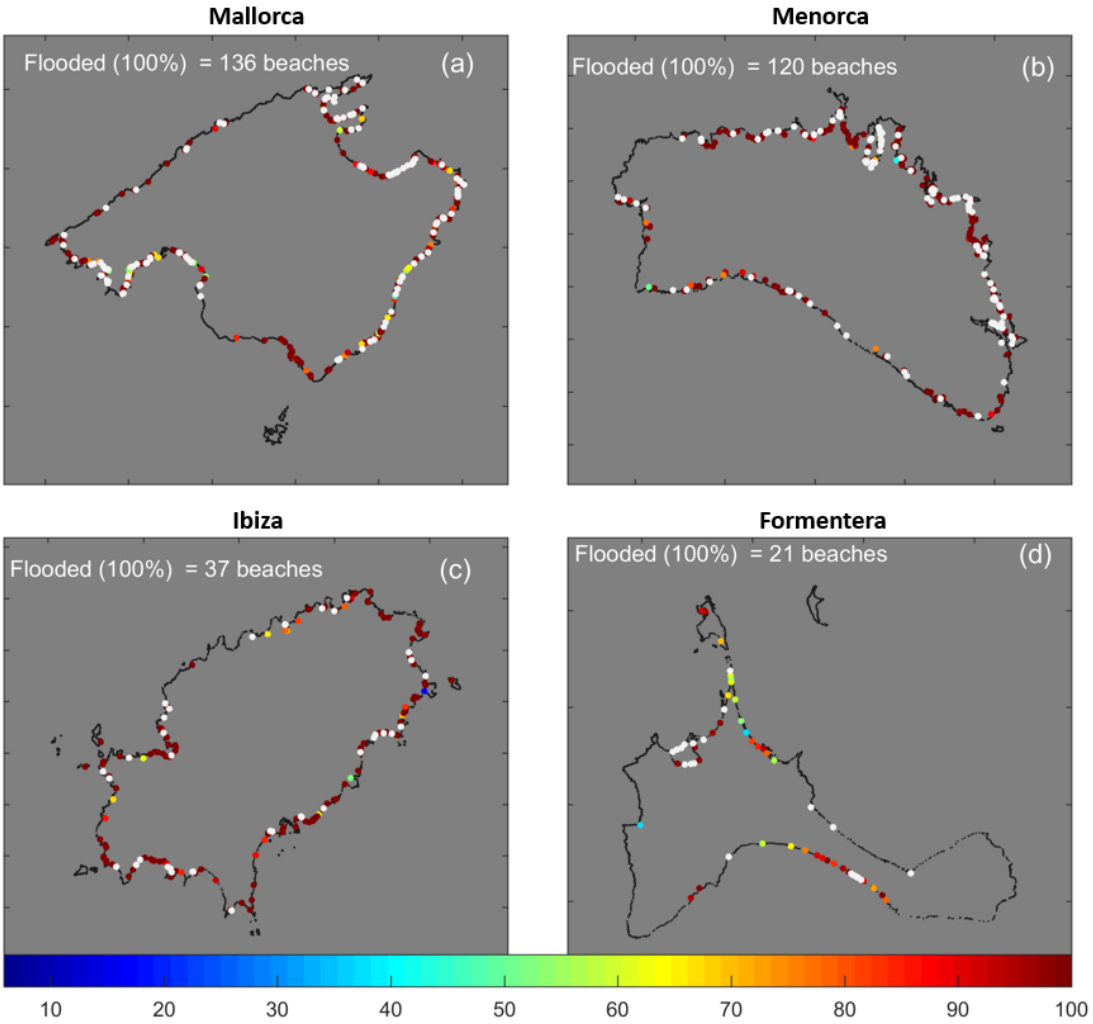

Figure 3. 8 Beach area loss (%) under extreme conditions at the end of the century (2080-2100) under scenario RCP8.5 for each island, Mallorca (a), Menorca (b), Ibiza (c) and Formentera (d). Beaches completely flooded are indicated by white dots.

3.5 Discussion

Projected changes of beach flooding during the XXI century under moderate and pessimistic GHG scenarios show a large reduction of dry beach area. Under mean conditions (i.e., calm situation in terms of storm surge or wind waves), the average coastal retreat would be 11.7 m (9.2 m) under scenario RCP8.5 (RCP4.5), at the end of the century. This would represent an average loss of beach area of 65.5% (55.9%), which would potentially have a big impact on coastal activities like sun and sand tourism but also on coastal protection. Under extreme conditions (i.e. storm surge and wind waves exceeding the 99th percentile), we find that the severity of the storms is not expected to increase, but to maintain or slightly decrease, in good agreement with previous studies (Androulidakis et al., 2015; De Leo et al., 2021). However, due to the effect of sea level rise, the flooding extension at beaches would reach 23.4 m (21.07 m) under scenario RCP8.5 (RCP4.5) at the end of the century, which in turn would imply an average loss of beach area of 86.4 % (83.5 %). Moreover, 314 (254) beaches of a total of 869 would be completely flooded during storms, that is, around 90 hours per year, spread over 4-5 events along the year (considering a typical storm duration of 18-24 hours). In those cases, the

protection offered by the beach to the frontline would be completely lost, so large impacts on the inland infrastructures and commodities can be foreseen.

To better understand and quantify the contribution of each driver (mean sea level, wave runup and storm surge) to the total flood distance, we have recomputed the coastline retreat considering separately each factor. The averaged contribution of each one is represented in Figure 3. 9. In mean conditions, at mid-century, for both GHG scenarios we find that the wave runup contributes to ~20 % of the total flood distance. The other 80% comes from the mean sea level rise (Figure 3. 9). At the end of the century, the wave runup is less important (15-20 %) respect to the mean sea level rise (80-85 %). In contrast, in extreme conditions the picture is totally different. The relative contribution of the wave runup respect to the coastline setback is much more important than the mean sea level. At mid-century wave runup would contribute to around 75 % of the flood distance. At the end of the century, the influence of the mean sea level and wave runup tends to be similar (~45 % each). The effect of the storm surge is not negligible with a contribution of ~2.2 m, that represents ~10 % of the total coastline retreat.

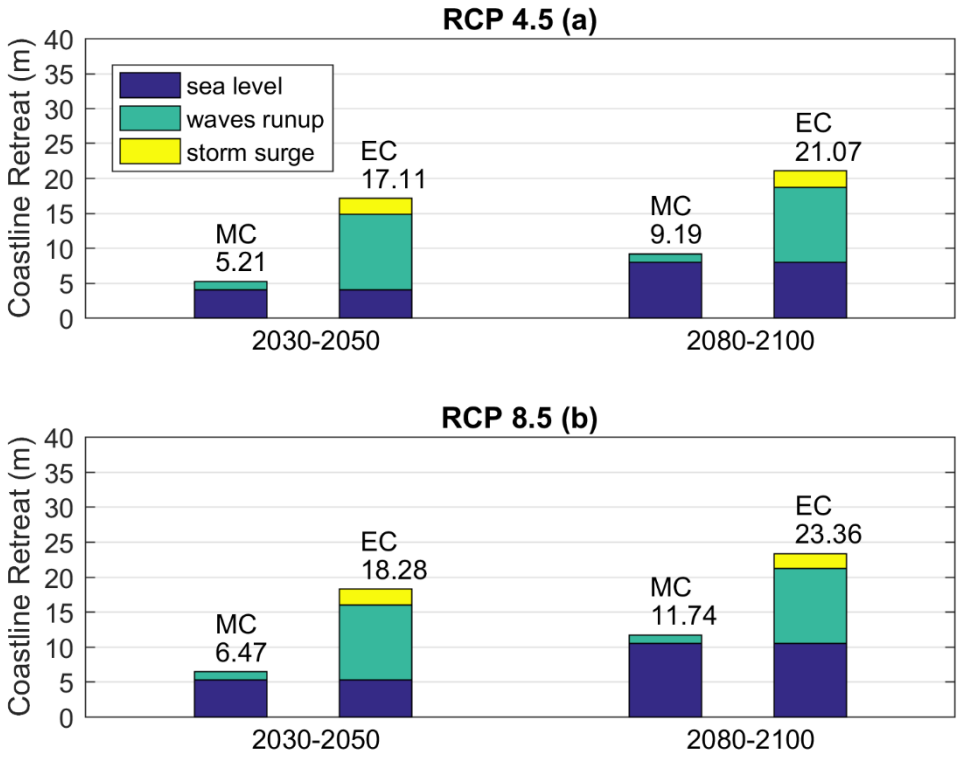

Figure 3. 9 Average value of the coastline retreat in meters for all the 869 beaches. The relative contribution of mean sea level rise (blue), wave runup (green) and storm surge (yellow), are presented under RPC4.5 scenario (a) and RCP8.5 scenario (b) for mid-century (2030-2050) and the end of the century (2080-2100). Results under mean conditions (MC, first and third columns) and under extreme conditions (EC, second and fourth columns).

In this work, we have addressed the changes in the beach coverage following a "bathtub" approximation. In other words, we have just considered the flooding due to changes in the sea level and waves, but we have not addressed the potential changes in the sediment transport processes. In a region like the Balearic Islands, without any river that can provide new sediments, beach morphodynamical equilibrium depends fundamentally on the onshore marine climate and on its interaction with the granulometry (Bernabéu et al., 2001). This balance may be affected both in longitudinal and transversal transport by anthropogenic actions on the coast

(e.g. construction of dikes, ports,…), leading to a gradual accumulation of sand in some areas and coastal erosion in others (Kudale, 2010; Ballesteros et al., 2018). In this regard, there are many factors that could modify the natural sediment transport on the coast at local scale (shape and size of the coastal infrastructure, exposure of the beach, nourishment, construction of dams, etc.). However, to predict and quantify the consequences of those actions in the forthcoming years is very difficult as there are no projections of those anthropogenic actions. Also, changes in the wave climate may modify the sediment transport balance at local scale, but it would mainly imply a redistribution of the sand, and not a net gain or loss of beach area. Then, we assume that the sedimentary balance at coast will remain the same in the future respect to the present conditions and, consequently the beach losses will be mostly induced by changes in the total water level.

In this study we have developed a cost-efficient methodology that has allowed to project the flooding of the coastline on 869 beaches. In order to assess whether the method is accurate enough, we have compared our results with previous detailed studies conducted in three locations: Playa de Palma and Cala Millor (Enríquez et al., 2017) and Son Bou (Enríquez et al., 2019). In particular, Enríquez et al., 2017 assessed the projected changes of the coastline on Playa de Palma and Cala Millor beaches using a high resolution bathymetry and propagating the nearshore wave climate using a phase resolving model (SWASH) in its 2D version with a grid resolution of 3m. Enríquez et al., 2019 focused on the Son Bou Beach and used a sophisticated combination of a phase resolved wave model (XBEACH) with a sediment transport model (Q2D-morpho) to characterize the sediment transport and the recovery of the shape profile after storms. In both studies they have used a similar database than the one used here for the mean sea level, storm surge and wave projections under RCP4.5 and RCP8.5 scenarios. In mean conditions, the results obtained in those studies are very close to those obtained here (Table 3. 2). Flooding differences are about 1-2 m, which represents a difference of 10-20 % of the total value. Under extreme conditions, the flood level obtained in Enríquez et al., 2017 are larger, up to 30-40 %. However, it is worth noting that Enríquez et al., 2017 have not considered wave attenuation by the damping effect of seagrasses meadows, and therefore they are probably overestimating the wave runup under storm conditions. Additionally, a recent study by (Luque et al., 2021) has also assessed the coastal retreat projections for the Balearic region. Although their approach is similar to the one followed here, there are two substantial differences. First, they do not take into account the effects of vegetation in the wave damping, as in the case of Enríquez et al., 2017. And second, we provide the projected flooding for both mean and extreme conditions for almost twice the number of beaches considered in that work, which provides a more comprehensive view of the expected impacts of climate change on sandy beaches.

	Playa de Palma		Cala Millor		Son Bou	
	MC	EC	MC	EC	MC	EC
RCP4.5	12.0 (11.3)	21.7 (30)	10.5 (11.7)	20.7 (29.4)	11.4 (~9.0)	23.8(~18.0)
RCP8.5	15.3 (14.8)	24.5 (30)	13.4 (17.5)	23.6 (38.0)	14.3 (~12.0)	26.4(~23.0)

Table 3. 2 Coastline retreat (in meters) under Mean Conditions (MC) and Extreme Conditions (EC), for Playa de Palma Beach, Cala Millor and Son Bou and under the RCP4.5 and RCP 8.5 scenarios. Values in brackets extracted from (Enríquez et al., 2017, 2019).

Regarding to large scale coastline retreat in a changing climate, it is worth mentioning the recent global analysis of coastline retreat on sandy beaches by Vousdoukas et al., 2020, which make use of a global beach slope database (Athanasiou et al., 2019). The main difference with our study is that we have considered detailed information on nearshore wave climate, local bathymetry and on shape and grain size for each beach of the archipelago. When comparing the (Vousdoukas et al., 2020) results for the Balearic Islands with our results, the differences are surprisingly large, as they project unrealistic accretion of more than 200 m in some beaches in the south of Menorca and west of Ibiza (see Figure S3. 11). This is mainly due to what they call "ambient change" and is obtained by extrapolating observed historical trend of coastline retreat computed from satellite images which proves to be a very dangerous choice. First, coastline evolution inferred from satellite imagery is prone to large uncertainties (Vos et al., 2019a) and become unrealistic when linearly projecting it for the next decades. Also, considering that the changes observed during the last 20 years would be the same for the next 80 years is a strong assumption. Another important issue is that reliable beach slopes are required when the nearshore total sea level rise must be transformed to coastline retreat. In Vousdoukas et al. (2020), the contribution of the sea level rise is almost twice than the one projected in this work (see Figure S3. 11b). This is probably due to the unrealistic beach slopes used in that work, which are based on the work of Athanasiou et al., (2019, see Figure S3. 12). The mean slope they use for our region is 0.190, much higher than those validated in this work. For example, a very thin grain size (d50 ~0.15 mm, like the one corresponding to the Playa de Palma Beach, located at the south of Mallorca, see point (A) in Figure 3. 1), leads to an equilibrium profile with a slope of 0.034. In contrast, a very coarse grain size (d50~1.00 mm), leads to a slope of ~0.075. Beach slopes out of this range are therefore unlikely to occur in the Balearic Islands. Finally, the storm surge induced coastline retreat they compute (see Figure S3. 11c) is underestimated. Storm surges in the Mediterranean basin are typically around ~0.15/0.20 cm (Androulidakis et al., 2015; Krestenitis et al., 2017, see Figure 7). That would imply a coastline retreat of around 2-3 m (Figure 3. 9, yellow), while (Vousdoukas et al., 2020) estimate it to be one order of magnitude lower (Figure S3. 11c). The main outcome of this comparison is that the estimates of coastline retreat are extremely sensitive to the quality of the data used, both in terms of climate forcing and especially in terms of beach characterization. Therefore, global estimates should be taken with extreme care, and regional assessments should be preferred for coastal management planning.

Finally, it is worth assessing if the results presented in this work for the Balearic Islands would be representative of the situation in other locations of the Mediterranean. Eventually, that would be the case if (a) the projections of sea level and wave evolution were similar in other Mediterranean locations and (b) the beach characteristics were comparable. Regarding the first point, projections suggest that regional differences in the sea level rise could be expected (Cherif et al., 2020), but they are significantly smaller than the expected basin average sea level rise. Namely, under scenario RCP8.5 at the end of the century regional differences due to changes in the circulation are expected to be lower than +15 % with respect to the basin average sea level rise (Cherif et al., 2020). Also wave projections suggest small reductions in the mean and extreme wave height through the whole basin (Lionello et al., 2017). Considering the beach characteristics, reports on beach morphology in different Mediterranean locations show similar values than those considered here (Falco et al., 2014; Aragonés et al., 2016; Jiménez and Valdemoro, 2019). Therefore, it is safe to assume that the reduction of beach area availability projected for the Balearic Islands can be extrapolated to the rest of the Mediterranean sandy beaches.

3.6 Conclusions

Sandy beaches are a key asset for coastal tourism and play a paramount role for coastal protection. Robust and detailed projections of flooding on sandy beaches in a climate change context are required for a timely and efficient adaptation. In this work, we have developed a cost-efficient methodology that allows propagating wave conditions in the open sea to the beach level for a large number of locations. Combining this with detailed information on beach characteristics (beach shape and granulometry) we have computed the flood level and coastline retreat for the 869 beaches of the Balearic Islands. This has been done for the historical period and projected for the 21st century under two scenarios of GHG emissions.

The flood level and coastal retreat will increase during this century and under both scenarios and will be dominated by the mean sea level rise. Storm surges and waves will slightly counteract the mean sea level rise effects due to a projected small decrease in the intensity of marine storms. At the end of the century, the averaged coastline retreat in the Balearic beaches in mean conditions will be ~9 m and ~12 m for scenarios RCP4.5 and RCP8.5, respectively. Under extreme conditions, the coastline will experience a much greater setback, reaching ~21 m and ~23 m respectively. In consequence, the average percentage of beach area loss will be ~55 % and ~65 %, in mean conditions, and around 83% and 86% in extreme conditions. Moreover, due to their shape, some beaches are projected to completely disappear. At the end of the century and under RCP4.5 scenario, 37 beaches would disappear in mean conditions, and this number would increase up to 254 during storms. Under scenario RCP8.5, the number of totally flooded beaches would be 72 in mean conditions and 314 during storms.

A comparison with previous studies has shown that global products that do not consider local characteristics may produce unrealistic results, in particular for the Balearic Islands. On the contrary, the approach followed in this work has proven to be accurate and flexible enough to provide robust results at the regional level. Finally, Mediterranean regions will experience similar evolution of sea level and waves in the next decades. Also, the beach morphology is very similar across the whole basin. Therefore, the results found for the Balearic Islands could be extrapolated to most locations in the Mediterranean (i.e., a large reduction of beach surface). Due to the paramount importance of sandy beaches for coastal protection and socioeconomic activities, adaptation measures should be put in place as soon as possible.

Supporting information for chapter 3

Figures

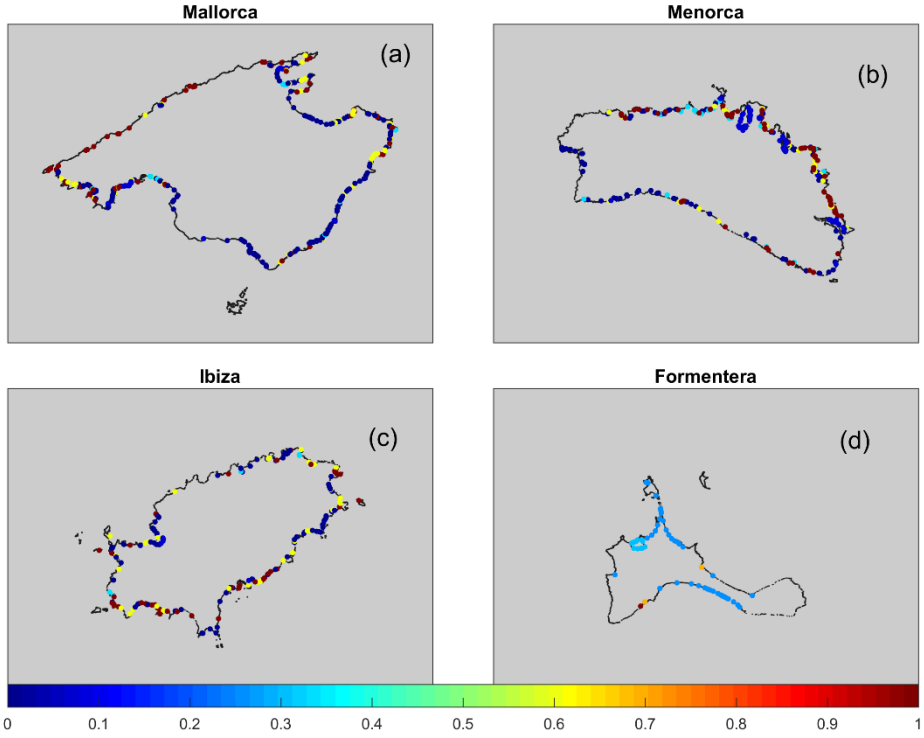

Figure S3. 1 Grain Size (D50mm) of the Balearic Sandy beaches (MITECO source). Mallorca (a), Menorca (b), Ibiza (c) and Formentera (d).

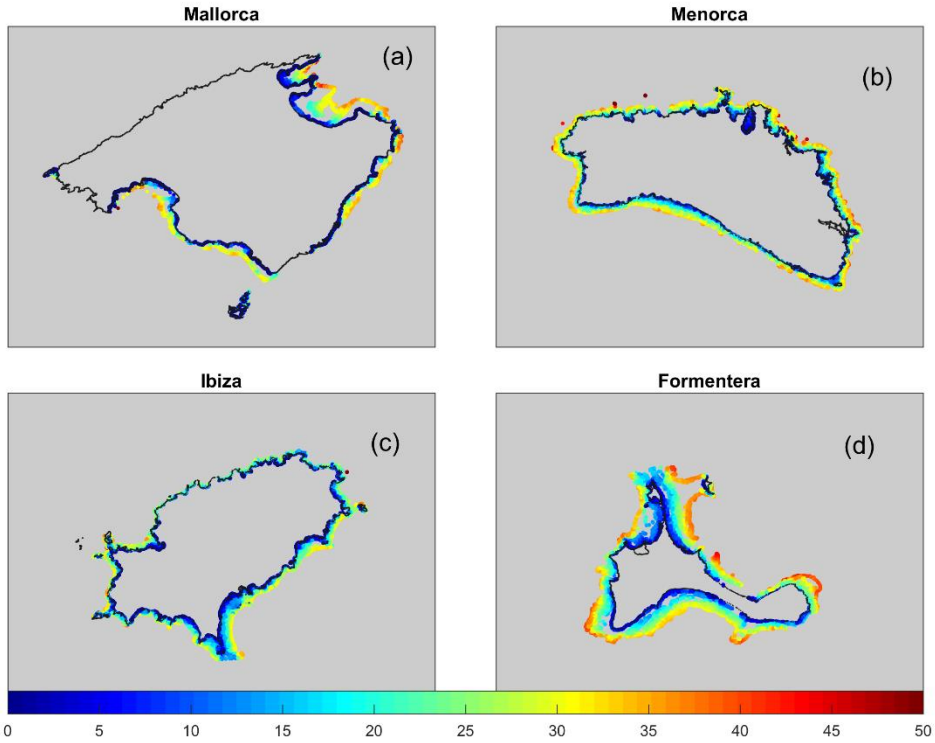

Figure S3. 2 Depth (in m) of seagrass meadows distribution in the Balearic Islands. Mallorca (a), Menorca (b), Ibiza (c) and Formentera (d).

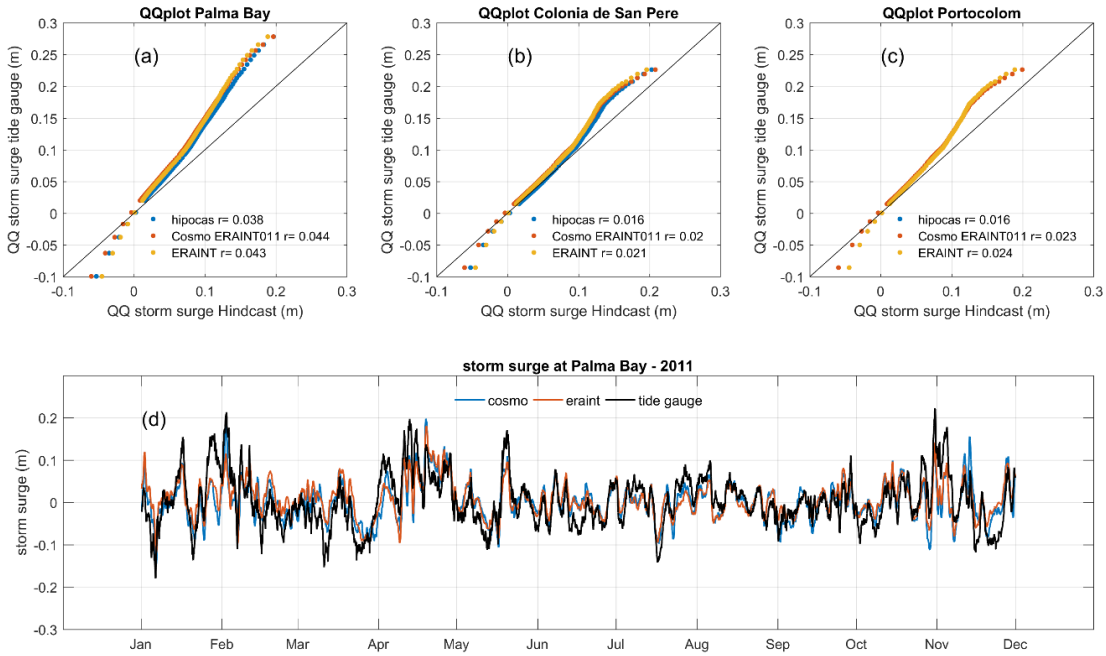

Figure S3. 3 Top panel: Quantile-Quantile plot between observed and modelled storm surges (m), at Palma Bay (a), Colonia de San Pere (b) and Portocolom (c). Bottom panel (d): temporal evolution of the storm surge for the year 2011 at Palma Bay. Cosmo simulation (blue), Era interim simulation (red) and observations after removing the astronomic tide signal (black).

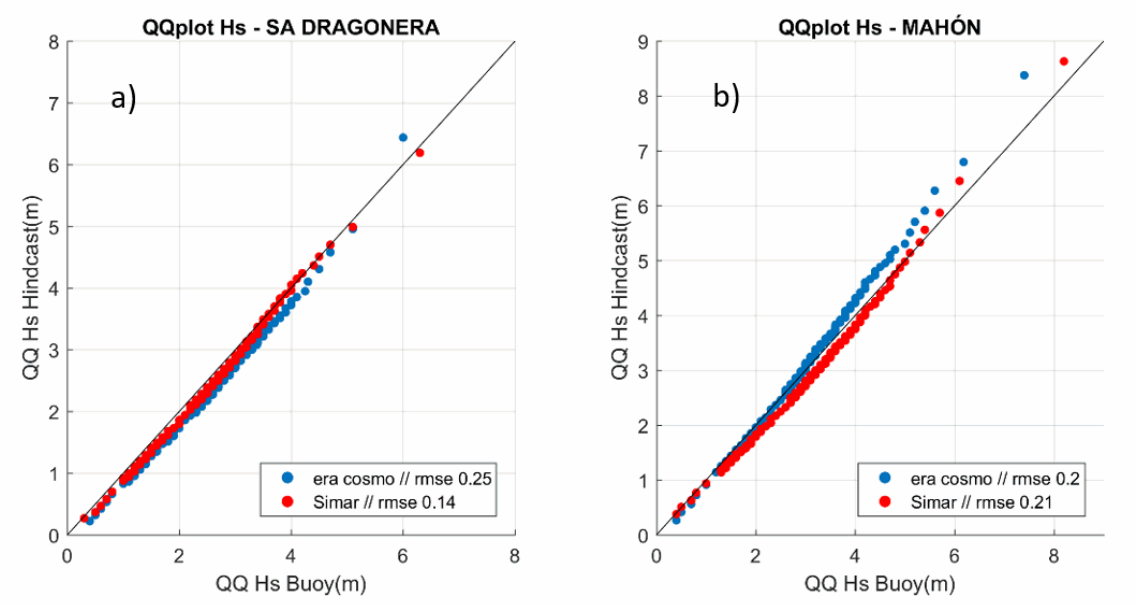

Figure S3. 4 Quantile-quantile plot of observed and simulated significant wave height (m) by Era Cosmo (blue dots) and Simar (red dots), at Sa Dragonera buoy (a) and at Mahón Buoy (b).

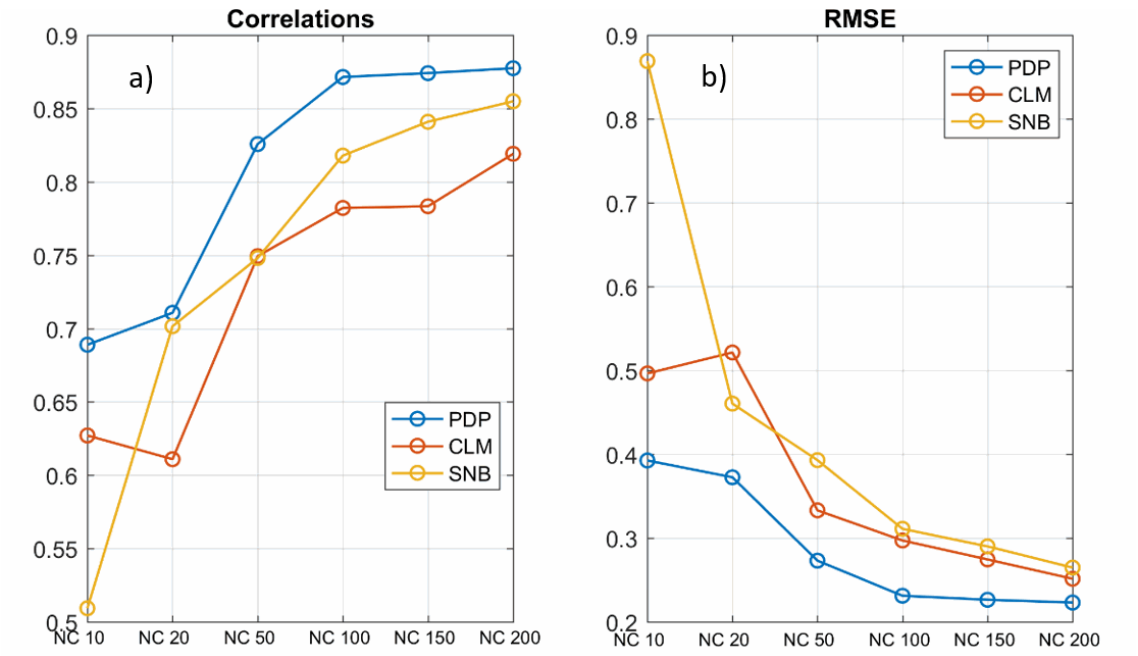

Figure S3. 5 Results of the sensitivity analysis comparing the wave climate propagated to the coast with observations at nearshore buoys (at Playa de Palma, PdP in blue, Cala Millor, CLM in red and Son Bou, SB in yellow), using different number of clusters in deep waters (see text for details). Correlations (a) and the Root Mean Square Error (b).

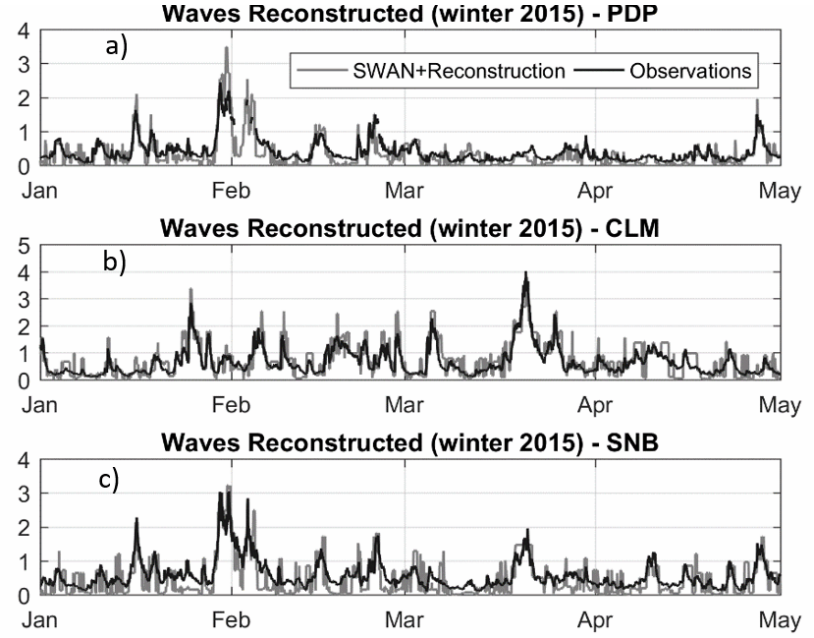

Figure S3. 6 Comparison of simulated (black) and observed (grey) significant wave height series for Playa de Palma (a), Cala Millor (b) and Son Bou (c).

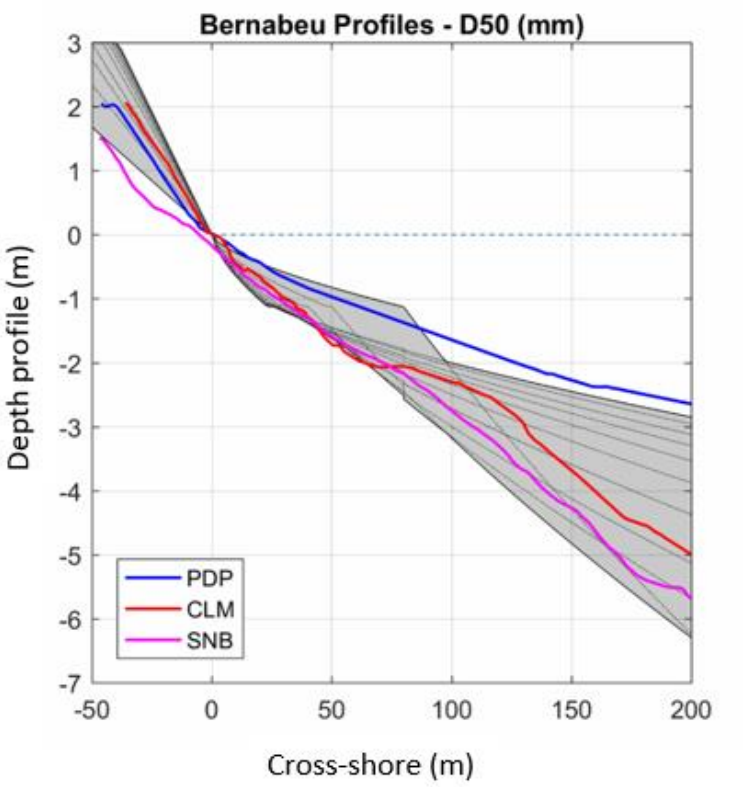

Figure S3. 7 Beach equilibrium profiles considered in this study following the Bernabeu formulation (dashed lines) and observed annual mean profiles at Playa de Palma (blue), Cala Millor (red) and Son Bou (magenta).

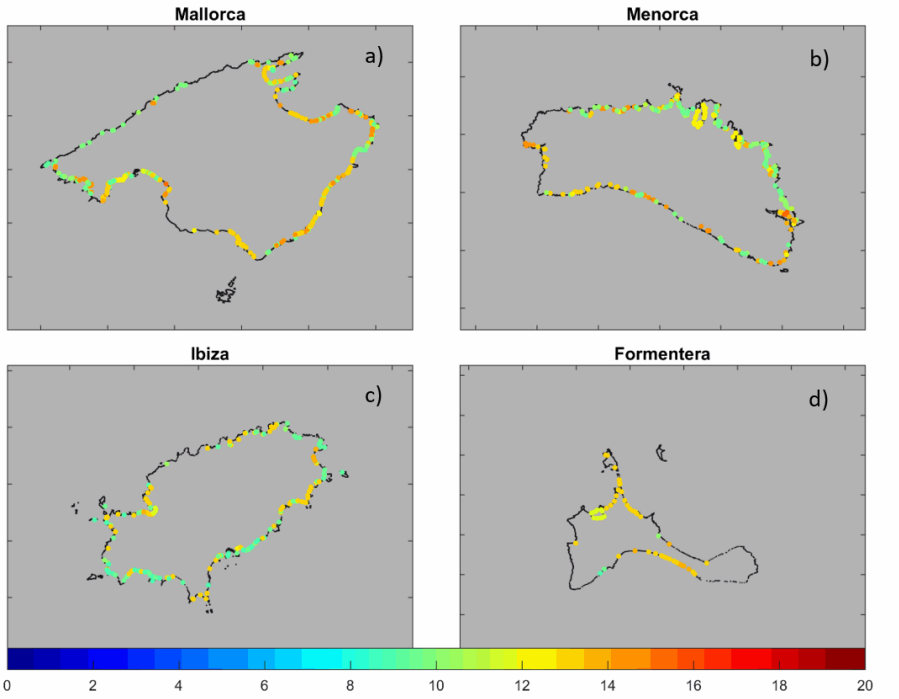

Figure S3. 8 Beach retreat (in meters) at the end of the century (2080-2100) under mean conditions for the RCP8.5 scenario. Mallorca (a), Menorca (b), Ibiza (c) and Formentera (d).

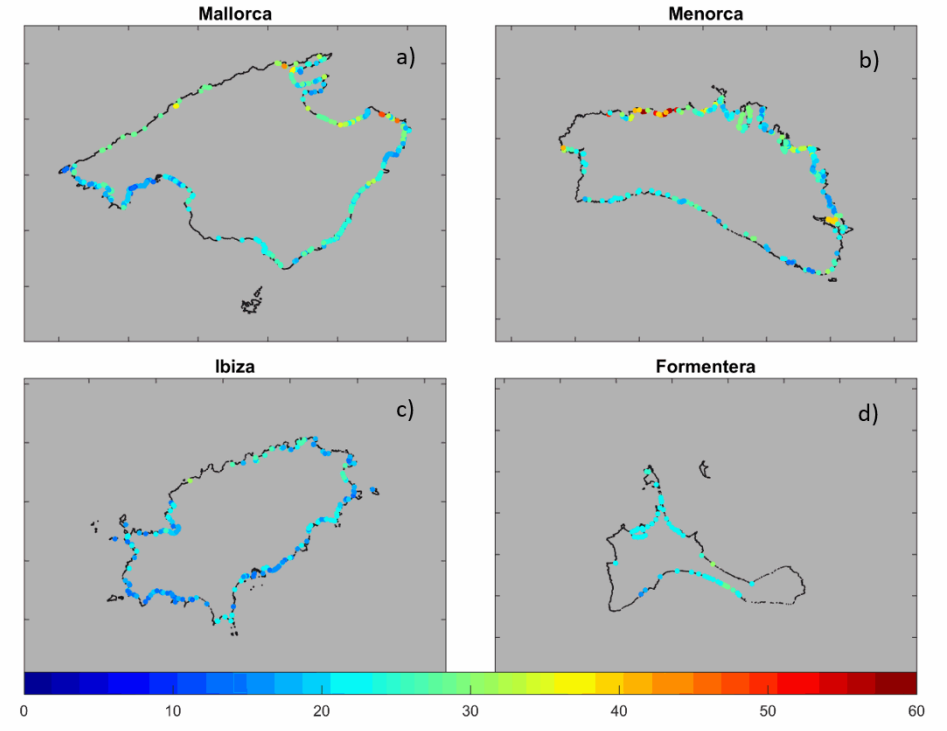

Figure S3. 9 Beach retreat (in meters) at the end of the century (2080-2100) under extreme conditions for the RCP8.5 scenario. Mallorca (a), Menorca (b), Ibiza (c) and Formentera (d). Note the different colorbar with respect to Figure S3. 8.

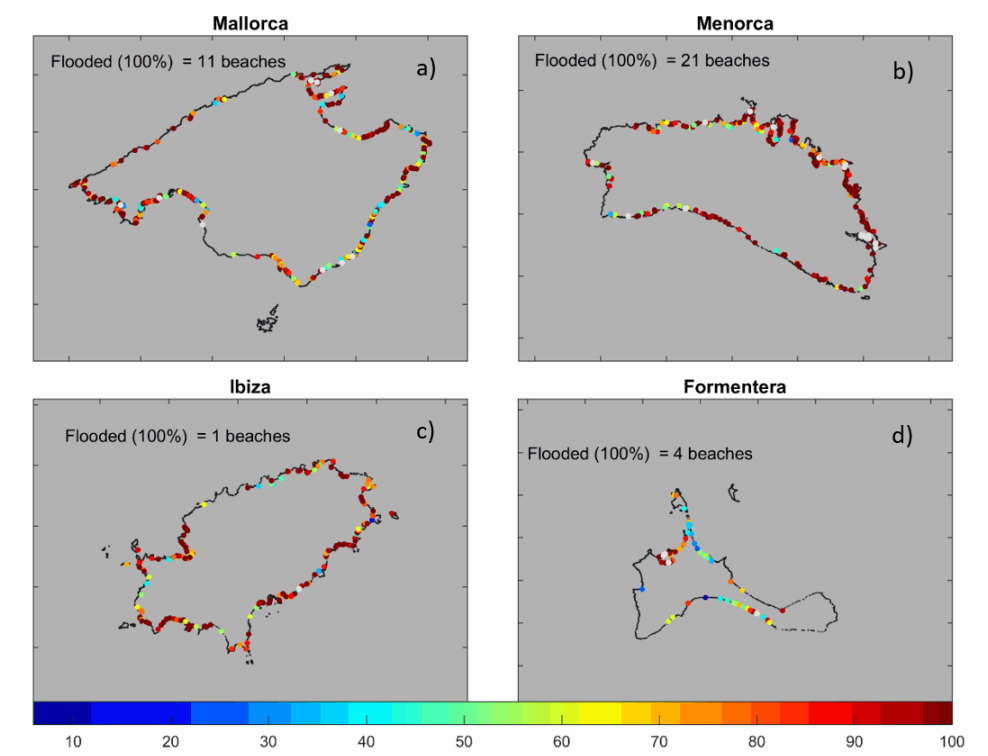

Figure S3. 10 Beach area loss (%) under mean conditions at the end of the century (2080-2100), under scenario RCP8.5. Beaches completely flooded are indicated by white dots. Mallorca (a), Menorca (b), Ibiza (c) and Formentera (d).

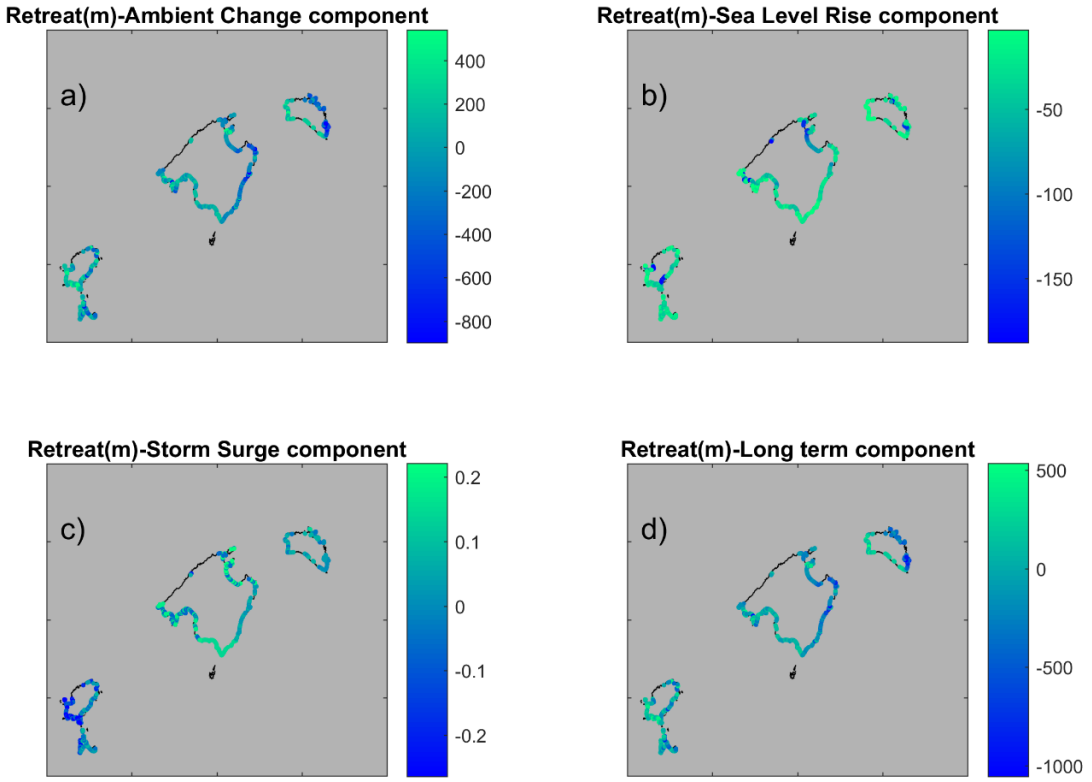

Figure S3. 11 Projections of coastline change (in m) for the Balearic Islands computed by Michalis I. Vousdoukas et al., 2020, a) change in due of Ambient Changes, b) change due to Sea Level Rise, c) change due to of 100-year Storm events and d) total change as the combination of all the others. Negative values, represent coastline retreat and positive values coastline advance.

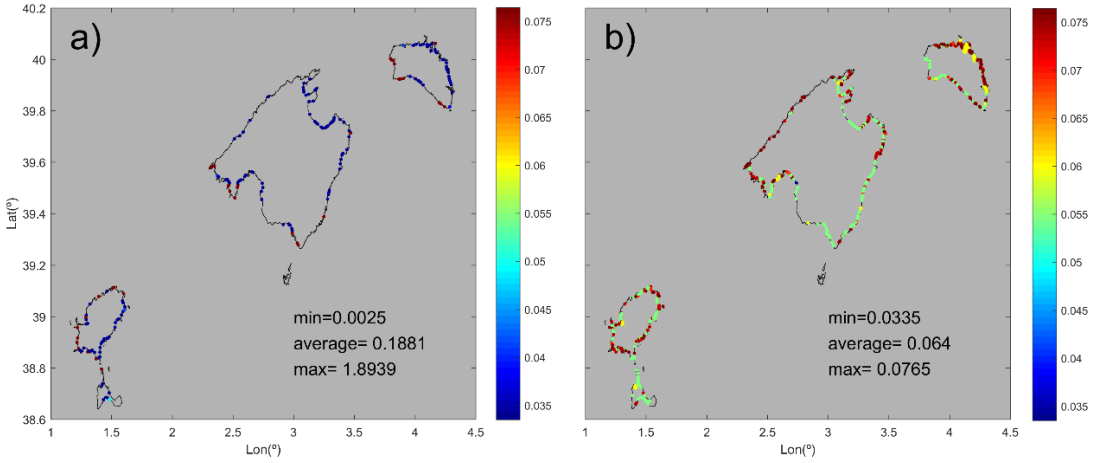

Figure S3. 12 (a) Beach slopes retrieved from Athanasiou et al., 2019 database and used by Vousdoukas et al., (2020). (b) Beach slopes considered in this work from the MITECO database. Note that the minimum, average and maximum values are showed in the panel itself.

Tables

Table S3.1 Flood distance and area reduction for the 869 beaches analysed.

Table S3.2 Pairs of Hs/Tp considered to propagate with XBEACH numerical model

This supplementary tables are published and can be downloaded here: https://www.frontiersin.org/articles/10.3389/fmars.2021.760725/full#supplementary-material

Chapter 4

4 Mediterranean Seagrasses provide valuable coastal protection under climate change.

This paper is to be submitted as:

Agulles, M., Marbà, N., Duarte, C.M., and Jordà, G., (2023). Mediterranean Seagrasses provide valuable coastal protection under climate change.

Chapter summary

Seagrass meadows are largely present in coastal areas of the Mediterranean Sea, providing an extremely important ecosystem service and natural coastal protection. Seagrass abundance, particularly *Posidonia Oceanica,* has declined abruptly in the last decades mainly due to global warming. Consequently, the future of Mediterranean seagrass is in danger and steep declines of abundance are expected for the coming decades, leading to reduce coastal protection against storms.

In this work, a regional assessment of the reduction of coastal impacts induced by the presence of seagrasses is performed under present and future climate. The study focuses on the Balearic Islands, as a representative region of Mediterranean Sea environment. Particularly, realistic scenarios of future seagrass evolution are considered to calculate changes in the extreme Total Water Level (TWL) along the century, based on observations of the shallowest seagrass front and shoot density during the last decades. In present climate, the total loss of seagrass would imply an increase in the extreme TWL of ~0.70m. Under future scenarios, if seagrass density degrades progressively along the century, losing two thirds parts respect to the present abundance, the extreme TWL would increase ~1.08m, of which 32% of that value is associated to seagrass degradation. Under the most pessimistic scenario, a total degradation of seagrass would lead to an increase on average in the extreme TWL of 1.46m, which 46% of that value belongs to the contribution of mean sea level rise (MSLR) and 54% due to loss of seagrass.

Consequently, these results highlight the importance of conserving seagrasses for coastal protection and provide valuable information for coastal management purposes in the coming decades.

4.1 Introduction

Coastal areas are a vital system for a significant proportion of the global population and economy (Pörtner et al., 2019). However, they are highly susceptible to the effects of climate change, with rising sea levels, increased storm surge flooding and wave attacks threatening human lives and coastal infrastructures (Vousdoukas et al., 2012b; Dangendorf et al., 2017). Traditional solutions to coastal protection from flooding, achieved through “hard engineering solutions” (e.g., seawalls, dikes), provide limited protection and involve long-term

environmental impacts. Hence, nature-based options, which incorporate ecology and ecosystem services to achieve coastal protection, is gaining prominence (Borsje et al., 2011) alone or combined with "hard engineering solutions" (Bouma et al., 2014). The presence of submerged vegetation can be an effective way to reduce the energy of the incoming waves and, thus, to minimize the impacts of marine storms as elements of coastal protection.

Posidonia Oceanica (hereafter P. Oceanica) is an endemic Mediterranean marine angiosperm that forms extensive, dense and highly productive submerged seagrass meadows (Borum et al., 2004). In the Mediterranean Sea, where about 1/3rd of the population live in the coastal zone (European Environment Agency, 2015), *P. Oceanica* meadows, cover between 25.000 and 50.000 km^2 of the coastal areas, or about 25% of the sea bottom between 0 and 40 m depth. *P. Oceanica* meadows play a key role in supporting Mediterranean fisheries production, carbon sequestration, and increase sediment retention which, therefore, reduces the erosion in the coastal zone (Gacia and Duarte, 2001; de los Santos et al., 2019). Consequently, seagrasses are an extremely important component of the coastal ecosystems (Borum et al., 2004) and their distribution and abundance reflect coastal environmental quality (de los Santos et al., 2019).

Seagrass meadows interact with flows, reducing by wave height by about 20-30 %, as demonstrated in both laboratory flume experiments (Fonseca and Cahalan, 1992; Koftis and Prinos, 2011) and field experiments (Infantes et al., 2012; Reidenbach and Thomas, 2018). Yet, most assessments of the role of seagrass meadows on the reduction of coastal impacts are local in nature and studies at higher spatial scales are still lacking, precluding incorporating seagrass into regional nature-based or hybrid solutions for coastal protection under climate change. The focus on local scales is due to the lack of adequate numerical modelling to generate regional-scale estimates. Fortunately, numerical tools have been developed to simulate wave propagation over benthic vegetation, including models that resolve the 3D Navier-stokes equations (Maza et al., 2013; van Rooijen et al., 2015). In addition, an analytical model for wave transformation over vegetation fields based on a non-linear formulation of the drag force was presented by (Mendez and Losada, 2004), subsequently implemented in the vegetation module of the numerical model XBEACH (Roelvink et al., 2015), in order to simulate wave propagation over seagrass meadows under different configurations (van Rooijen et al., 2015).

The role of seagrass in coastal protection has been, however, compromised due to losses derived from coastal development and deteriorated water quality (Waycott et al. 2009) as well as, more recently, marine heatwaves with climate change, to which *P. Oceanica* is particularly vulnerable (Marbà and Duarte, 2010; Garrabou et al., 2022). Losses of *P. Oceanica* in the Mediterranean sea are estimated at about 6.9% per year over the last 50 years due to several causes like pollution, mechanical stress and recently, the spread of invasive exotic species, (Marbà et al., 2014), although loss rate decelerated since 1990's (de los Santos et al., 2019). Moreover, future projections suggest that warming could lead to the functional extinction of *P. Oceanica* meadows during the second half of this century (Jordà et al., 2012; Marbà et al., 2022). However, the impact of future seagrass losses on coastal protection due to sea level rise remains unassessed.

The goal of this work is to perform a regional assessment of the reduction of coastal impacts induced by the presence of seagrasses under present and future climate. The study focuses on the Balearic Islands, as a representative region of Mediterranean Sea environment (Figure 4. 1). To reach the study's goal, a numerical modelling system able to reproduce the wave-seagrass interactions is implemented and validated with field observations. Next, an analysis of the evolution of seagrass characteristics during the last decades in the region is performed to set up

realistic scenarios of future seagrass evolution. Then, different simulations are performed to quantify the total water level reduction under different scenarios of climate and seagrass evolution.

The work is organized as follows. In Section 2, data and site description are presented. The methodology to develop a numerical model system and seagrass characterization is presented in section 3. Results of the different methodologies proposed are shown in section 4. To conclude, discussion and conclusions are presented in section 5.

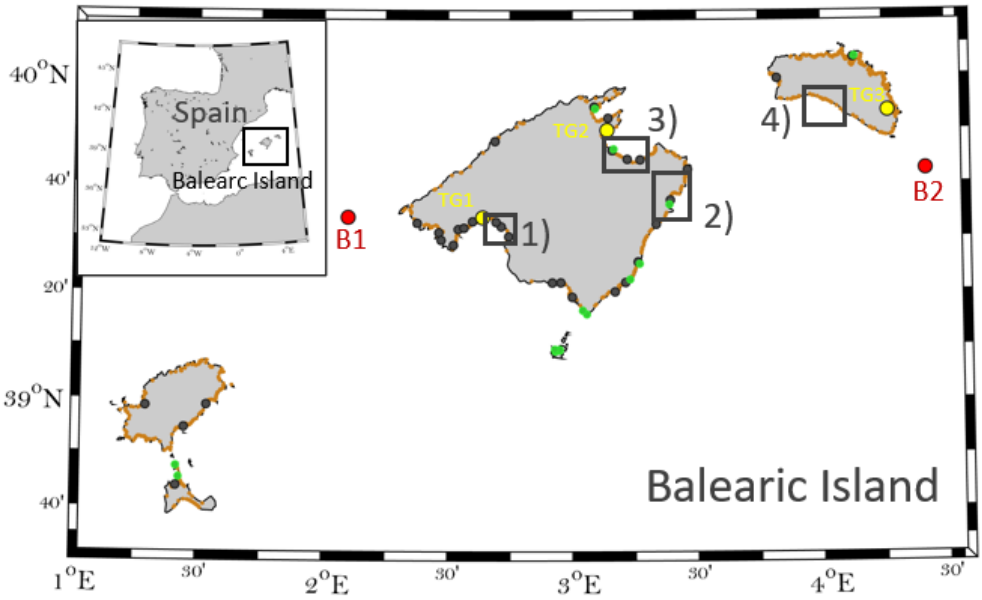

Figure 4. 1 Map of the study region including in-situ observations of shoot density of P. Oceanica (green dots, (de los Santos et al., 2019)*) beach locations (orange dots) and port locations (black dots). The sites selected for the analysis of the evolution of seagrass meadow shallowest frontier indicated by the black squares (1-Platja de Palma, PDP, 2-Cala Millor beach, CLM, 3- Bahia d'Alcudia, BDA, and 4-Son Bou beach SNB). Red dots denoted the buoy locations for waves offshore validation (B1-Sa Dragonera and B2-Mahón). The Tide gauges used for sea level validation are located in yellow dots, from Palma Port (TG1), Alcudia Port (TG2) and Mahón Port (TG3).*

4.2 Data

4.2.1 Bathymetry and coastal typology

Bathymetric information is obtained primarily from the GEBCO datasets (General Bathymetric Charts of Ocean, http://www.gebco.net), provided in a 30 arc-second grid. In order to increase the spatial resolution in shallow waters, the bathymetric information is supplemented with higher resolution data from the shoreline to 40 meters depth provided by the Spanish coastal authority (MITECO, https://www.miteco.gob.es/es/costas/temas/proteccion-costa/actuaciones-proteccion-costa/illes-balears/default.aspx). In this work, we consider two typologies of coastal protection (beaches and artificial structures). On one side, beach characteristics were derived from the MITECO database, including information on the shape contour and granulometry of 869 beaches along the Balearic archipelago (Figure 4. 1, orange dots). Throughout equilibrium profile theory (Bernabeu Tello et al., 2001), we obtained the beach profile considering the physical interaction between the granulometry and wave's energy in front of the beach (Agulles et al., 2021).

Regarding the coastal structures, we consider two typical ones that protect the port's dock from storms: a breakwater with a relatively gentle slope and a vertical wall. There are 34 main ports in the region (5 commercial ports belonging to the National Harbour Authority, Puertos del Estado, and 29 recreational ports managed by regional authorities, see Figure 4. 1). For the commercial ports we assume a toe's depth of 20m, which is characteristic of this kind of structures in the Mediterranean sea (Gutiérrez Serret and Grassa Garridob, 2015) and for the recreational ones 5 meters depth at the same location (see Table S4. 1 for detailed information).

4.2.2 Present marine climate

4.2.2.1 Sea level characterization

The characterization of sea level variability has been done by merging two datasets. On the one hand, we use a daily coastal sea level reconstruction based on tide gauge observations covering the whole archipelago for the period from 1980 to 2015. The reconstruction is based on an optimal interpolation of tide gauge observations which provides an accurate representation of sea level variability from daily to interannual scales along all the coastal region (Ramos Alcántara et al., 2022). The product is available at https://doi.org/10.1594/PANGAEA.945345. On the other hand, the subdaily variability responsible for extreme sea level has been characterized using the shallow water Hydrostatic Padua Surface Elevation (HYPSE) model to simulate storm surges (Lionello et al., 2005). The model was forced by the atmospheric fields provided by the COSMO-ERAINT011 (12 km resolution covering from 1979 to 2013 at 3 hourly resolution (Lionello et al., 2017).

Both datasets have been validated using the observations of the tide gauges at three different locations in the Balearic Islands (in Palma, Alcudia and Mahón, denoted by TG1, TG2 and TG3 in Figure 4. 1, respectively). Daily sea level shows an RMSE of 0.016, 0.015 and 0.018 and a time correlation of 0.99, 0.99 and 0.98 for the tide gauges TG1, TG2 and TG3, respectively. Three hourly storm surge (removing daily sea level signal) shows a RMSE of 0.015, 0.014 and 0.014 and a time correlation of 0.67, 0.73 and 0.73 for the tide gauges TG1, TG2 and TG3, respectively. An example of the good agreement of the datasets with observations is presented in Figure S2. 4 for January to June 2012.

4.2.2.2 Waves

Wind wave variability for the period 1979-2013 in deep waters has been characterized using a wave model simulation done with the WAM model (Hasselmann et al., 1988) and forced by the winds from COSMO-ERAINT011 (Lionello et al., 2017). The simulated 3 hourly wave data was validated using observations from two different offshore buoys (Dragonera and Mahón), with a RMSE of 0.20 m and 0.25 m, respectively and a correlation over 0.85 in both cases (see Figure S4. 2).

4.2.3 Future marine climate

4.2.3.1 Mean Sea Level

Projections of future mean sea level include all the factors that play a role at a global scale (mass variations linked to the addition or removal of water from the ocean and thermal expansion due to ocean warming) and at regional scale (gravitational fingerprint of changes in the ocean mass, changes in the circulation patterns, mass redistribution by atmospheric pressure and wind and land motion). In this work, we use the projections described by (Cherif et al., 2020) and (Agulles

et al., 2021). These are mainly based on the results of (Slangen et al., 2014) which include the global and regional signals of the changes in the mass component and the dynamic contribution in the Atlantic. Under GHG scenario RCP8.5, mean sea level in the region is projected to rise between 0.50 to 1.10 m, while under GHG scenario RCP4.5 it would rise between 0.42 to 0.65 m by 2100.

4.2.3.2 Storm surge and Waves

Projected changes in storm surge and open ocean waves for the Balearic Islands are very small under scenarios RCP8.5 and RCP4.5. The projected changes are about ~0.01 m and ~0.1m, for the storm surge and the extreme waves, respectively (Agulles et al., 2021). Therefore, we can consider that the extreme value characterization done for the storm surge and the wave components for the present climate will also be representative of the future climate.

4.2.4 Seagrass parameters

4.2.4.1 Regional area extent

To identify the presence of seagrass at a regional scale, we use information of the seagrass distribution provided by the Spanish Seagrass Atlas (Ruiz et al., 2015), which consists on a database fed by field observations from different research and regional institutions. This database provides the location and depth of seagrass meadows around the Balearic Islands (Figure S3. 2, note that this figure is in the previous chapter), while lacking information on changes of seagrass distribution.

4.2.4.2 Depth of the shallowest seagrass front

Aiming at assessing the variability of the position of the seagrass shallowest front (hereafter referred as seagrass front) along the years, two databases have been used for four study sites (Platja de Palma, PDP; Badia d'Alcúdia, BDA; Cala Millor, CLM; and Son Bou, SNB, Figure 4. 1). First, we used orthophotos covering the period between 1956 and 2015 with a spatial resolution of 0.5 m from the Government of the Balearic Islands (http://ideib.caib.es/visor/). There are 4, 6, 2 and 3 valid orthophotos for PDP, BDA, CLM and SNB, respectively. Second, we used satellite images from SENTINEL 2, with a spatial resolution of 10 m and covering the period from 2015 to 2021 at monthly resolution (https://scihub.copernicus.eu/dhus/#/home). A subjective quality control has been performed to keep only those images clear enough to identify the seagrass front. Overall, the dataset includes a total of 230 images distributed as follows: 14 for PDP for the time period from 2006 to 2021, 70 at CLM from 1956 to 2021, 76 at BDA from 2002 to 2021 and 70 at SNB from 1984 to 2021.

4.2.4.3 Posidonia Oceanica shoot density.

We used seagrass shoot density values measured annually, from 2000 to 2012 (de los Santos et al., 2019)(see Figure 4. 1 green dots, for locations, and Table S4. 2 for details of the sampling). Shoot density counts were conducted by divers in permanent representative plots (between 0.06 m^2 and 0.25 m^2) mostly in summer.

4.3 Methods

4.3.1 Numerical modelling system

Total water level (TWL) at the coast can be represented as a combination of several components: the mean sea level, the storm surge and the wave runup. The two first components can be faithfully represented by the databases presented above. However, the wave runup at the coast can largely differ from the open sea waves provided by the above-mentioned regional models. In consequence, a numerical modelling system able to simulate the wave runup has been implemented. The system is composed by nesting two different numerical models. Firstly, we use a model able to propagate open sea waves up to the nearshore and secondly, a model able to simulate the wave runup at the coast in the presence of submerged vegetation.

4.3.1.1 Nearshore maritime climate

Physical processes as refraction, diffraction, white-capping, bottom friction and breaking, among others, modify the waves parameters on their way from deep to shallow waters (Roland and Ardhuin, 2014). Therefore, the wave fields simulated in deep waters need to be transferred up to the nearshore. To do so, we implement an hybrid downscaling methodology using a clustering algorithm (Camus et al., 2011a) and the SWAN numerical model (Booij and Holthuijsen, 1987) to propagate the historical deep waves to shallow waters (for more details see (Agulles et al., 2021). As a result, we obtain a 3 hourly nearshore wave reconstruction for the period (1979-2013) covering the whole Balearic Islands with a spatial resolution of 200 m.

4.3.1.2 Wave runup in presence of submerged vegetation

The most important transformation of wave characteristics occurs in the shoaling and swash zone, where diffraction, shoaling and breaking highly reduce the waves energy (Lin and Liu, 1998). Moreover, in this critical zone, the bottom friction plays a paramount role in the energy wave dissipation, especially over vegetated grounds (Duarte et al., 2013; Beck et al., 2018; Menéndez et al., 2020).

In order to simulate these processes, the XBEACH model has been implemented (Roelvink et al., 2015). The model solves phase-averaged coupled 2D horizontal equations for wave propagation, flow, sediment transport, and bottom changes, that allows, among other parameters, to obtain the wave runup at the swash zone (Agulles et al., 2021). Additionally, we consider the vegetation module of XBEACH, which includes wave damping and wave breaking over vegetation fields at variable depths. Based on a nonlinear formulation of the drag force, either irregular or monochromatic waves can be modelled considering geometric and physical characteristics of the vegetation field (Mendez and Losada, 2004; van Rooijen et al., 2015) where the time-averaged energy dissipation through a vegetation field can be expressed with the following equation:

$$< \varepsilon_v >= \frac{1}{2\sqrt{\pi}} \rho C_D b_v N \left(\frac{kg}{2\sigma}\right)^3 \frac{sinh^3(k\alpha h) + 3sinh(k\alpha h)}{3kcosh^3(kh)} {H_{rms}}^3 \quad (1)$$

Where b_v is the vegetation stem diameter, N is the vegetation density, k is the wave number, g is the gravitational acceleration, σ is the wave frequency, h is the water depth, C_D is the drag coefficient and H_{rms} is the root mean square wave height.

Four sensitivity runs have been performed forcing the 1D version of XBEACH with observed nearshore waves and changing the damping coefficient due to wave-seagrass interaction (Table

1). In order to calibrate the vegetation module, the results have been compared with observed swash, retrieved from timestack images provided by the Balearic Islands Coastal Observing and Forecasting Facility (SOCIB), (Tintoré et al., 2013) in PDP and CLM beaches. The results show that the inclusion of the vegetation module improves the results in both beaches (see Table 4. 1 and Figure S4. 3). Without vegetation, the correlation is 0.79 (0.64) and the RMSE 0.19 m (0.15 m) for PDP (CLM). With the optimal drag coefficient (Test 3), the correlation is almost the same 0.80 (0.63) but the RMSE is strongly reduced to 0.08 m (0.13 m).

Tests	Ah (m)	Bv (m)	N (shoots/m2)	Cd	RMSE (m)		Correlation	
					PDP	CLM	PDP	CLM
Test 0	-	-	-	-	0.19	0.15	0.79	0.64
Test 1	0.35	0.02	615	0.20	0.13	0.17	0.79	0.59
Test 2	0.35	0.02	615	0.10	0.10	0.13	0.78	0.61
Test 3	0.35	0.02	615	0.05	0.08	0.13	0.80	0.63

Table 4. 1 Parameters used in the sensitivity tests for the calibration of the drag coefficient calibration and results of the validation in terms of RMSE (in m) and correlation. The parameters considered are the mean shoot length (Ah), stem width (Bv), vegetation density (N) and drag coefficient (Cd). The symbol (-) indicates that no vegetation module has been included in the XBEACH simulations.

Once the vegetation module has been calibrated an additional validation of the model has been carried out using waves observations from another field experiment (Infantes et al., 2012). In that experiment, the wave H_{rmse} was measured along a cross-shore transect in CLM beach during the period from 7 to 23 July 2009 (see Figure 4. 2). In that beach, seagrass was present up to a depth of 6 m and the nearshore wave height observed during the experiment ranged from 0.3 to 1.2 m when a moderate storm hit the area. The wave propagation during the same period was simulated using XBEACH with and without considering the presence of seagrass. In this case, the drag coefficient is set to Cd=0.05 but we consider a leaf length (Av) of 0.80 m, according to the seagrass characteristics reported for that location during the experiment (Infantes et al., 2012). The results show that, at the deepest location (~17m depth), there are no differences in the simulation without and with seagrass, with an RMSE of 0.23 and 0.22m, respectively (P1 in Figure 4. 2). However, as the wave steepness (H_{rmse}/depth) increases closer to the coast, the simulation with the vegetation module shows better skills, with a RMSE reduction at the shallower depth (P4 in Figure 4. 2) from 0.27 m to 0.11 m.

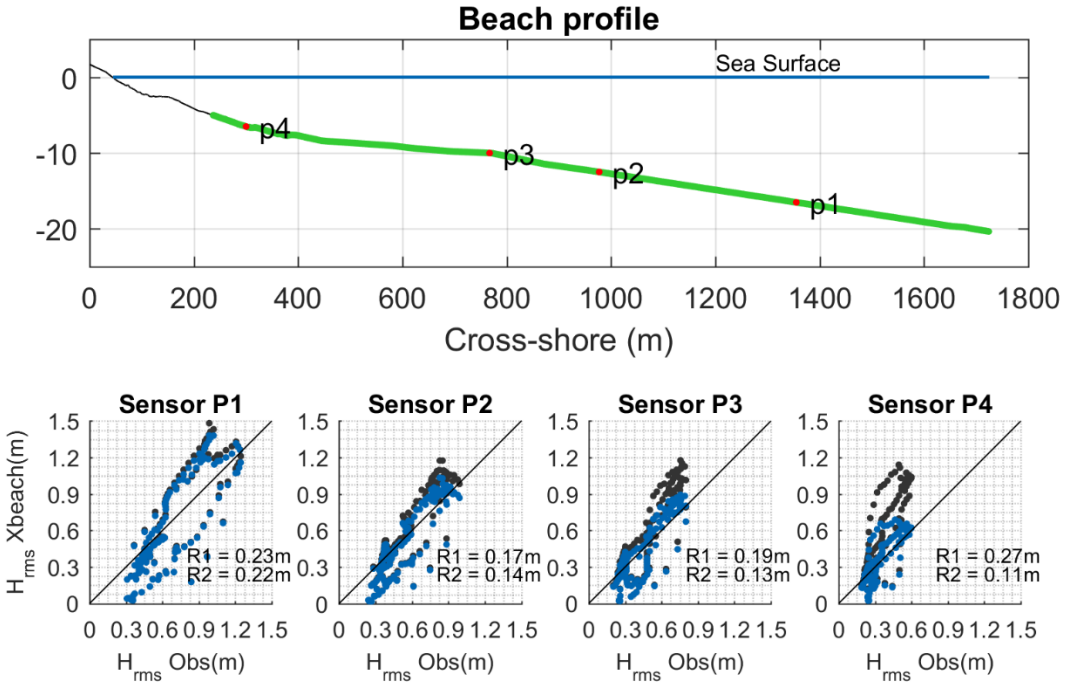

Figure 4. 2 Validation of the XBEACH model outputs in Cala Millor along a cross-shore transect (upper panel). The location of the wave observations is denoted by the red dots (P1 to P4). The lower panels show the comparison of observed and modelled H_{rms} (in m) for the four observation points. The corresponding RMSE (in m) is included in the insets for the simulation without the vegetation module (R1, corresponding to the black dots) and with the calibrated vegetation module (R2, corresponding to the blue dots).

4.3.2 Seagrass characterization

4.3.2.1 Seagrass front variability

Recently, satellite images have been used along with machine learning algorithms to characterize seagrasses meadows (location, depth, type, etc.) with satisfactory results (Traganos and Reinartz, 2018; Traganos, 2020). However, those techniques need a huge number of images and robust pre- and post-quality control. In our case, we only aimed at identifying the position of the seagrass front, to obtain the minimum relative depth (water depth/plant height) which plays a role in the wave energy dissipation (equation 1). Thus, instead of using automated algorithms, the shallowest limit of the meadow is identified by visual inspection over a georeferenced image based on the color contrast, and the polyline is drawn by hand (see an example in Figure 4. 3). Once defined, the corresponding average depth and standard deviation (STD) of the seagrass front, for each image, is obtained from the bathymetric data. Finally, from the analysis of all the available images, time series of the shallowest seagrass depth has been generated for the four study sites shown in Figure 4. 1, black squares.

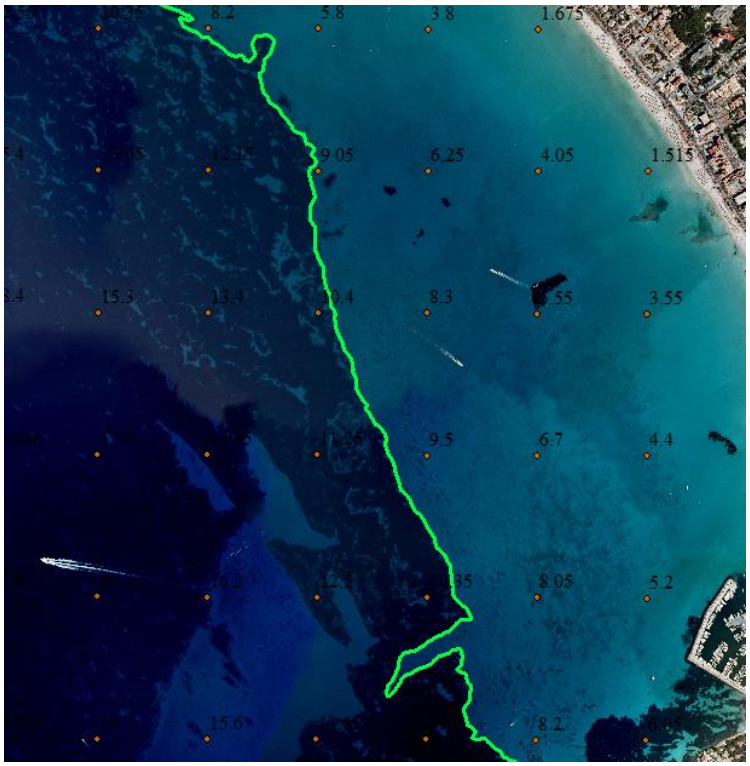

Figure 4. 3 Example of the polyline defining the upper limit of the seagrass meadow (green line), obtained for Platja de Palma in 2008

4.3.2.2 Meadow density

Seagrass meadow density plays an important role in the wave energy dissipation (equation 1). From the one side, we use average shoot density representative of the last 2 decades provided by the Spanish Seagrass Atlas (Ruiz et al., 2015) to model wave runup in coastal areas which are nowadays colonized by *P. Oceanica*. From the other side, scenarios of seagrass shoot density are considered to calculate wave runup along the century, based on linear decay trends observed between 2000 and 2012 in meadows shallower than 10 m and deeper than 10 m (de los Santos et al., 2019)..

4.3.3 Look-up tables

Running XBEACH for all locations (869 beaches and 34 ports) and for the whole period of the study (1979-2014) is computationally too expensive. Therefore, to obtain a high-resolution wave runup (3 hourly time series), we use a cost-effective methodology already tested by Agulles et al. (2021). In particular, 39 sea states (i.e., pairs of Hs-Tp) that encompass all range of the nearshore wave climate obtained by the SWAN model simulation (see section 3.1) are defined. Then, XBEACH is used to propagate, from intermediate depths up to the swash zone, these 39 sea states under different conditions of bathymetry, seagrass coverage and seagrass abundance to generate several look-up tables. These tables allow to directly link nearshore sea states with the wave characteristics at the coast without the need of running the model again. The look-up tables are thus used to transform 3-hourly time series of nearshore waves for present climate (1979-2014) to waves at the dikes toe or to wave runup at the beach, using the look-up table that corresponds to the local bathymetry and seagrass characteristics (see a sketch of the procedure in Figure S4. 4).

In this process, we have considered 11 bottom equilibrium profiles, 5 scenarios of seagrass coverage and two meadow densities. The beach profiles correspond to different granulometries of sand beaches (from a grain size of 0.015 to 0.075) and have been obtained based on the formulation of (Bernabeu and Vidal, 2001). The scenarios of seagrass coverage considered are (1) no presence of seagrass, (2), seagrass up to the shoreline, (3) up to 2 m depth, (4) up to 5m depth and (5) up to 7m depth. The meadow densities considered are 615 shoots/m^2 and 200 shoots/m^2, which are representative of a well-preserved meadow and a deteriorated one, respectively. Overall, we have performed 4290 (39 x 11 x 5 x 2) simulations of XBEACH that covers all possible combinations of sea states, beach profiles and seagrass coverage in the region (Figure S4. 4).

XBEACH explicitly provides the wave runup on the beaches but it has not been created originally for coastal dikes or seawalls. For those cases, the common approach is to use empirical formulation based on laboratory and field controlled experiments (Eurotop, 2018). For dikes with a relatively gentle slope (28 out of 34 in our case, see Table S4. 1) the wave runup is estimated as follows (equation 1):

$$RU_{2\%} = H_{mo} * 1.65 * \boldsymbol{\gamma}_b * \boldsymbol{\gamma}_f * \boldsymbol{\gamma}_\beta * \varepsilon_{m-1,0} \quad (1)$$

Where H_{mo} is the wave height at dike's toe estimated from the XBEACH simulations, and $\boldsymbol{\gamma}_b$, $\boldsymbol{\gamma}_f$, $\boldsymbol{\gamma}_\beta$ and $\varepsilon_{m-1,0}$ are parameters that represents the berm characteristics, roughness, wave attack and breaker parameter, respectively. In our case, we consider a dike with relatively gentle slope as a design approach, with the simplest parametrization. That is, no berm ($\boldsymbol{\gamma}_b$=1), equivalent roughness of 0.4 (rocks with two layers and permeable core), perpendicular wave attack against structure ($\boldsymbol{\gamma}_\beta = 1$) and a breaker parameter equal to 3, which is the typical configuration of Mediterranean coastal structures used to design harbors (Gutiérrez Serret and Grassa Garridob, 2015). For those ports that have been designed with a vertical wall as the main protection structure (6 out of 34), we use another approximation showed also by Eurotop 2018 manual, (equation 2):

$$RU_{2\%} = H_{mo} * 1.8 \quad (2)$$

4.3.4 Scenarios of total water level evolution

In order to produce future scenarios of TWL at beaches and ports, we need projections of future sea level and waves and projections of seagrass characteristics. Unfortunately, it is difficult to provide robust projections for the future of the *P. Oceanica* in the coming decades, because whereas its resilience against the increase of the sea temperature and marine heat waves largely depends on populations thermal threshold (Bennett et al., 2021; Marbà et al., 2022), which are quite well established for the Balearic Islands, there is a lack of information about its vulnerability to severe storms, despite evidence that they can trigger *P. Oceanica* losses (Gera et al., 2014; Alcoverro et al., 2020). Also, anthropogenic factors (e.g., pollution, anchoring) can lead to losses. Therefore, we have opted to define three scenarios for the seagrass evolution, starting with observed seagrass density to consider that the meadows (1) remain in steady state, (2) disappear by the end of the century due to global warming, and (3) an intermediate scenario where the meadows are progressively degraded from 615 shoots/m^2 to 200 shoots/m^2 by end of century.

In summary, five numeric experiments were performed (Table 4. 2). Two of them are devoted to the analysis of the role of seagrass in coastal protection under present climate conditions (PRES_NS and PRES_WS). The other three focus on the future evolution of TWL, assuming sea level evolves as it is projected under the RCP8.5 GHG scenario but with different scenarios for seagrass evolution (FUT_NS, FUT_615 and FUT_200).

Scenarios of TWL	Time coverage	No Seagrass	Well Preserved Seagrass (615sh/m^2)	Degraded Seagrass (200sh/m^2)
PRES_NS	1979-2014	X		
PRES_WS	1979-2014		X	
FUT_NS	2015-2100	X		
FUT_615	2015-2100		X	
FUT_200	2015-2100			X

Table 4. 2 Numerical experiments performed for different time periods and under different scenarios of seagrass evolution.

4.4 Results

4.4.1 Evolution of seagrass characteristics

4.4.1.1 Evolution of the seagrass front

The analysis of the images reveals that the water depth of the shallowest meadow front remained practically constant over the time period examined (1956- 2021) at the four sites examined (Figure 4. 4). In PDP (Figure 4. 4, 1-PDP), the seagrass front is situated at 8.31 ± 0.38 m depth. At SNB (Figure 4. 4, bottom panel) it is located at 8.34 m depth but exhibits more variability along the years (± 0.57 m). In CLM and BDA, the fronts are located at 6.28 ± 0.39 m and 7.17 ± 0.41 m, respectively. In order to cover as long a period as possible, the analysis has been carried out by concatenating results from orthophotos and satellite images.

The orthophotos show a regression of the PDP seagrass front from 7.4 to 8.1 m in 58 years (1956-2014), which the satellite images further extend to 8.8 m recently (2020-2021). However, this must be taken with caution because observations are not uniformly distributed across the time period examined (Figure 4. 4, 1-PDP). In CLM, the orthophotos suggest a recess from 6.0 m to 6.8 m from 1959 to 2021. However, the satellite images show a very variable depth ranging from 5.3 to 7.2 m in the last 6 years. This suggests that there is a non-negligible level of observational noise (i.e., maybe due to dead leaves remaining in the bottom) that probably also affected the values obtained from the orthophotos. The same behavior is observed in BDA and SNB from the satellite images (the record from the orthophotos in those locations is too short to be considered). In summary, we have not found consistent evidence for a long-term regression of the seagrass shallow limit, except in the case of PDP. Therefore, the shallow limit of the meadow was kept constant in the simulations performed.

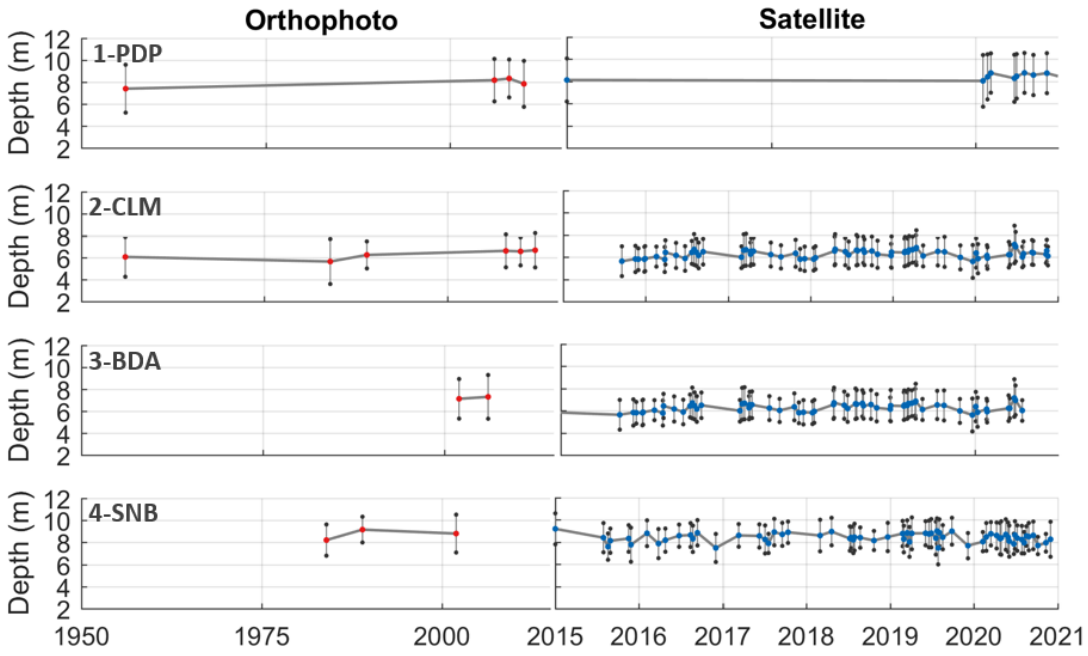

Figure 4. 4 Average depth of seagrass front for; 1) Platja de Palma (PDP), 2) Cala Millor (CLM), 3) Badia d'Alcúdia (BDA) and 4) Son Bou (SNB). In the left panel, results of depth average (red dots) and STD (vertical gray lines) retrieved from orthophoto images and in the right panel, results of depth average (blue dots) and STD (vertical gray lines) retrieved from satellite images. Note that the scale of the horizontal axis is different among left and right panels.

4.4.1.2 Shoot density evolution

For seagrass meadow shallower than 10 m, the average shoot density ranged from 300 to 1000 shoot/m^2, with large interannual variability (temporal std of 103 sh/m^2), and an underlying decline rate at -8.8 $\pm$ 2.1 sh/m^2/yr. Mean shoot density of meadows deeper than 10 m, was lower, ranging from 100 to 500 sh/m^2 and with less interannual variability (70 sh/m^2). However, deep meadows showed a stronger negative trend at -17 $\pm$ 1.2 sh/m^2/yr (Figure S4. 5). In other words, the rate of the meadow degradation below 10 m is double the rate observed in shallower waters. It is dangerous to extrapolate those trends for the next decades as far as the dynamics of the meadows and the impact of climate change may be strongly non-linear, but if they would hold, by the end of this century coastal areas in the region would be devoid of *P. Oceanica*, (see Table S4. 2 and Figure S4. 5).

If the observed evolution continues similarly in the next decades, the seagrasses would disappear by the end of the century (simulation FUT_NS). Adopting strong measures to reduce the seagrass decline (e.g., with replanting or with new protection policies) may lead to a moderate decline, reaching ~200 sh/m^2 by the end of the century (simulation FUT_200). Finally, the scenario that assumes no decline at all (simulation FUT_615) seems unrealistic but serves a valuable purpose for the sake of comparison with present conditions.

4.4.2 Role of seagrass for coastal protection in present climate

Extreme TWL in dikes is higher than on beaches (Figure 4. 5), as these are more effective damping the wave runup. The values of the extreme TWL in the beaches range from 0.45m in the southern coast to 2.45m in the northwest of Mallorca and northern coast of Menorca with an average value of 0.87 ± 0.39 m, depending on the different orientation of the beaches relative

to the incoming storms, the beach slopes and the seagrass coverage. In the ports, the TWL ranges from 1.80 m in Palma Bay to 6.67 m in northern coast of Mallorca and Menorca, with an averaged value of 3.74 ± 1.2m. In addition to the previously mentioned factors, the type of dike also plays a role in TWL with the vertical walls inducing higher runups in ports.

Loss of *P. Oceanica* meadows lead, on average, an increase of about 0.7 m in the extreme TWL both on beaches and dikes, with larger increases (>1.2 m) on the Northern coast of Menorca and south part of Mallorca (Figure 4. 6), which would affect 77 beaches out of 869 (Figure 4. 6 C) and in 2 ports out of 34 (Figure 4. 6, D). Conversely, extreme TWL is less vulnerable to seagrass loss on the north beaches of Mallorca and beaches and ports in the Palma Bay, where the expected TWL increase with seagrass loss is estimated to be about 0.30 m, 130 beaches and 2 dikes.

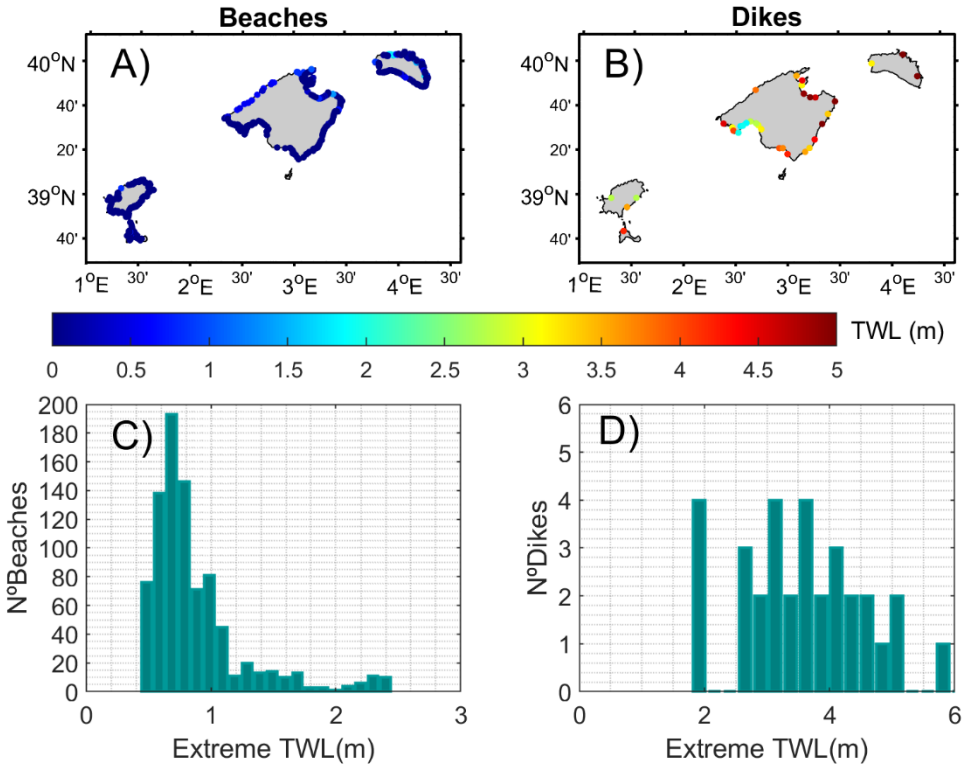

Figure 4. 5 Simulated 99th percentile of the total water level in the Balearic Islands (experiment PRES_WS). The results are presented for the beaches (a) and the dikes (b). The histograms of the values mapped are presented in the bottom row.

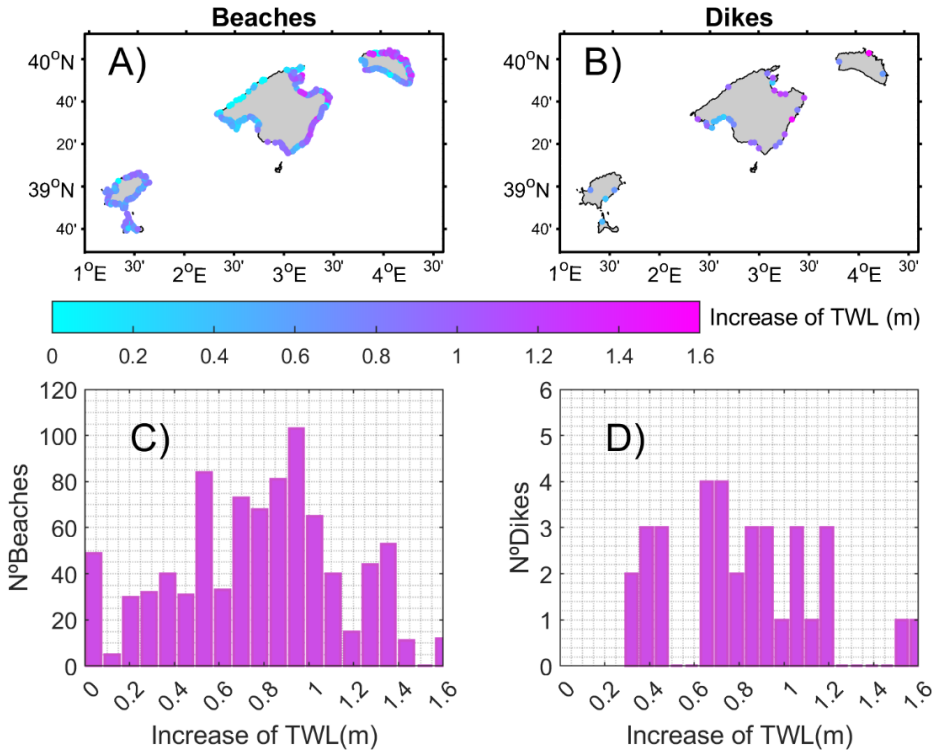

Figure 4. 6 Increase of extreme TWL in the absence of seagrasses (difference between experiment PRES_NS and experiment PRES_WS). The results are presented for the beaches (a) and the dikes (b). The histograms of the values mapped are presented in the bottom row.

4.4.3 Role of seagrasses for coastal protection under future scenarios

Extreme TWL in beaches is projected to go from 1.07 m (on average) to 1.74 m at the end of the century if seagrass meadows are conserved, while extreme TWL would go from 3.96 m to 4.63 m in ports, induced by the projected mean sea level rise. Seagrass decline is estimated to have a large effect on the extreme TWL, with moderate degradation of the meadow (density declining by 2/3 down to 200 sh/m^2 at the end of the century) leading to an increase of the extreme TWL in beaches of 1.08 m, on average, increasing from the present 1.07 m to 2.15 m (Figure 4. 7). In ports, TWL is predicted to increase from 3.96 up to 5.18 m with 2/3 loss of seagrass density. Complete seagrass loss leads to TWL increase by 1.46 m, on average, on beaches, 0.79 m of this attributable to seagrass loss, while TWL will increase by 1.49 m on ports, of which 0.82 m are attributable to seagrass loss (see Figure 4. 7 A, B and Table 4. 3). Thus, conserving seagrass meadows avoids an average 40% increase in extreme TWL on beaches under present conditions and 30% at the end of the century, compared to Balearic shorelines devoid of seagrass meadows. Under present conditions, the seagrass reduces the extreme TWL in dikes by 18% (see Figure 4. 7 C). There is, however, broad variability in these forecasts, depending on local

characteristics (Table 4. 3). This means that in some locations, the loss of seagrass can induce an increase in the extreme TWL of up to 2.35 m.

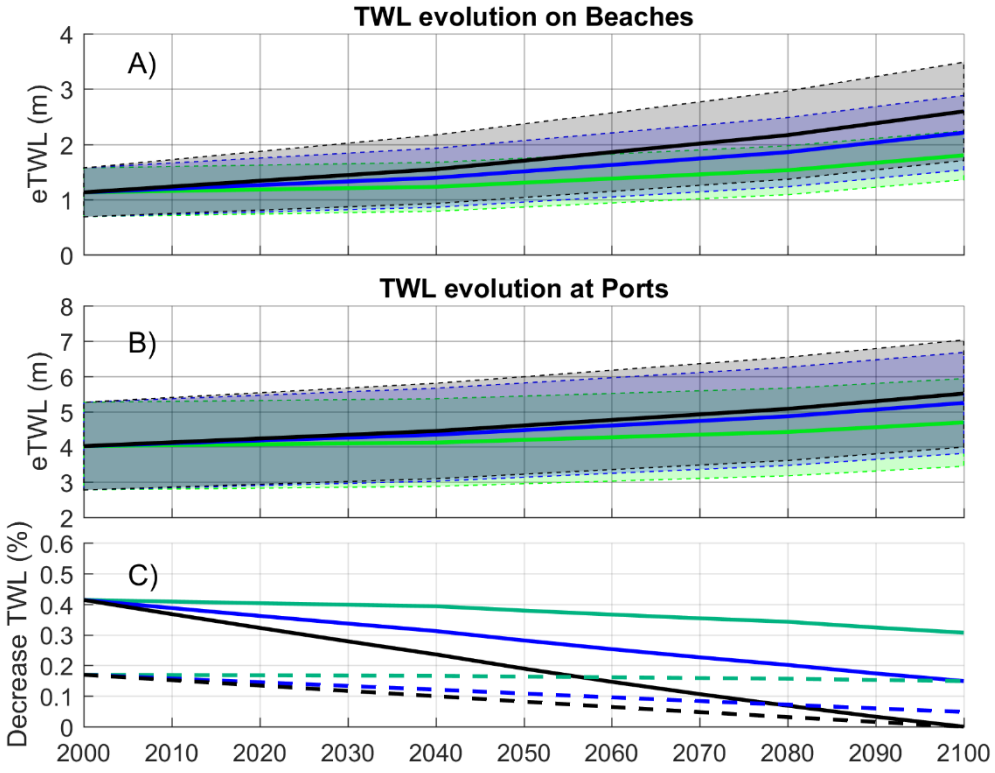

Figure 4. 7 Average evolution of extreme TWL in the Balearic Islands beaches (a) and ports (b) under RCP8.5 GHG scenario and under different scenarios for the evolution of seagrass meadows. No degradation (green lines, simulation FUT_615), moderate degradation (blue lines, simulation FUT_200) and total degradation (black lines, simulation FUT_NS). Patches represent the spatial Standard Deviation (STD) of the extreme TWL. The bottom panel, (c) represents the contribution of PO to reduce the TWL in percentage (%) with respect NS scenario.

BEACHES						
Run	Seagrass degradation in 2100	TWL_PRES Mean(min-max)	TWL_FUT Mean(min-max)	Difference Mean(min-max)	Average Contribution of MSLR (%)	Average Contribution of loss of seagrass (%)
FUT_NS	Total	1.07(0.49-2.81)	2.54(1.50-3.97)	1.46(0.64-2.35)	46	54
FUT_200	Moderate	1.07(0.49-2.81)	2.15(1.35-3.48)	1.08(0.67-1.64)	62	38
FUT_615	No degradation	1.07(0.49-2.81)	1.74(1.16-3.48)	0.67	100	0
PORTS						
Run	Seagrass degradation in 2100	TWL_PRES Mean(min-max)	TWL_FUT Mean(min-max)	Difference (m)	Average Contribution of MSLR (%)	Average Contribution of loss of seagrass (%)
FUT_NS	Total	3.96(1.93-6.99)	5.45(2.99-9.29)	1.49(0.96-2.30)	45	55
FUT_200	Moderate	3.96(1.93-6.99)	5.18(2.87-8.77)	1.22(0.87-1.77)	55	45
FUT_615	No degradation	3.96(1.93-6.99)	4.63(2.59-7.66)	0.67	100	0

Table 4. 3 Average contribution of mean sea level rise (MSLR) and loss of seagrass to extreme TWL under different scenarios of seagrass evolution. The range of values in the region is presented in brackets.

The return levels (RL) , computed using the peaks over threshold approach (Kyselý et al., 2010) associated to extreme events (see Figure S4. 7 for more details of the methodology followed), provide additional insights into the role of seagrass. An extreme TWL associated to a RL of 50 years, as could be the case of the Gloria storm in January 2020 (Amores et al., 2020), could reach a value of about 2 m in the northern beaches and 10 m on the northern dikes (Figure 4. 8 A, B black patches). In the south of Mallorca Island, the RLs are lower, being ~1.2 m and ~6.5 m for beaches and dikes, respectively. Under present marine conditions but in the absence of seagrass meadows, a one in 50 years storm like Gloria would have induced a higher TWL reaching 3.3 m and 10 m in northern beaches and dikes (Figure 4. 8 A and B blue patches) and 2.5 m and 8.0 m in the southern beaches and dikes (Figure 4. 8 C and D blue lines). Moreover, the impacts of such storm would be felt much more often: every year in beaches and every 5 years in dikes.

Assuming seagrass meadows to be conserved (Figure 4. 8 yellow), the storm-induced impacts that occur every 50 years on average at present will occur in the northern and southern dikes of the region every 23 and 12 years, respectively (Figure 4. 8). On beaches, the effects of the sea level rise would be even more acute, and the impacts associated with any storm would be similar to those that occurred with the extreme Gloria storm. Loss of seagrass meadows and sea level rise will expose the northern and southern coasts of Mallorca will be exposed to Gloria-type impacts every 3 and 2 years, respectively and the extreme TWL on the beaches would be very high, reaching 4 and 3.3 m every year, respectively, much higher than what was experienced during the Gloria storm.

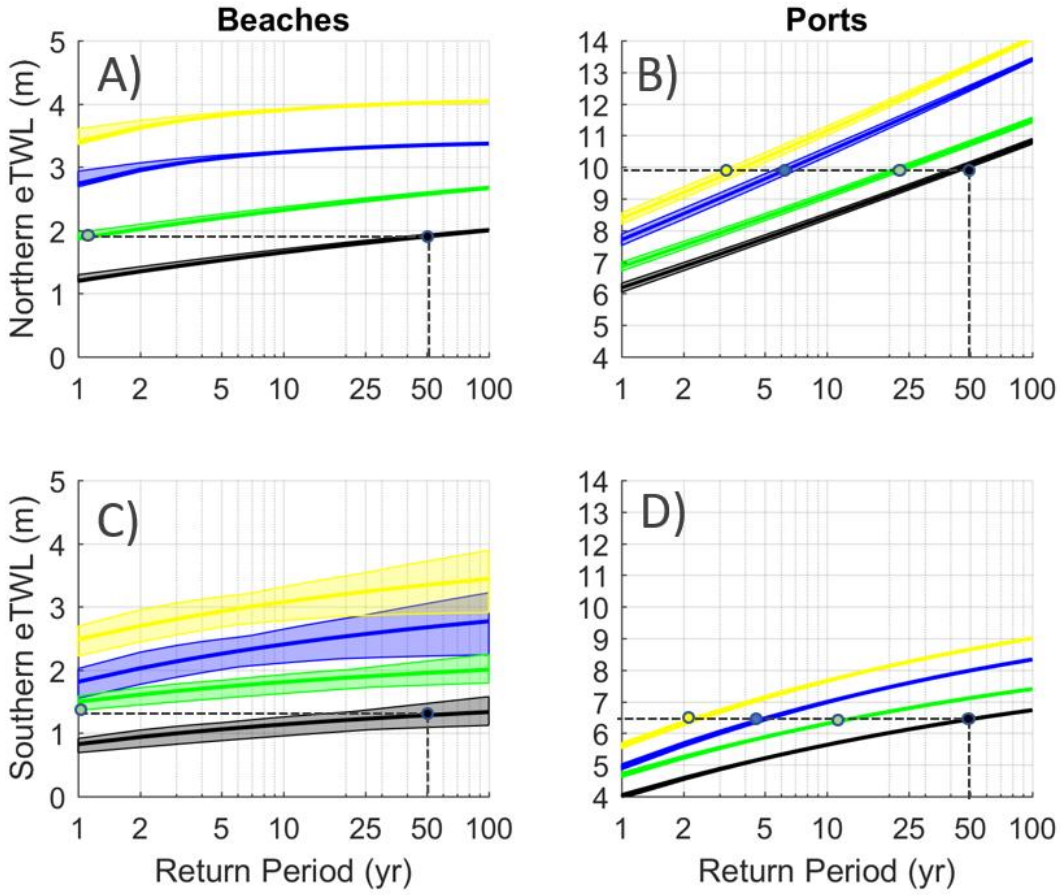

Figure 4. 8 Return Levels on beaches (left panels) and ports (right panels), in the northern (top panels) and the southern (bottom panels) coasts of Mallorca, for different scenarios of seagrass conservation and different time frames. Present conditions (black), present conditions with seagrass absence (blue), 2100 conditions with well-preserved seagrasses (green), and 2100 conditions with seagrass absence (yellow).

4.5 Discussion and conclusions

Seagrass meadows play a significant role in wave energy dissipation and, consequently, in the intensity of the coastal flooding. However, the role of seagrass conservation in protecting shorelines under climate change has not yet been quantified. Consequently, the estimates presented here provide a necessary foundation linking conservation and adaptation planning. Specifically, our model calculations show that seagrass reduces the incoming wave height by 20-30%, at the position where the ratio (depth/Hrms) is lowest (Figure 4. 2, sensor P4), in comparison to bare seabed, consistent with results from flume experiments (Fonseca and Cahalan, 1992; Koftis and Prinos, 2011; Stratigaki et al., 2011). Similar seagrass effects have been observed in field experiments, with wave height being reduced by 25-49% when compared to adjacent bare seabeds (Reidenbach and Thomas, 2018). Seagrass effects on wave damping are more intense when incoming wave energy is higher (i.e., under storm conditions), while the presence of seagrasses does not change significantly the TWL under calm conditions (Figure S4. 6). The effectiveness of the role of seagrass in attenuating wave action is also higher at shallower depths than at deeper ones, thus meadows with the upper limit located closer to the shore reduce the wave energy more effectively. Conversely, the effect of the seagrass is negligible at depths approaching the depth limit *P. Oceanica* meadows (30-40 m, (Duarte et al 2007). The effect of seagrass on wave reduction is larger at locations with gentle slopes, as the wave-

seagrass interaction lasts longer. Therefore, seagrass can reduce the extreme wave runup between 10% and 60% at beaches and between 10% and 20% in ports across the Balearic Islands, depending on the level of exposure and seagrass characteristics.

Our analyses assumes that the seabed becomes sandy when seagrass dies (i.e., bottom friction coefficient of 0.02), which is an oversimplification, since following plant dead the roots remain in the ground for a certain time forming a seabed of dense vegetation that could be considered as a reef or a rocky base in terms of friction (Manning bottom friction coefficient of 0.030-0.035). Although there is not enough information for that process to be more accurately incorporated in our scenarios, we estimated that if dead plants would form a reef, the wave runup during extreme events could be reduced 5-10% (Figure S4. 8), which has little impact on our findings.

Our assessment focused on a single emissions scenario (RCP8.5) for simplicity. Under GHG scenario RCP4.5 the mean sea level rise by 2100 is estimated to be ~0.50 m (Cramer et al., 2020; Agulles et al., 2021) and therefore the extreme TWL at the end of the century would be smaller. However, *P. Oceanica* meadows are expected to play a key role in the coastal protection under any GHG emission scenario, with their contribution to reduce extreme TWL ranging from ~30% (in the worse sea level rise scenario) to ~40% (considering no change in sea level, Figure 4. 7).

Our results show that the loss of the seagrasses would have an impact comparable to that of the projected impact of mean sea level rise, thereby doubling the impact of climate change on Balearic coastal areas. For the beaches, Agulles et al. (2021) showed that the projected mean sea level rise would imply the loss of 86 % of beach area in the Balearic Islands under storm conditions. This is similar to the effect of seagrass losses alone on beach erosion.

The dikes and seawalls of ports are typically designed to resist events with a return period of 50 years. Thus, dikes and seawalls should be re-designed, and seagrass conservation and restoration should become a priority in coastal defense plans in order to adapt to sea level rise. If coastal protection against projected sea level rise is based exclusively on hard coastal defense structures, dikes and seawalls should be re-designed to be even greater. The inclusion of seagrass meadows in coastal defense, in addition, would provide co-benefits beyond coastal protection such as mitigation of climate change, biodiversity and good water quality. Sensitivity analyses show that wave dissipation is greater when seagrass meadows reach shallow depths, have long leaves, wide stems or high shoot density, both for moderate and strong storms. These seagrass traits have similar contributions to energy dissipation, except for the extreme case that seagrass grow to 1 m depth (Figure 4. 9).

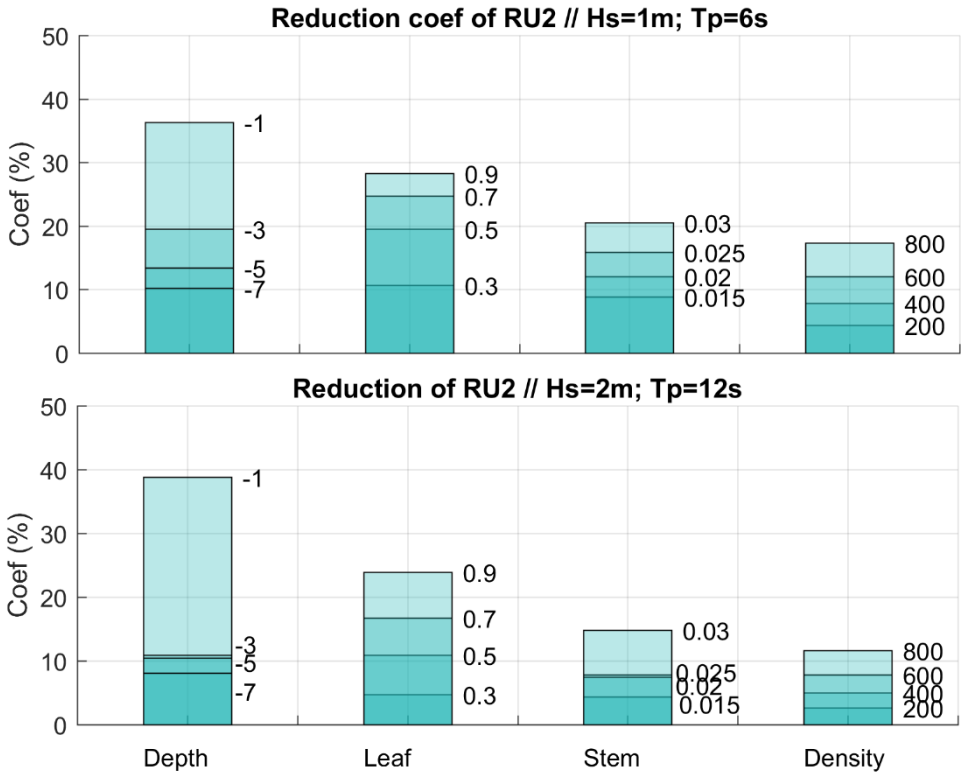

Figure 4. 9 Sensitivity experiments of wave runup reduction in the Cala Millor Beach with different characteristics of the seagrass meadow with respect to the case of not having any seagrass. First column, minimum depth of seagrass in meters. Second column, leaf in meters. Third column, Stem diameter in meters and the last column, the shoot density in number of shoots per meter square.

The results presented here reveal a prominent role of P. *Oceanica* seagrass in the defense of Balearic coastal areas. The present distribution and abundance of *P. Oceanica* around the archipelago induce a reduction of the extreme total water level (eTWL) of 0.7 m, on average, both on beaches and ports. This represents, respectively, a remarkable 40% and 15% reduction relative to the TWL expected if the region would be devoid of *P. Oceanica*. Hence, loss of seagrass would lead to the impacts that are now experienced every 50 years (e.g., Gloria storm) to recur every year on beaches and every 5 years on ports. Future impacts will be aggravated due to sea level rise and the projected loss of P. *Oceanica* with increased intensity and recurrence of marine heat waves, (Jordà et al., 2012).

Specifically, seagrasses loss would imply an average increase of the eTWL of 1.46m by end of century, with 46% of that value induced by the sea level rise and 54% due to the loss of seagrasses. If seagrass could be conserved throughout the century, the increase in the eTWL would be reduced to half, i.e., about 0.67 m, almost entirely due to the contribution of the sea level rise. In terms of the impacts associated to extreme storms, this means that impacts similar to those under the Gloria storm would be experienced, at the end of the century, every year on beaches and every 5 years on ports due to the sea level rise. If seagrasses were completely lost, such destructive impacts would be expected several times per year on beaches and every 2 years on ports. The results provide a compelling quantification of the fundamental role that seagrass meadows play in coastal defense currently and the importance of conserving seagrass to mitigate the impacts of sea level rise and increased storm activity on vulnerable coasts. Indeed, our main finding is that seagrass loss and sea level rise can have similar, and additive impacts in magnitude on Balearic coasts by the end of the century. With much of the GDP of the Balearic

Island depending on coastal tourism, similar to other island destinations around the world, the prospect is rather adverse, particularly because conservation efforts may be undermined by the vulnerability of *P. Oceanica* to climate change. Deriving innovative approaches to conserve and restore P. *Oceanica* seagrass Meadows and confer resistance to marine heat waves should be a priority to reduce impacts of sea level rise on coastal infrastructure and human lives.

Supporting information for chapter 4

Figures

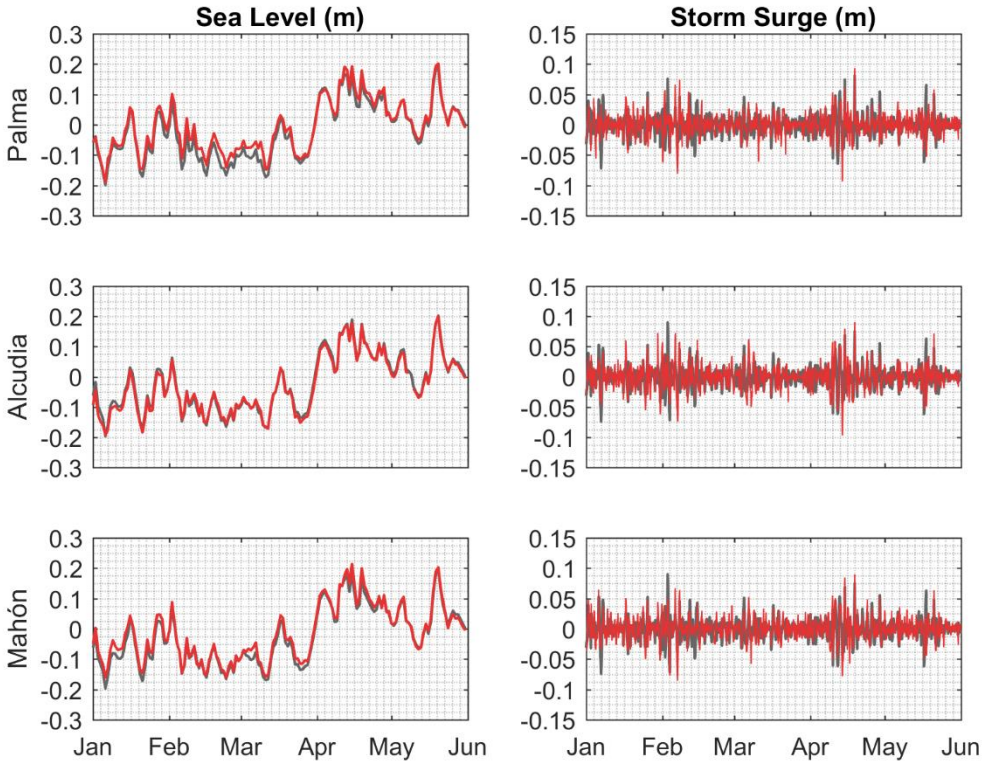

Figure S4. 1 Validation of the sea level (left panels) and storm surge (right panels) at the port of Palma (first row), Alcudia (middle row) and Mahón (bottom row). Sea level observations are represented in grey, sea level reconstruction (in red, left panel) and simulation of storm surge (in red, right panel).

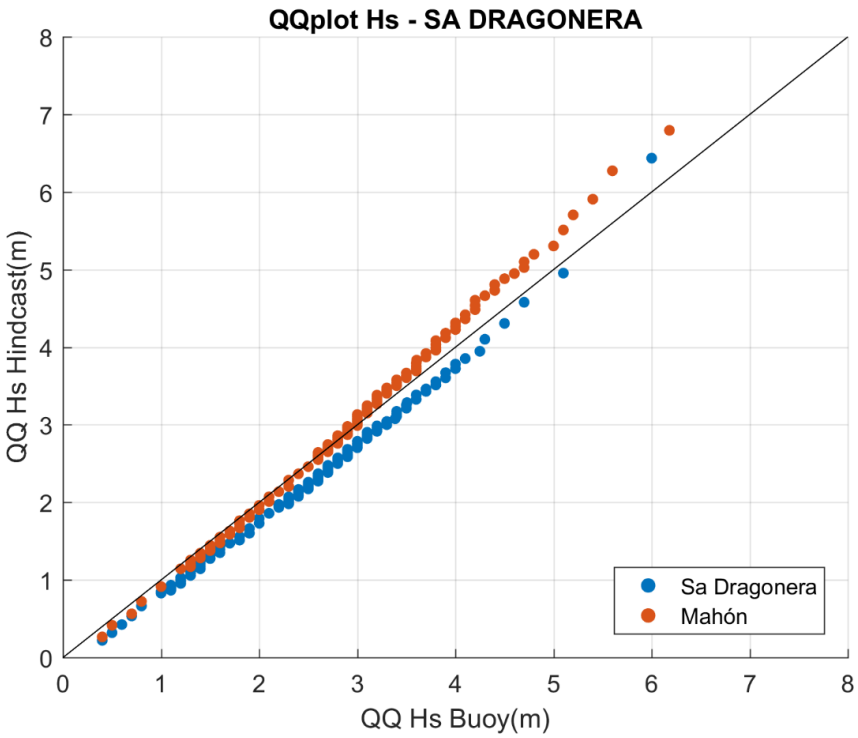

Figure S4. 2 Quantile-quantile plot of observed and simulated significant wave height (m) by Era Cosmo at Sa Dragonera buoy (blue dots) and at Mahón buoy (red dots).

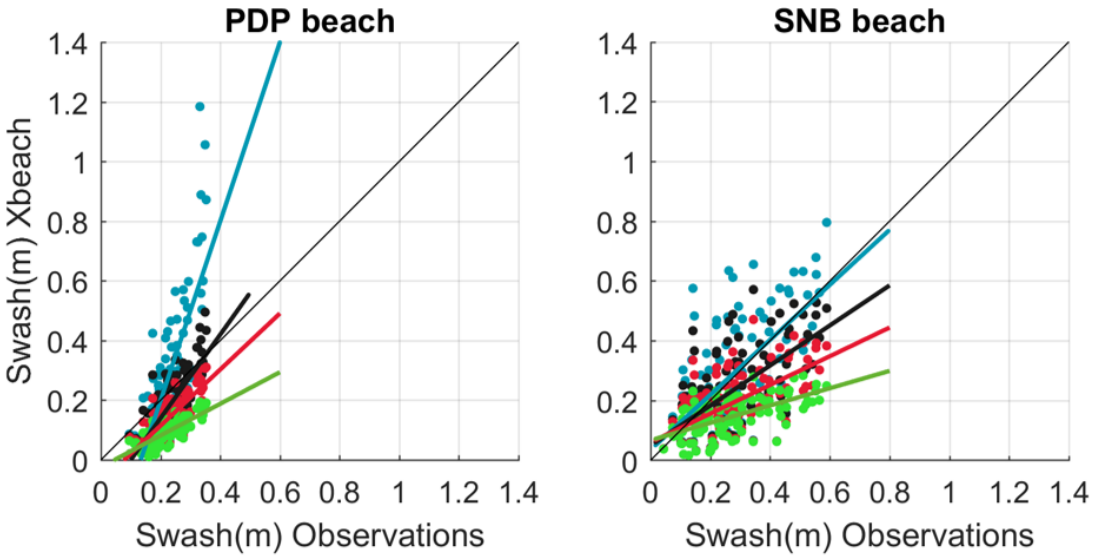

Figure S4. 3 Results of the calibration tests for the vegetation module in PDP beach (left panel) and SNB beach (right panel). Absence of seagrass (blue), with seagrass drag of 0.20 (green), 0.10 (red) and 0.05 (black).

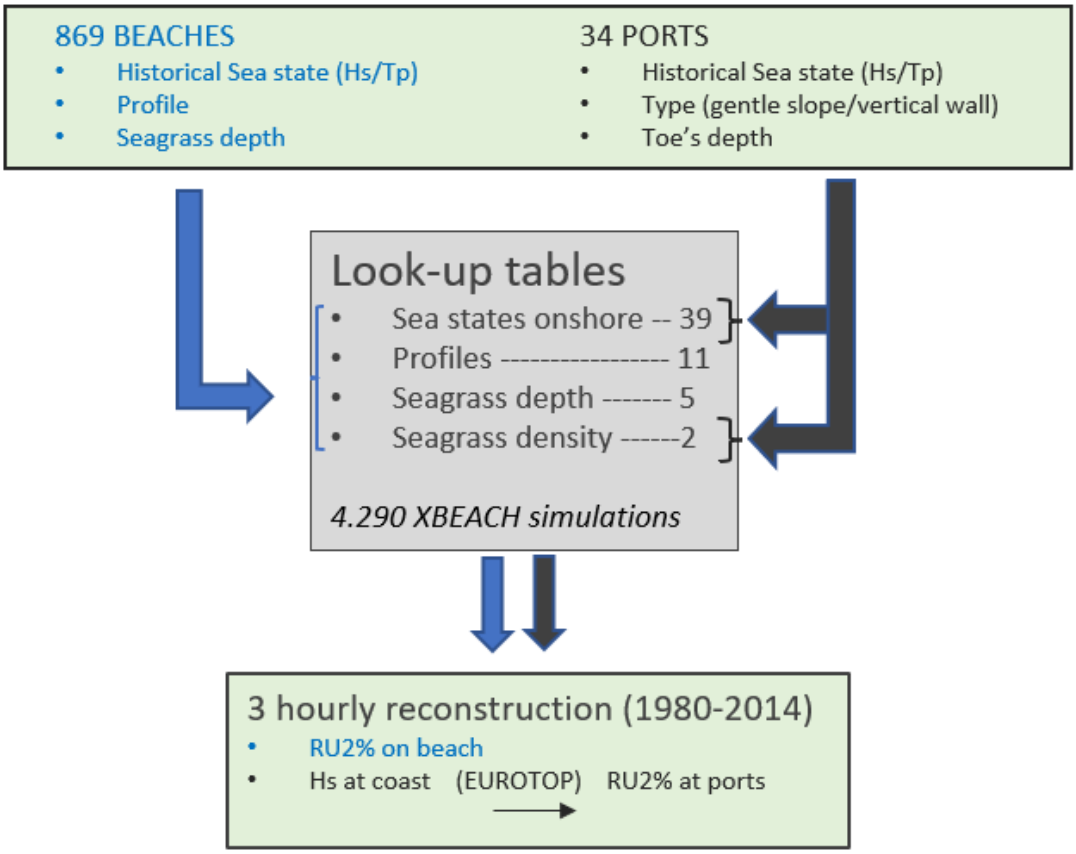

Figure S4. 4 Diagram of the procedure used to construct the look up tables that link nearshore sea states with wave runup at the coast depending on the coastal typology. Left path, for beaches (in blue) and right path, for ports (in black).

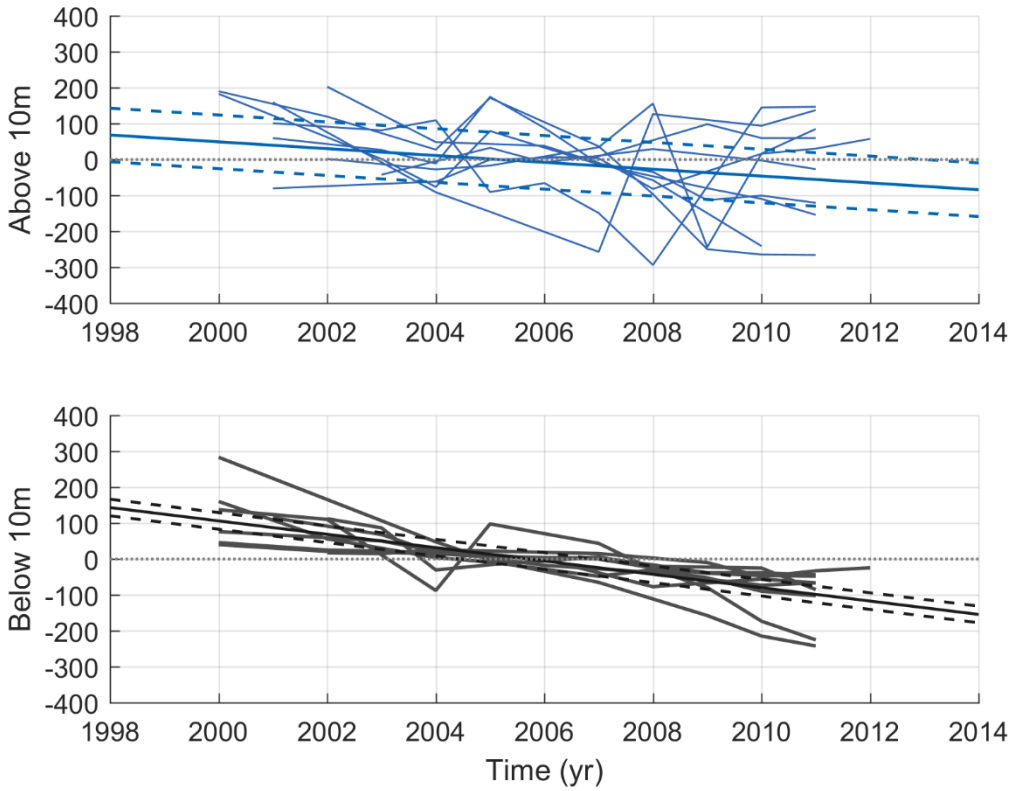

Figure S4. 5 Annual Shoot density (sh/m^2) anomaly at the 19 sampled sites from a depth shallower than 10 meters (top panel) and deeper than 10 meters (bottom panel). The linear trend is represented with a continuous line while the 0.05-0.95 confidence interval is plotted with dashed lines.

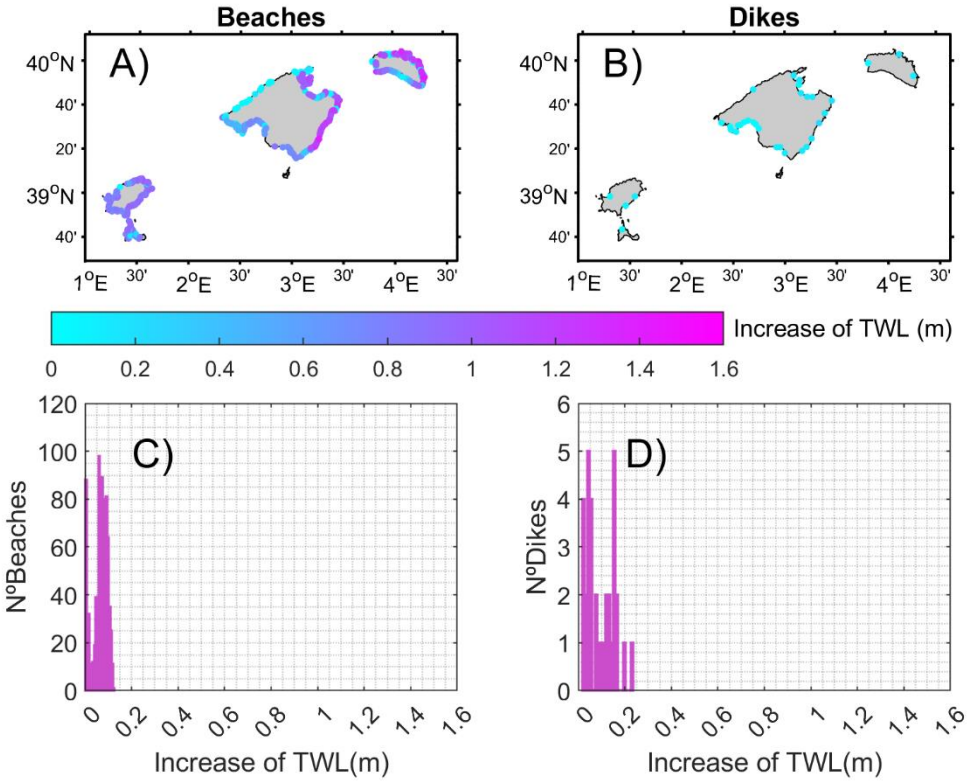

Figure S4. 6 Increase of TWL under mean conditions in the absence of seagrasses (difference between experiment PRES_NS and experiment PRES_WS). The results are presented for the beaches (left panels) and dikes (right panels). The histograms of the values mapped are presented in the bottom row.

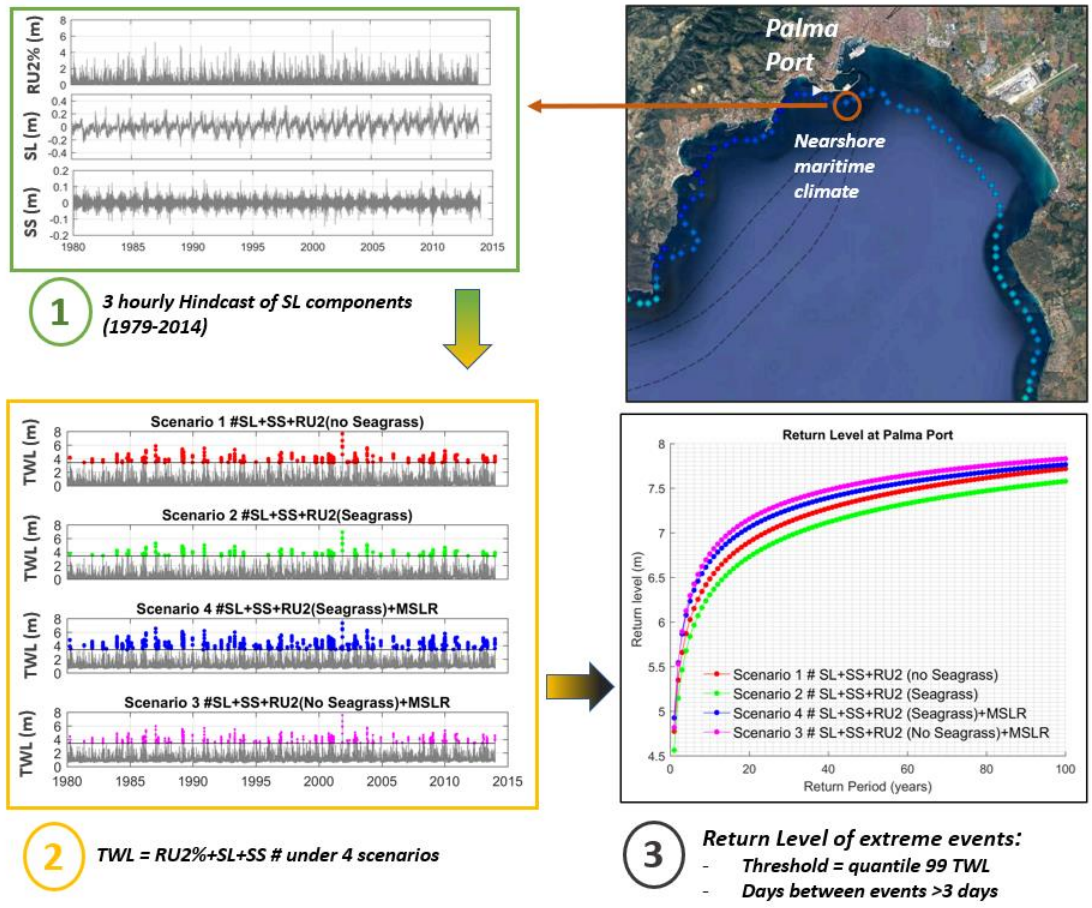

Figure S4. 7 Methodological scheme for obtaining Return Levels according to considered scenarios.

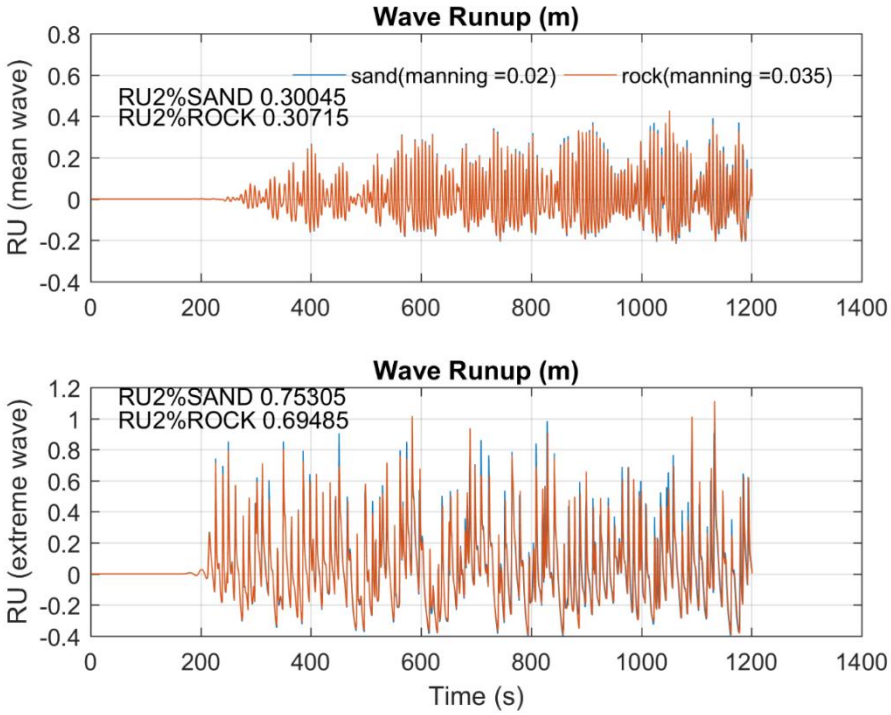

Figure S4. 8 XBEACH simulation that shows the instant wave runup under a sea state of Hs = 1m and Tp = 6s, (top panel) and a sea state of Hs = 2m and Tp = 12s (bottom panel), over sandy seabed (blue) and rock seabed (orange).

Tables

Table S4. 1 Basic information of the dikes considered in this work.

Table S4. 2 Shoot density observations in the Balearic Islands retrieved from De Los Santos et al., 2019.

This supplementary tables can be downloaded throughout this link:

https://drive.google.com/drive/folders/1EAtNTMFvVygi1rZnoXhnlUqZ78obSxDF?usp=share_link

Chapter 5

5 Conclusions

The main goal of this thesis was to contribute to the improvement of the quantification of the coastal impacts, particularly the flooding on sandy beaches in a changing climate.

First, uncertainties associated to the wave runup on sandy beaches have been obtained based on different strategies (chapter 2). To do so, we have implemented several systems based on empirical and numerical approaches and compared their results with swash observations in two different sandy beaches (Playa de Palma and Cala Millor). The results show that, depending on the choice of lateral boundary conditions, the RMSE can double, and a large bias can be induced, in the case of offshore waves are used instead of nearshore observations. Besides, uncertainties associated to unknown bathymetry, or the type of seabed considered can increase the estimation error of wave runup with the same order of magnitude. Furthermore, the approximation to calculate wave runup that considers the most sophisticated modelling system with the best information on boundary conditions, bottom topography, and seabed roughness lead to a wave runup RMSE comparable to the standard deviation of the observed runup. An important result of our study was that uncertainties associated to wave runup computations are comparable to the uncertainties associated to mean sea level rise projections. Therefore, the uncertainty associated to wave runup modelling should be considered when developing future projections of beach flooding. The results of our work could be used to get a first estimate of those uncertainties depending on the modelling system configuration.

The second goal of this thesis was to develop and apply a new methodology able to quantify beach flooding at a regional scale. In chapter 3, we have demonstrated that providing robust results of coastal flooding at a regional scale is feasible. In particular, we have developed a new and robust methodology that allows the massive analysis of flooding for a large number of beaches. This methodology allows much more reliable results than those provided by global estimates which are unable to capture local characteristics which completely determine the future evolution of the coastlines. Furthermore, the results of our approach are comparable to those performed with more sophisticated and time-consuming approaches typically implemented in single locations. The methodology has been used to quantify the beach surface loss under different climate scenarios and different wave regimes in the Balearic Islands. The results showed that, under plausible scenarios of future GHG emissions, beach flooding will increase during this century mainly because of the mean sea level rise. In contrast, storm surges and waves will slightly counteract the effects of mean sea level rise due to a projected small decrease in the intensity of marine storms in the western Mediterranean Sea. At the end of the century, the average permanent coastline retreat in the Balearic Islands will be around 10 meters. Under extreme temporary conditions, the coastline will experience a much greater setback, reaching over 23 meters in average under the most pessimistic scenario. Therefore, the average percentage of beach areas that will be permanently lost by 2100 will be slightly more than half of the beach area available nowadays. During storm conditions, more than eighty percent of the present beach area will be lost. Furthermore, those beaches that are exposed the most, with a gentle slope and relatively small beach area, will likely completely disappear by the end of the century.

The final specific goal of this thesis was to assess the role of submerged vegetation to reduce coastal impacts. This goal was addressed in chapter 4, where we performed a regional

assessment of the reduction of coastal impacts induced by the presence of seagrasses under present and future climate. To do so, a numerical modelling system able to reproduce the wave-seagrass interactions has been implemented and validated with field observations. Then, an analysis of the evolution of seagrass characteristics (i.e., front location and meadow density) during the last decades in the region was carried out to define realistic scenarios of future seagrass evolution. Finally, different simulations were performed to quantify the expected extreme total water level under different scenarios of climate and seagrass evolution. The main results showed that, in present climate, a complete loss of seagrass would imply an increase in extreme flood level of 0.7m. This would be similar to the effect of the mean sea level rise projected by the end of the century under the most pessimistic scenario. Considering future scenarios with a progressive reduction of seagrass density along with a rise of mean sea level, lead to a dramatic increase of extreme total water level (i.e., 1.5m by 2100 with respect to present conditions). Consequently, the return periods associated to extreme events will abruptly change in the coming decades. For instance, the impacts associated to marine storms that nowadays occur every 50 years (i.e., Gloria storm), would be felt every 2-3 years in ports, while, on beaches every year will experience much higher impacts than those experienced during the Gloria storm. In conclusion, the preservation and restoration of seagrasses are key actions that would help to mitigate the impacts of global warming on the Mediterranean coasts.

References

Agulles, M., Jordà, G., and Lionello, P. (2021). Flooding of Sandy Beaches in a Changing Climate. The Case of the Balearic Islands (NW Mediterranean). *Frontiers in Marine Science* 8, 1–15. doi:10.3389/fmars.2021.760725.

Alcoverro, T., Marco-Méndez, C., Minguito-Frutos, M., Boada, J., Prado, P., Sanmartí, N., et al. (2020). Efectes del temporal Gloria en els ecosistemes de Posidonia oceanica al llarg de la costa catalana.

Alvarez-ellacuria, A., Or, A., Gómez-pujol, L., Simarro, G., and Obregon, N. (2011). Geomorphology Decoupling spatial and temporal patterns in short-term beach shoreline response to wave climate. 128, 199–208. doi:10.1016/j.geomorph.2011.01.008.

Álvarez, E., Grau, A. M., Marba, N., and Carreras, D. (2015). Praderas de angiospermas marinas de Baleares. *Atlas de las praderas marinas de espana. IEO/IEL/UICN*, 179–219.

Amores, A., Marcos, M., Carrió, D. S., and Gómez-Pujol, L. (2020). Coastal impacts of Storm Gloria (January 2020) over the north-western Mediterranean. *Natural Hazards and Earth System Sciences* 20, 1955–1968.

Androulidakis, Y. S., Kombiadou, K. D., Makris, C. V, Baltikas, V. N., and Krestenitis, Y. N. (2015). Storm surges in the Mediterranean Sea: Variability and trends under future climatic conditions. *Dynamics of Atmospheres and Oceans* 71, 56–82.

Aragonés, L., Serra, J. C., Villacampa, Y., Saval, J. M., and Tinoco, H. (2016). Geomorphology New methodology for describing the equilibrium beach pro fi le applied to the Valencia ' s beaches. *Geomorphology* 259, 1–11. doi:10.1016/j.geomorph.2015.06.049.

Athanasiou, P., Van Dongeren, A., Giardino, A., Vousdoukas, M., Gaytan-Aguilar, S., and Ranasinghe, R. (2019). Global distribution of nearshore slopes with implications for coastal retreat. *Earth System Science Data* 11, 1515–1529. doi:10.5194/essd-11-1515-2019.

Atkinson, A. L., Power, H. E., Moura, T., Hammond, T., Callaghan, D. P., and Baldock, T. E. (2017). Assessment of runup predictions by empirical models on non-truncated beaches on the south-east Australian coast. *Coastal Engineering* 119, 15–31. doi:10.1016/j.coastaleng.2016.10.001.

Ballesteros, C., Jiménez, J. A., Valdemoro, H. I., and Bosom, E. (2018). Erosion consequences on beach functions along the Maresme coast (NW Mediterranean, Spain). *Natural Hazards* 90, 173–195. doi:10.1007/s11069-017-3038-5.

Barnard, P. L., Erikson, L. H., Foxgrover, A. C., Hart, J. A. F., Limber, P., Neill, A. C. O., et al. (2019). Dynamic flood modeling essential to assess the coastal impacts of climate change. 1–13. doi:10.1038/s41598-019-40742-z.

Beck, M. W., Losada, I. J., Menéndez, P., Reguero, B. G., Díaz-Simal, P., and Fernández, F. (2018). The global flood protection savings provided by coral reefs. *Nature Communications* 9. doi:10.1038/s41467-018-04568-z.

Bennett, S., Alcoverro, T., Kletou, D., Antoniou, C., Boada, J., Buñuel, X., et al. (2021). Resilience of seagrass populations to thermal stress does not reflect regional differences in ocean climate. *New Phytologist*. doi:10.1111/nph.17885.

Bernabeu, A. M., and Vidal, C. (2001). Estudio morfológico del perfil de playa: modelo de perfil de equilibrio en dos tramos.

Bernabéu, A., Medina, R., Vidal, C., and Muñoz Pérez, J. J. (2001). Estudio morfológico del perfil de playa: modelo de perfil de equilibrio en dos tramos.

Bernabeu Tello, A., Vidal, C., and Medina, R. (2001). Estudio morfológico del perfil de playa: modelo de perfil de equilibrio en dos tramos: modelo de perfil de equilibrio en dos tramos. *Revista de la Sociedad Geológica de España* 14, 227–236.

Bidlot, J. R. (2017). Twenty-one years of wave forecast verification. *ECMWF Newsletter* 150, 31–36.

Blackwell, B. D., Raybould, M., and Lazarow, N. (2013). Beaches as societal assets: Council expenditures, recreational returns, and climate change. *Handbook of Tourism Economics: Analysis, New Applications and Case Studies*, 443–467. doi:10.1142/9789814327084_0020.

Blair, T. C., and McPherson, J. G. (1999). Grain-size and textural classification of coarse sedimentary particles. *Journal of Sedimentary Research* 69, 6–19. doi:10.2110/jsr.69.6.

Bonaduce, A., Pinardi, N., Oddo, P., Spada, G., and Larnicol, G. (2016). Sea-level variability in the Mediterranean Sea from altimetry and tide gauges. *Climate Dynamics* 47, 2851–2866. doi:10.1007/s00382-016-3001-2.

Booij, N., and Holthuijsen, L. H. (1987). Propagation of ocean waves in discrete spectral wave models. *Journal of Computational Physics* 68, 307–326.

Borsje, B. W., van Wesenbeeck, B. K., Dekker, F., Paalvast, P., Bouma, T. J., van Katwijk, M. M., et al. (2011). How ecological engineering can serve in coastal protection. *Ecological Engineering* 37, 113–122. doi:10.1016/j.ecoleng.2010.11.027.

Borum, J., Duarte, C. M., Greve, T. M., and Krause-Jensen, D. (2004). *European seagrasses: an introduction to monitoring and management*. M & MS project.

Bouma, T. J., van Belzen, J., Balke, T., Zhu, Z., Airoldi, L., Blight, A. J., et al. (2014). Identifying knowledge gaps hampering application of intertidal habitats in coastal protection: Opportunities & steps to take. *Coastal Engineering* 87, 147–157. doi:10.1016/j.coastaleng.2013.11.014.

Bruun, P. (1962). Sea-level rise as a cause of shore erosion. *Journal of the Waterways and Harbors division* 88, 117–130.

Caffyn, A., Prosser, B., and Jobbins, G. (2002). Socio-economic framework–a framework for the analysis of socio-economic impacts on beach environments. *Baseline research for the integrated sustainable management of Mediterranean sensitive coastal ecosystems*, 37–51.

Camus, P., Mendez, F. J., and Medina, R. (2011a). A hybrid efficient method to downscale wave climate to coastal areas. *Coastal Engineering* 58, 851–862. doi:10.1016/j.coastaleng.2011.05.007.

Camus, P., Mendez, F. J., Medina, R., and Cofiño, A. S. (2011b). Analysis of clustering and selection algorithms for the study of multivariate wave climate. *Coastal Engineering* 58, 453–462. doi:10.1016/j.coastaleng.2011.02.003.

Camus, P., Mendez, F. J., Medina, R., Tomas, A., and Izaguirre, C. (2013). High resolution downscaled ocean waves (DOW) reanalysis in coastal areas. *Coastal Engineering* 72, 56–68. doi:10.1016/j.coastaleng.2012.09.002.

Cebrián, J., Duarte, C. M., Marbà, N., Enríquez, S., Gallegos, M., and Olesen, B. (1996).

Herbivory on Posidonia oceanica: Magnitude and variability in the Spanish Mediterranean. *Marine Ecology Progress Series* 130, 147–155. doi:10.3354/meps130147.

Chen, G., Xiong, Q., Morris, P. J., Paterson, E. G., Sergeev, A., and Wang, Y. (2014). OpenFOAM for computational fluid dynamics. *Notices of the AMS* 61, 354–363.

Cherif, S., Doblas-Miranda, E., Lionello, P., Borrego, C., Giorgi, F., Iglesias, A., et al. (2020). Chapter 2 Drivers of Change. *Climate and Environmental Change in the Mediterranean Basin – Current Situation and Risks for the Future. First Mediterranean Assessment Report*, 1–26.

Chust, G., González, M., Fontán, A., Revilla, M., Alvarez, P., Santos, M., et al. (2022). Climate regime shifts and biodiversity redistribution in the Bay of Biscay. *Science of the Total Environment* 803. doi:10.1016/j.scitotenv.2021.149622.

Cobb, K. M., Rojas, M., Chen, D., Samset, B. H., Diongue-Niang, A., Edwards, P. N., et al. (2021). Framing, context, and methods. in *AGU Fall Meeting 2021* (AGU).

Coccossis, H., and Koutsopoulou, A. (2020). Measuring and monitoring sustainability of coastal tourism destinations in the Mediterranean. *Tourism: An International Interdisciplinary Journal* 68, 482–498.

Cramer, W., Guiot, J., Marini, K., Secretariat, M., and Bleu, P. (2020). Climate and environmental change in the mediterranean basin–current situation and risks for the future. *First Mediterranean Assessment Report. MedECC (Mediterranean Experts on Climate and Environmental Change). Union for the Mediterranean, Plan Bleu, UNEP/MAP, Marseille, France*.

Crossland, C. J., Baird, D., Ducrotoy, J.-P., Lindeboom, H., Buddemeier, R. W., Dennison, W. C., et al. (2005). The Coastal Zone — a Domain of Global Interactions. 1–37. doi:10.1007/3-540-27851-6_1.

Dangendorf, S., Marcos, M., Wöppelmann, G., Conrad, C. P., Frederikse, T., and Riva, R. (2017). Reassessment of 20th century global mean sea level rise. *Proceedings of the National Academy of Sciences of the United States of America* 114, 5946–5951. doi:10.1073/pnas.1616007114.

De Leo, F., Besio, G., and Mentaschi, L. (2021). Trends and variability of ocean waves under RCP8.5 emission scenario in the Mediterranean Sea. *Ocean Dynamics* 71, 97–117. doi:10.1007/s10236-020-01419-8.

de los Santos, C. B., Krause-Jensen, D., Alcoverro, T., Marbà, N., Duarte, C. M., van Katwijk, M. M., et al. (2019). Recent trend reversal for declining European seagrass meadows. *Nature Communications* 10, 1–8. doi:10.1038/s41467-019-11340-4.

Dean, R. G., and Dalrymple, R. A. (1991). *Water wave mechanics for engineers and scientists*. World Scientific Publishing Company.

Di Luccio, D., Benassai, G., Budillon, G., Mucerino, L., Montella, R., and Pugliese Carratelli, E. (2018). Wave run-up prediction and observation in a micro-tidal beach. *Natural Hazards and Earth System Sciences* 18, 2841–2857. doi:10.5194/nhess-18-2841-2018.

Didier, D., Bernatchez, P., Boucher-Brossard, G., Lambert, A., Fraser, C., Barnett, R. L., et al. (2015). Coastal flood assessment based on field debris measurements and wave runup empirical model. *Journal of Marine Science and Engineering* 3, 560–590. doi:10.3390/jmse3030560.

Duarte, C. M., Losada, I. J., Hendriks, I. E., Mazarrasa, I., and Marbà, N. (2013). The role of coastal plant communities for climate change mitigation and adaptation. *Nature Climate Change* 3, 961–968. doi:10.1038/nclimate1970.

Enríquez, A. R., and Bujosa Bestard, A. (2020). Measuring the economic impact of climate-induced environmental changes on sun-and-beach tourism. *Climatic Change* 160, 203–217. doi:10.1007/s10584-020-02682-w.

Enríquez, A. R., Marcos, M., Álvarez-Ellacuría, A., Orfila, A., and Gomis, D. (2017). Changes in beach shoreline due to sea level rise and waves under climate change scenarios: Application to the Balearic Islands (western Mediterranean). *Natural Hazards and Earth System Sciences* 17, 1075–1089. doi:10.5194/nhess-17-1075-2017.

Enríquez, A. R., Marcos, M., Falqués, A., and Roelvink, D. (2019). Assessing beach and dune erosion and vulnerability under sea level rise: A Case study in the Mediterranean Sea. *Frontiers in Marine Science* 6, 1–12. doi:10.3389/fmars.2019.00004.

European Environment Agency (2015). Mediterranean Sea region briefing - The European environment ? state and outlook 2015. *European Environment Agency*, 1–6. Available at: https://www.eea.europa.eu/soer-2015/countries/black-sea.

Eurotop (2018). Eurotop 2018; Manual on wave overtopping of sea defences and related structures. An overtopping manual largely based on European research, but for worldwide application. 320. Available at: www.overtopping-manual.com.

Falco, G. De, Budillon, F., Conforti, A., Muro, S. De, Martino, D., Innangi, S., et al. (2014). Sandy beaches characterization and management of coastal erosion on western Sardinia island (Mediterranean Sea). Sandy beaches characterization and management of coastal erosion on western Sardinia island (Mediterranean Sea). doi:10.2112/SI70-067.1.

Fonseca, M. S., and Cahalan, J. A. (1992). A preliminary evaluation of wave attenuation by four species of seagrass. *Estuarine, Coastal and Shelf Science* 35, 565–576. doi:10.1016/S0272-7714(05)80039-3.

Gacia, E., and Duarte, C. M. (2001). Sediment Retention by a Mediterranean Posidonia oceanica Meadow : The Balance between Deposition and Resuspension. 505–514. doi:10.1006/ecss.2000.0753.

Galofré, J., Medina, R., Vidal Pascual, C., Bernabeu Tello, A., and González, M. (2001). Modelado de la morfodinámica de playas por medio de formulaciones de “Equilibrio.” *Física de la tierra*, 95–117. doi:10.5209/rev_FITE.2001.n13.12771.

Garrabou, J., Gómez-Gras, D., Medrano, A., Cerrano, C., Ponti, M., Schlegel, R., et al. (2022). Marine heatwaves drive recurrent mass mortalities in the Mediterranean Sea. *Global Change Biology* 28, 5708–5725.

Garrett, J. K., Clitherow, T. J., White, M. P., Wheeler, B. W., and Fleming, L. E. (2019). Coastal proximity and mental health among urban adults in England: The moderating effect of household income. *Health and Place* 59, 102200. doi:10.1016/j.healthplace.2019.102200.

Gera, A., Pagès, J. F., Arthur, R., Farina, S., Roca, G., Romero, J., et al. (2014). The effect of a centenary storm on the long-lived seagrass posidonia oceanica. *Limnology and Oceanography* 59, 1910–1918. doi:10.4319/lo.2014.59.6.1910.

Giorgi, F. (2010). Uncertainties in climate change projections, from the global to the regional scale. *EPJ Web of Conferences* 9, 115–129. doi:10.1051/epjconf/201009009.

Gomes da Silva, P., Coco, G., Garnier, R., and Klein, A. H. F. (2020). On the prediction of runup, setup and swash on beaches. *Earth-Science Reviews* 204, 103148. doi:10.1016/j.earscirev.2020.103148.

Gomes da Silva, P., Medina, R., González, M., and Garnier, R. (2018). Infragravity swash parameterization on beaches: The role of the profile shape and the morphodynamic beach state. *Coastal Engineering* 136, 41–55. doi:10.1016/j.coastaleng.2018.02.002.

Gómez-pujol, L., Or, A., Álvarez-ellacuría, A., and Tintoré, J. (2011). Geomorphology Controls on sediment dynamics and medium-term morphological change in a barred microtidal beach (Cala Millor , Mallorca , Western Mediterranean). 132, 87–98. doi:10.1016/j.geomorph.2011.04.026.

Gomis, D., Tsimplis, M., Marcos, M., Fenoglio-Marc, L., Pérez, B., Raicich, F., et al. (2012). *Mediterranean sea-level variability and trends*. doi:10.1016/B978-0-12-416042-2.00004-5.

Gutiérrez Serret, R., and Grassa Garridob, J. M. (2015). Diseno, construccion y explotacion de diques de abrigo portuario en Espana desde finales del siglo XX. *Ribagua* 2, 80–96. doi:10.1016/j.riba.2015.10.004.

Harley, M., Armaroli, C., and Ciavola, P. (2011). Evaluation of XBeach predictions for a real-time warning system in Emilia-Romagna, Northern Italy. *Journal of Coastal Research*, 1861–1865.

Hasselmann, K., Hasselmann, S., Bauer, E., Janssen, P. A. E. M., Komen, G. J., Bertotti, L., et al. (1988). The WAM model - a third generation ocean wave prediction model. *J. Phys. Oceanogr.* 18, 1775–1810. doi:10.1175/1520-0485(1988)018<1775:twmtgo>2.0.co;2.

Hawkins, E., and Sutton, R. (2009). The potential to narrow uncertainty in regional climate predictions. *Bulletin of the American Meteorological Society* 90, 1095–1108.

Holman, R. A. (1986). Extreme value statistics for wave run-up on a natural beach. *Coastal Engineering* 9, 527–544. doi:10.1016/0378-3839(86)90002-5.

Holman, R. A., and Guza, R. T. (1984). Measuring run-up on a natural beach. *Coastal Engineering* 8, 129–140. doi:10.1016/0378-3839(84)90008-5.

Horton, B. P., Khan, N. S., Cahill, N., Lee, J. S. H., Shaw, T. A., Garner, A. J., et al. (2020). Estimating global mean sea-level rise and its uncertainties by 2100 and 2300 from an expert survey. *npj Climate and Atmospheric Science* 3, 1–8. doi:10.1038/s41612-020-0121-5.

Infantes, E., Orfila, A., Simarro, G., Terrados, J., Luhar, M., and Nepf, H. (2012). Effect of a seagrass (Posidonia oceanica) meadow on wave propagation. *Marine Ecology Progress Series* 456, 63–72. doi:10.3354/meps09754.

Jiménez, J. A., and Valdemoro, H. I. (2019). *Shoreline Evolution and its Management Implications in Beaches Along the Catalan Coast : Dynamic Processes , Sediments and Management Chapter 32 Shoreline Evolution and its Management Implications in Beaches Along the Catalan Coast*. Springer International Publishing doi:10.1007/978-3-319-93169-2.

Jordà, G., Marbà, N., and Duarte, C. M. (2012). Mediterranean seagrass vulnerable to regional climate warming. *Nature Climate Change* 2, 821–824. doi:10.1038/nclimate1533.

Kernkamp, H. W. J., Van Dam, A., Stelling, G. S., and De Goede, E. D. (2011). Efficient scheme

for the shallow water equations on unstructured grids with application to the Continental Shelf. *Ocean Dynamics* 61, 1175–1188. doi:10.1007/s10236-011-0423-6.

Kirchner, J. (2001). Data analysis toolkit# 5: uncertainty analysis and error propagation. *University of California Berkeley Seismological Laboratory. Available online at: http://seismo. berkeley. edu/~ kirchner/eps_120/Toolkits/Toolkit_05. pdf*.

Koftis, T. K., and Prinos, P. (2011). Spectral wave attenuation over Posidonia Oceanica. *34th IAHR Congress 2011 - Balance and Uncertainty: Water in a Changing World, Incorporating the 33rd Hydrology and Water Resources Symposium and the 10th Conference on Hydraulics in Water Engineering*, 935–942.

Krestenitis, Y., Pytharoulis, I., Karacostas, T. S., Androulidakis, Y., Makris, C., Kombiadou, K., et al. (2017). Severe Weather Events and Sea Level Variability Over the Mediterranean Sea: The WaveForUs Operational Platform. 63–68. doi:10.1007/978-3-319-35095-0_9.

Kudale, M. D. (2010). Impact of port development on the coastline and the need for protection. *Indian Journal of Marine Sciences* 39, 597–604.

Kyselý, J., Picek, J., and Beranová, R. (2010). Estimating extremes in climate change simulations using the peaks-over-threshold method with a non-stationary threshold. *Global and Planetary Change* 72, 55–68.

Lange, A. M. Z., Fiedler, J. W., Becker, J. M., Merrifield, M. A., and Guza, R. T. (2022). Estimating runup with limited bathymetry ☆. *Coastal Engineering* 172, 104055. doi:10.1016/j.coastaleng.2021.104055.

Lin, P., and Liu, P. L.-F. (1998). A numerical study of breaking waves in the surf zone. *Journal of fluid mechanics* 359, 239–264.

Lionello, P., Mufato, R., and Tomasin, A. (2005). Sensitivity of free and forced oscillations of the Adriatic Sea to sea level rise. *Climate Research* 29, 23–39. doi:10.3354/cr029023.

Lionello, P., Ozsoy, E., Planton, S., and Zanchetta, G. (2017). Climate variability and change in the Mediterranean region. *Global Planet. Change* 151, 1–3.

Loarca, A. L., Cobos, M., Millares, A., Besio, G., and Baquerizo, A. (2020). Integrated extreme sea level events in the Mediterranean coast of Spain. Copernicus Meetings.

Luijendijk, A., Hagenaars, G., Ranasinghe, R., Baart, F., Donchyts, G., and Aarninkhof, S. (2018). The State of the World's Beaches. *Scientific Reports* 8, 1–11. doi:10.1038/s41598-018-24630-6.

Luque, P., Gómez-Pujol, L., Marcos, M., and Orfila, A. (2021). Coastal Flooding in the Balearic Islands During the Twenty-First Century Caused by Sea-Level Rise and Extreme Events. *Frontiers in Marine Science* 8, 1–21. doi:10.3389/fmars.2021.676452.

Marbà, N., Díaz-Almela, E., and Duarte, C. M. (2014). Mediterranean seagrass (Posidonia oceanica) loss between 1842 and 2009. *Biological Conservation* 176, 183–190.

Marbà, N., and Duarte, C. M. (2010). Mediterranean warming triggers seagrass (Posidonia oceanica) shoot mortality. *Global Change Biology* 16, 2366–2375. doi:10.1111/j.1365-2486.2009.02130.x.

Marbà, N., Jordà, G., Bennett, S., and Duarte, C. M. (2022). Seagrass Thermal Limits and Vulnerability to Future Warming. *Frontiers in Marine Science* 9, 1–10. doi:10.3389/fmars.2022.860826.

Marcos, M., and Tsimplis, M. N. (2007). Forcing of coastal sea level rise patterns in the North Atlantic and the Mediterranean Sea. *Geophysical Research Letters* 34. doi:10.1029/2007GL030641.

Maza, M., Lara, J. L., and Losada, I. J. (2013). A coupled model of submerged vegetation under oscillatory flow using Navier-Stokes equations. *Coastal Engineering* 80, 16–34. doi:10.1016/j.coastaleng.2013.04.009.

Medvedev, O., Shepherd, D., and Hautus, M. J. (2015). The restorative potential of soundscapes: A physiological investigation. *Applied Acoustics* 96, 20–26. doi:10.1016/j.apacoust.2015.03.004.

Mejjad, N., Rossi, A., and Pavel, A. B. (2022). The coastal tourism industry in the Mediterranean: A critical review of the socio-economic and environmental pressures & impacts. *Tourism Management Perspectives* 44, 101007. doi:10.1016/j.tmp.2022.101007.

Mendez, F. J., and Losada, I. J. (2004). An empirical model to estimate the propagation of random breaking and nonbreaking waves over vegetation fields. *Coastal Engineering* 51, 103–118. doi:10.1016/j.coastaleng.2003.11.003.

Menéndez, P., Losada, I. J., Torres-Ortega, S., Narayan, S., and Beck, M. W. (2020). The Global Flood Protection Benefits of Mangroves. *Scientific Reports* 10. doi:10.1038/s41598-020-61136-6.

Molinari, R. L., and Mestas-Nunez, A. M. (2003). North Atlantic decadal variability and the formation of tropical storms and hurricanes. *Geophysical Research Letters* 30, 1996–1999. doi:10.1029/2002gl016462.

Monserrat, S., Vilibić, I., and Rabinovich, A. B. (2006). Meteotsunamis: atmospherically induced destructive ocean waves in the tsunami frequency band. *Natural hazards and earth system sciences* 6, 1035–1051.

Morton, R. A., and Sallenger, A. H. (2003). Morphological impacts of extreme storms on sandy beaches and barriers. *Journal of Coastal Research* 19, 560–573.

Oddo, P. C., Lee, B. S., Garner, G. G., Srikrishnan, V., Reed, P. M., Forest, C. E., et al. (2020). Deep Uncertainties in Sea-Level Rise and Storm Surge Projections: Implications for Coastal Flood Risk Management. *Risk Analysis* 40, 153–168. doi:10.1111/risa.12888.

Ondiviela, B., Losada, I. J., Lara, J. L., Maza, M., Galván, C., Bouma, T. J., et al. (2014). The role of seagrasses in coastal protection in a changing climate. *Coastal Engineering* 87, 158–168. doi:10.1016/j.coastaleng.2013.11.005.

Oppenheimer, M., Glavovic, B., Hinkel, J., van de Wal, R., Magnan, A. K., Abd-Elgawad, A., et al. (2019). Sea level rise and implications for low lying islands, coasts and communities.

Orams, M. B. (2003). Sandy beaches as a tourism attraction: a management challenge for the 21 st century. *Journal of Coastal Research*, 74–84.

Orejarena-Rondón, A. F., Sayol, J. M., Marcos, M., Otero, L., Restrepo, J. C., Hernández-Carrasco, I., et al. (2019). Coastal Impacts Driven by Sea-Level Rise in Cartagena de Indias. *Frontiers in Marine Science* 6. doi:10.3389/fmars.2019.00614.

Pickering, M. D., Horsburgh, K. J., Blundell, J. R., Hirschi, J. J. M., Nicholls, R. J., Verlaan, M., et al. (2017). The impact of future sea-level rise on the global tides. *Continental Shelf Research* 142, 50–68. doi:10.1016/j.csr.2017.02.004.

Pilar, P., Soares, C. G., and Carretero, J. C. (2008). 44-year wave hindcast for the North East

Atlantic European coast. *Coastal Engineering* 55, 861–871. doi:10.1016/j.coastaleng.2008.02.027.

Pörtner, H.-O., Roberts, D. C., Masson-Delmotte, V., Zhai, P., Tignor, M., Poloczanska, E., et al. (2019). Technical summary. *IPCC special report on the ocean and cryosphere in a changing climate. Available: www. ipcc. ch/site/assets/uploads/sites/3/2019/11/04_SROCC_TS_FINAL. pdf.(July 2020)*, 61.

Qiu, Z., Qiao, F., Jang, C. J., Zhang, L., and Song, Z. (2021). Evaluation and projection of global marine heatwaves based on CMIP6 models. *Deep-Sea Research Part II: Topical Studies in Oceanography* 194, 104998. doi:10.1016/j.dsr2.2021.104998.

Ramos Alcántara, J., Gomis, D., and Jordà, G. (2022). Reconstruction of Mediterranean coastal sea level at different timescales based on tide gauge records. *EGUsphere*, 1–32.

Ranftl, S., von der Linden, W., and Committee, M. 2021 S. (2021). Bayesian surrogate analysis and uncertainty propagation. in *Physical Sciences Forum* (MDPI), 6.

Ratsimandresey, A. W., Sotillo, M. G., Álvarez Fanjul, E., Carretero Albiach, J. C., Pérez Gómez, B., and Hajji, H. (2008). A 44-year (1958-2001) sea level residual hindcast over the Mediterranean Basin. *Physics and Chemistry of the Earth* 33, 250–259. doi:10.1016/j.pce.2007.02.002.

Reidenbach, M. A., and Thomas, E. L. (2018). Influence of the Seagrass, Zostera marina, on wave attenuation and bed shear stress within a shallow coastal bay. *Frontiers in Marine Science* 5, 1–16. doi:10.3389/fmars.2018.00397.

Rodrigue, J.-P., and Notteboom, T. (2020). Ports and economic development. *T. Nottleboom, P. Athanasios, & J.-P. Rodrigue, Port Economics, Management and Policy. New York: Routledge*.

Rodríguez, E. M. G. (1995). Morfologia de playas en equilibrio. Planta y perfil.

Roelvink, D., McCall, R., Mehvar, S., Nederhoff, K., and Dastgheib, A. (2018). Improving predictions of swash dynamics in XBeach: The role of groupiness and incident-band runup. *Coastal Engineering* 134, 103–123. doi:10.1016/j.coastaleng.2017.07.004.

Roelvink, D., van Dongeren, A., McCall, R., Hoonhout, B., van Rooijen, A., van Geer, P., et al. (2015). XBeach Technical Reference : Kingsday Release. 1–141. doi:10.13140/RG.2.1.4025.6244.

Roland, A., and Ardhuin, F. (2014). On the developments of spectral wave models: Numerics and parameterizations for the coastal ocean Topical Collection on the 7th International Conference on Coastal Dynamics in Arcachon, France 24-28 June 2013. *Ocean Dynamics* 64, 833–846. doi:10.1007/s10236-014-0711-z.

Rovira Soto, M. T., and Anton Clavé, S. (2017). Second homes and urban landscape patterns in Mediterranean coastal tourism destinations. *Land Use Policy* 68, 117–132. doi:10.1016/j.landusepol.2017.07.018.

Ruiz, J. M., Guillén, E., Ramos Segura, A., and Otero, M. (2015). *Atlas de las praderas marinas de España*. Instituto Español de Oceanografía.

Ruti, P. M., Somot, S., Giorgi, F., Dubois, C., Flaounas, E., Obermann, A., et al. (2016). Med-CORDEX initiative for Mediterranean climate studies. *Bulletin of the American Meteorological Society* 97, 1187–1208. doi:10.1175/BAMS-D-14-00176.1.

Satta, A., Puddu, M., Venturini, S., and Giupponi, C. (2017). Assessment of coastal risks to

climate change related impacts at the regional scale: The case of the Mediterranean region. *International Journal of Disaster Risk Reduction* 24, 284–296. doi:10.1016/j.ijdrr.2017.06.018.

Serafin, K. A., Ruggiero, P., Barnard, P. L., and Stockdon, H. F. (2019). The influence of shelf bathymetry and beach topography on extreme total water levels: Linking large-scale changes of the wave climate to local coastal hazards. *Coastal Engineering* 150, 1–17. doi:10.1016/j.coastaleng.2019.03.012.

Shimura, T., Pringle, W. J., Mori, N., Miyashita, T., and Yoshida, K. (2022). Seamless Projections of Global Storm Surge and Ocean Waves Under a Warming Climate. *Geophysical Research Letters* 49, 1–8. doi:10.1029/2021GL097427.

Shukla, P. R., Skea, J., Buendia, E. C., Masson-Delmotte, V., Pörtner, H.-O., Roberts, D. C., et al. (2019a). IPCC, 2019: Summary for Policymakers. In: Climate Change and Land: an IPCC special report on climate change, desertification, land degradation, sustainable land management, food security, and greenhouse gas fluxes in terrestrial ecosystems. 1–864.

Shukla, P. R., Skea, J., Slade, R., Diemen, R. van, Haughey, E., Malley, J., et al. (2019b). *Foreword Technical and Preface*.

Simarro, G., Ribas, F., Álvarez, A., Guillén, J., Chic, Ò., and Orfila, A. (2017). ULISES: An Open Source Code for Extrinsic Calibrations and Planview Generations in Coastal Video Monitoring Systems. *Journal of Coastal Research* 335, 1217–1227. doi:10.2112/jcoastres-d-16-00022.1.

Slangen, A. B. A., Carson, M., Katsman, C. A., van de Wal, R. S. W., Köhl, A., Vermeersen, L. L. A., et al. (2014). Projecting twenty-first century regional sea-level changes. *Climatic Change* 124, 317–332. doi:10.1007/s10584-014-1080-9.

Soto-Navarro, J., Jordá, G., Amores, A., Cabos, W., Somot, S., Sevault, F., et al. (2020). *Evolution of Mediterranean Sea water properties under climate change scenarios in the Med-CORDEX ensemble*. doi:10.1007/s00382-019-05105-4.

Stockdon, H. F., Holman, R. A., Howd, P. A., and Sallenger, A. H. (2006). Empirical parameterization of setup, swash, and runup. *Coastal Engineering* 53, 573–588. doi:10.1016/j.coastaleng.2005.12.005.

Stockdon, H. F., Thompson, D. M., Plant, N. G., and Long, J. W. (2014). Evaluation of wave runup predictions from numerical and parametric models. *Coastal Engineering* 92, 1–11. doi:10.1016/j.coastaleng.2014.06.004.

Stratigaki, V., Manca, E., Prinos, P., Losada, I. J., Lara, J. L., Sclavo, M., et al. (2011). Large-scale experiments on wave propagation over Posidonia oceanica. *Journal of Hydraulic Research* 49, 31–43. doi:10.1080/00221686.2011.583388.

Suárez de Vivero, J. L. (1999). Delimitación y definición del espacio litoral. *Actas de las Jornadas sobre el litoral de Almería*, 13–23.

Telesca, L., Belluscio, A., Criscoli, A., Ardizzone, G., Apostolaki, E. T., Fraschetti, S., et al. (2015). Seagrass meadows (Posidonia oceanica) distribution and trajectories of change. *Scientific Reports* 5, 1–14. doi:10.1038/srep12505.

Tintoré, J., Vizoso, G., Heslop, E., Martínez-ledesma, M., Torner, M., Diedrich, A., et al. (2013). SOCIB : The Balearic Islands Coastal Ocean Observing and Forecasting System Responding to Science, Technology and Society Needs. *Marine Technology Society Journal* 47, 1–17. doi:10.4031/MTSJ.47.1.10.

Tolman, H. L. (1989). The numerical model WAVEWATCH. *Communications on hydraulic and geotechnical engineering, No. 1989-02*.

Traganos, D. (2020). Development of seagrass monitoring techniques using remote sensing data.

Traganos, D., and Reinartz, P. (2018). Mapping Mediterranean seagrasses with Sentinel-2 imagery. *Marine Pollution Bulletin* 134, 197–209. doi:10.1016/j.marpolbul.2017.06.075.

Tsimplis, M. N., Proctor, R., and Flather, R. A. (1995). A two-dimensional tidal model for the Mediterranean Sea. *Journal of Geophysical Research: Oceans* 100, 16223–16239.

Turner, R. K., and Bower, B. T. (1999). Principles and Benefits of Integrated Coastal Zone Management (ICZM). *Perspectives on Integrated Coastal Zone Management*, 13–34. doi:10.1007/978-3-642-60103-3_2.

UNWTO (2018). International Tourism Trends 2017. *World Tourism Orgnization*, 1–20.

Van der Meer, J., Allsop, N., Bruce, T., De Rouck, J., Kortenhaus, A., Pullen, T., et al. (2018). EurOtop, 2018. Manual on wave overtopping of sea defences and related structures. *An overtopping manual largely based on european research, but for worldwide application. Available www. overtopping-manual. com*.

van Rooijen, A. A., van Thiel de Vries, J. S. M., McCall, R. T., van Dongeren, A. R., Roelvink, J. A., and Reniers, A. J. H. M. (2015). Modeling of wave attenuation by vegetation with XBeach. *E-proceedings of the 36th IAHR World Congress*, 7.

Villatoro, M., Silva, R., Méndez, F. J., Zanuttigh, B., Pan, S., Trifonova, E., et al. (2014). An approach to assess flooding and erosion risk for open beaches in a changing climate. *Coastal Engineering* 87, 50–76. doi:10.1016/j.coastaleng.2013.11.009.

Vogiatzakis, I., Griffith, G., and Morse, S. (2005). MEDITERRANEAN COASTAL LANDSCAPES Management Practices , Typology and Sustainability FINAL REPORT Management Practices , Typology and Sustainability FINAL REPORT The University of Reading July 2005 Address for Correspondence : The Living Landscapes Project.

Vos, K., Harley, M. D., Splinter, K. D., Simmons, J. A., and Turner, I. L. (2019a). Sub-annual to multi-decadal shoreline variability from publicly available satellite imagery. *Coastal Engineering* 150, 160–174. doi:10.1016/j.coastaleng.2019.04.004.

Vos, K., Vos, K., Splinter, K. D., Harley, M. D., Simmons, J. A., and Turner, I. L. (2019b). CoastSat : A Google Earth Engine-enabled Python toolkit to extract shorelines from publicly available satellite imagery CoastSat : A Google Earth Engine-enabled Python toolkit to extract shorelines from publicly available satellite imagery. *Environmental Modelling and Software* 122, 104528. doi:10.1016/j.envsoft.2019.104528.

Vousdoukas, M. I., Ferreira, Ó., Almeida, L. P., and Pacheco, A. (2012a). Toward reliable storm-hazard forecasts: XBeach calibration and its potential application in an operational early-warning system. *Ocean Dynamics* 62, 1001–1015. doi:10.1007/s10236-012-0544-6.

Vousdoukas, M. I., Ranasinghe, R., Mentaschi, L., Plomaritis, T. A., Athanasiou, P., Luijendijk, A., et al. (2020). Sandy coastlines under threat of erosion. *Nature Climate Change* 10, 260–263. doi:10.1038/s41558-020-0697-0.

Vousdoukas, M. I., Wziatek, D., and Almeida, L. P. (2012b). Coastal vulnerability assessment based on video wave run-up observations at a mesotidal, steep-sloped beach. *Ocean Dynamics* 62, 123–137.

Wttc, W. (2016). Travel and Tourism Economic Impact 2016 annual update summary.

Xie, D., Zou, Q. P., Mignone, A., and MacRae, J. D. (2019). Coastal flooding from wave overtopping and sea level rise adaptation in the northeastern USA. *Coastal Engineering* 150, 39–58. doi:10.1016/j.coastaleng.2019.02.001.

Zhang, K., Douglas, B. C., and Leatherman, S. P. (2004). Global warming and coastal erosion. *Climatic change* 64, 41–58.

Zhang, Y. J., Ye, F., Stanev, E. V, and Grashorn, S. (2016). Seamless cross-scale modeling with SCHISM. *Ocean Modelling* 102, 64–81.

Zhongming, Z., Linong, L., Xiaona, Y., Wangqiang, Z., and Wei, L. (2021). AR6 Climate Change 2021: The Physical Science Basis.

Zijlema, M., Stelling, G., and Smit, P. (2011). SWASH: An operational public domain code for simulating wave fields and rapidly varied flows in coastal waters. *Coastal Engineering* 58, 992–1012. doi:10.1016/j.coastaleng.2011.05.015.

List of Figures

List of Tables

List of terms and abbreviations

PDP	Playa de Palma
CLM	Cala Millor
SNB	Son Bou
RCP	Representative Concentration Pathways
UNWTO	World Organization a Union Nations Specialized Agency
GDP	Gross Domestic Product
WTTC	World Travel and Tourism Council
AT	Astronomical Tide
SS	Storm Surge
WR	Wave Runup
TWL	Total Water Level
SCHISM	Semi-implicit Cross-scale Hydroscience Integrated System Model
WWIII	WaveWatch III
WAM	Wave Model
SWAN	Simulating Waves Nearshore
SWASH	Simulating Waves till shore
IPCC	Intergovernmental Panel on Climate Change
GHG	Greenhouse Gases
SSP	Shared Socioeconomic Pathway
MHWs	Marine Heat Waves
GMSLR	Global Mean Sea Level Rise
TC	Tropical Cyclones
CN	Centro Nacional
IEO	Instituto Español de Oceanografía
CSIC	Centro Superior de Investigaciones Científicas
IMEDEA	Instituto Mediterráneo de Estudios Avanzados
UIB	Universitat de les Illes Balears
TEMPERSEA	Temperature of the Red Sea
MOCLI	Modelización Climática
SOCLIMPACT	DownScaling Climate ImPACTs
VENOM	Variabilitat Espacial del Nivel del Mar en el Mediterrani Occidental
UNCHAIN	Unpacking Climate Impact Chains
NW	Northwest
RMSE	Root Mean Square Error
S2006	Stockdon et al 2006
SOCIB	Balearic Islands Coastal Observing and Forecasting System
Hs	Significant wave height
Tp	Peak period
SSW	South-Southwest
SW	Southwest
NNE	North-northeast
SSE	South-southeast
E	East
RTK-GPS	Real time Kinematic Global Position System
$\boldsymbol{\beta_f}$	Beach slope
MSL	Mean Sea Level
AWACs	Acoustic Wave and Currents

$< \eta >$	Setup
S	Swash
STD	Standard Deviation
H_O	Wave height in deep waters
L_O	wavelength
EMP-OFF	Empirical offshore
EMP-ON	Empirical onshore
EMP-OBS	Empirical observations
NUM1D-OBS	Numerical 1D observations
NUM2D-OBS	Numerical 2D observations
BATHY	Bathymetry
FRIC	Friction
Ah	Mean shoot length
Bv	Stem width
N	Vegetation density
Cd	Drag coefficient
GEBCO	General Bathymetric Charts of Ocean
MITECO	Ministerio para la Transición ecológica y el reto demográfico
HYPSE	Hydrostatic Padua Surface Elevation model
ECMWF	European Center for Medium-Range Weather Forecasts
MedCORDEX	Mediterranean CORDEX
SLR	Sea level Rise
FL	Flood Level
MAXDISS	Maximum Dissimilarity Algorithm
RU2%	2% exceeding individual wave runup
h_{bz}	Maximum depth in breaking the zone
h_{sz}	Maximum depth in the shoaling zone
Ω	Dean parameter
H	Wave height under mean conditions
w	Sedimentation speed
T	Mean period
D50	Mean grain size
JONSWAP	Joint North Sea Wave Project
FD	Flood distance
MC	Mean conditions
EC	Extreme conditions
RSRC	Red Sea Research Center
CBRC	Computational Bioscience Research Center
MSLR	Mean Sea Level Rise
PO	Posidonia Oceanica
$\mathcal{E}_v$	Time average energy dissipation
k	Wave number
σ	Wave frequency
H_{rms}	Root mean square wave height
γ_b	Berm characteristics parameter
γ_f	Roughness parameter
γ_β	Wave attack angle parameter
$\varepsilon_{m-1,0}$	Breaker parameter
H_{mo}	Wave height at dike's toe
PRES_NS	Present No seagrass
PRES_WS	Present With seagrass

FUT_NS	Future No seagrass
FUT_615	Future With seagrass 615 sh/m2
FUT_200	Future With seagrass 200 sh/m2
BDA	Bahía De Alcudia
TWL_PRES	Total water level in present climate
TWL_FUT	Total water level in future climate
RL	Return level
eTWL	Extreme total water level

Additional research

In this annex I show a summary of other works in which I have been involved in during the last 5 years. These projects have allowed me to acquire relevant knowledge related to coastal oceanography and climate variability.

1-Temporal evolution of temperatures in the Red Sea and the Gulf of Aden base on in situ observations

M. Agulles, G. Jordà, B. Jones, S. Agustí, C. M. Duarte

Reference:

Agulles, M., Jordà, G., Jones, B., Agustí, S., and Duarte, C. M.: Temporal evolution of temperatures in the Red Sea and the Gulf of Aden based on in situ observations (1958–2017), Ocean Sci., 16, 149–166, https://doi.org/10.5194/os-16-149-2020, 2020.

Abstract:

The Red Sea holds one of the most diverse marine ecosystems in the world, although fragile and vulnerable to ocean warming. Several studies have analysed the spatio-temporal evolution of temperature in the Red Sea using satellite data, thus focusing only on the surface layer and covering the last ∼30 years. To better understand the long-term variability and trends of temperature in the whole water column, we produce a 3-D gridded temperature product (TEMPERSEA) for the period 1958–2017, based on a large number of in situ observations, covering the Red Sea and the Gulf of Aden. After a specific quality control, a mapping algorithm based on optimal interpolation have been applied to homogenize the data. Also, an estimate of the uncertainties of the product has been generated. The calibration of the algorithm and the uncertainty computation has been done through sensitivity experiments based on synthetic data from a realistic numerical simulation.

TEMPERSEA has been compared to satellite observations of sea surface temperature for the period 1981–2017, showing good agreement especially in those periods when a reasonable number of observations were available. Also, very good agreement has been found between air temperatures and reconstructed sea temperatures in the upper 100 m for the whole period 1958–2017, enhancing confidence in the quality of the product.

The product has been used to characterize the spatio-temporal variability of the temperature field in the Red Sea and the Gulf of Aden at different timescales (seasonal, interannual and multidecadal). Clear differences have been found between the two regions suggesting that the Red Sea variability is mainly driven by air–sea interactions, while in the Gulf of Aden the lateral advection of water plays a relevant role. Regarding long-term evolution, our results show only positive trends above 40 m depth, with maximum trends of 0.045 + 0.016 ◦C decade^{-1} at 15 m, and the largest negative trends at 125 m (◦C decade^{-1}). Multidecadal variations have a strong impact on the trend computation and restricting them to the last 30–40 years of data can bias high the trend estimates.

2-Assessment of the Red Sea temperatures in CMIP5 models for present and future climate

M. Agulles, G. Jordà, I. Hoteit, S. Agustí, and C.M. Duarte

Reference:

Agulles M, Jordà G, Hoteit I, Agustí S, Duarte CM (2021) Assessment of Red Sea temperatures in CMIP5 models for present and future climate. PLoS ONE 16(7): e0255505. https://doi.org/10.1371/journal.pone.0255505

Abstract:

The increase of the temperature in the Red Sea basin due to global warming could have a large negative effect on its marine ecosystem. Consequently, there is a growing interest, from the scientific community and public organizations, in obtaining reliable projections of the Red Sea temperatures throughout the 21st century. However, the main tool used to do climate projections, the global climate models (GCM), may not be well suited for that relatively small region. In this work we assess the skills of the CMIP5 ensemble of GCMs in reproducing different aspects of the Red Sea 3D temperature variability. The results suggest that some of the GCMs are able to reproduce the present variability at large spatial scales with accuracy comparable to medium and high-resolution hindcasts. In general, the skills of the GCMs are better inside the Red Sea than outside, in the Gulf of Aden. Based on their performance, 8 of the original ensemble of 43 GCMs have been selected to project the temperature evolution of the basin. Bearing in mind the GCM limitations, this can be an useful benchmark once the high resolution projections are available. Those models project an averaged warming at the end of the century (2080–2100) of 3.3 ±> 0.6°C and 1.6 ±> 0.4°C at the surface under the scenarios RCP8.5 and RCP4.5, respectively. In the deeper layers the warming is projected to be smaller, reaching 2.2 ±> 0.5°C and 1.5 ±> 0.3°C at 300 m. The projected warming will largely overcome the natural multidecadal variability, which could induce temporary and moderate decrease of the temperatures but not enough to fully counteract it. We have also estimated how the rise of the mean temperature could modify the characteristics of the marine heatwaves in the region. The results show that the average length of the heatwaves would increase ~15 times and the intensity of the heatwaves ~4 times with respect to the present conditions under the scenario RCP8.5 (10 time and 3.6 times, respectively, under scenario RCP4.5).

3-Risk of loss of tourism attractiveness in the Western Mediterranean under climate change.

Miguel Agulles, Camilo Melo-Aguilar and Gabriel Jordà

Reference:

AGULLES, M., Melo-Aguilar, C., & Jordà, G. Risk of loss of tourism attractiveness in the Western Mediterranean under climate change. Frontiers in Climate, 191.

Abstract:

The sun and sea tourism are key for economy of the southern European countries. This economic sector is expected to be severely affected by climate change due to the projected loss of beaches, loss of thermal comfort, water restrictions or extreme events, among other impacts. Thus, adaptation strategies need to be developed urgently. To do so, it is necessary to first conduct an assessment of the risk of loss of tourism attractiveness to guide the development of such strategies. Furthermore, uncertainties in the different factors are considered into the risk analysis. In this study we analyze the risk of loss of tourism attractiveness due to climate change in the Spanish Mediterranean destinations, in the Western Mediterranean, as a case study. To do so, the Vulnerability Sourcebook methodology is adopted and modified to incorporate the uncertainties in the different elements of the impact chains. The increase in heat stress and the loss of beach availability have been identified as the climate change induced hazards that will affect the most the region attractiveness. Also, the impact chains have been constructed and several climatic and socioeconomic indicators have been considered after a knowledge co-production process with selected stakeholders. The weights assigned to each indicator have been obtained from an analytic hierarchy process based on the results of a consultation with sector experts. The results of the impact chain operationalization have shown that exposure and vulnerability in all the touristic destinations in the region are very similar and that the hazard will largely increase in the next decades, specially under the future scenario SSP585 or the RCP8.5. However, the final risk does not seem to suffer a large increase because of the relatively small weight assigned to the hazard. In other words, the exposure (e.g., typology of the tourists and touristic activities) or the vulnerability (e.g., capacity to put in place adaptation strategies) would be more important than the projected change in the hazard (e.g., heat stress increase or beach reduction). The benefits and limitations of the methodology are discussed and some suggestions for the validation of the assessment are proposed.

4-Introducing Uncertainties in the impact Chain Risk Assessment Framework: The Untic tool.

Camilo Melo-Aguilar, Miguel Agulles, and Gabriel Jordà

Reference:
Melo-Aguilar, C.; Agulles, M.; Jordà, G. Introducing Uncertainties in the Impact Chain Risk Assessment Framework: The UNTIC tool. Preprints 2022, 2022090436 (doi: 10.20944/preprints202209.0436.v1).

Abstract:

The use of composite indices is widespread in many fields of knowledge, but a common problem associated to those type of indices is how to introduce uncertain knowledge on them. One example would be the Impact Chain framework for risk assessment. This methodology has proven to be a robust and effective approach to set up the conceptual framework associated to a given risk allowing to naturally consider the different components that shape that risk. However, the operationalization of the impact chain may not be straightforward, in particular, due to the inherent uncertainties associated to the selected indicators and the assigned weights. In this paper, we propose to use a probabilistic framework that would allow to consider uncertain knowledge in the composite indicator computation. Moreover, in the framework of

the UNCHAIN project, a web-based tool has been developed to ease the task of implementing that methodology. This web-based application is designed as a multidimensional tool to consider uncertainties in any type of composite indicator, thus, its scope goes beyond the Impact Chain and risk analysis framework. For illustrative purposes, the tool has been applied to a case study on the risk of loss of tourist attractiveness due to heat stress conditions on the Balearic Island, Spain. This case study is used to show how uncertainties in different components of the impact chain can affect the robustness of the final risk assessment. Also, the tool provides an estimate of the sensitivity of the final risk to each component, which can be used to guide risk mitigation strategies. Finally, a proposal for the validation of the risk assessment
is presented.

5-Influence of biotic and abiotic factors of seagrass Posidonia Oceanica recruitment: Identifying suitable microsites.

Pereda-Briones, L. , Tomas, F. , Agulles, M. a, Terrados, J

Reference:

Pereda-Briones, L., Terrados, J., Agulles, M., & Tomas, F. (2020). Influence of biotic and abiotic factors of seagrass Posidonia oceanica recruitment: identifying suitable microsites. Marine Environmental Research, 162, 105076.

Abstract:

The period between seed germination and successful seedling establishment is considered the most vulnerable phase for plant development. To better predict recruitment patterns within plant communities, it is essential to identify the abiotic constrains and biotic interactions that allow for the colonization of substrates by plant species. We evaluated which combination of factors are associated with successful survival and development of seedlings of the seagrass *Posidonia oceanica* in order to identify the most important microsite features acting together on recruitment success. Our results show that *P. oceanica* seedlings are rather specific in their environmental requirements during their first 18 months of life, when their development and survival are favored in microsites of consolidated substratum (solid rock, and to a lesser extent *P. oceanica* matte) covered by macroalgae (mainly crustose algae) and located in sheltered locations (with energy flux values not exceeding 7×10^5 kg s^{-2} m s^{-1}). After this phase, their probability of surviving becomes more independent from external conditions.

6-Research advancements for Impact Chain based Climate Risk and Vulnerability Assessments

Linda Menk, Erich Rome, Daniel Lückerath, Katharina Milde, Carlo Aall, Åsa Gerger Swartling, Mathilda Englund, Karin André, Mark Meyer, Saskia Reuschel, Kathrin Renner, Gabriel Jordá Sànchez, Julie Gobert, Adeline Cauchy, Muriel Bour, Emmanuel M.N.A.N. Attoh, Brigt Dale, Florence Rudolf, Stefan Kienberger, Miguel Agulles, Camilo Melo-Aguilar, Marc Zebisch

Abstract:

With the climate crisis progressing, the demand for scientifically sound evidence from Climate Risk and Vulnerability Assessments (CRVA) has increased significantly in the last decade. Impact chain-based CRVA (IC-based CRVA), e.g., detailed in the Vulnerability Sourcebook, are capable of producing scientifically sound and actionable results that regularly find their way into decision-making. While past applications of IC-based CRVA revealed potential for methodical improvements, their overall success also sparked interest to apply the method in areas it was not originally designed for. The research project UNCHAIN was initiated, i.a. to investigate the methods' state of the art, identify methodical challenges and opportunities, and subsequently to address challenges, leverage opportunities and test new application areas. This article presents findings from eleven case studies conducted in different countries and sectors in Europe with the aims of a) advancing IC-based CRVA through methodical innovations, and b) assessing the applicability of the assessment method in new areas.

We herein summarize history, challenges, and opportunities apparent in IC-based CRVA. We, furthermore, present the research pipeline established in UNCHAIN to ensure comparability of results across case studies and we finally present the methodical innovations and their respective application areas. In this article's results, each case study contributes either a recommendation for a methodical innovation or shares experiences made with a new application area. The results span methodical innovations of the stakeholder engagement process, to integrating uncertainty measures, via integrating models of future socioeconomic exposure, to applying the method to address transboundary risks and to conduct CRVA for industry stakeholders.

7-Mechanisms contributing to extreme sea level events in the western Mediterranean

J. Ramos[1-2], M. Agulles[1], D. Gomis[2] and G. Jordà[1]

8-Impacts of sea level variability on sea water intrusion into Mediterranean coastal aquifers

Camilo Melo-Aguilar[1-2], Miguel Agulles[3], and Gabriel Jordà[1-3]

9-The VENOM network: A low-cost ultra-dense tide gauge network in the western Mediterranean

A.Frank-Comas*[1], M.Agulles[2], J.Puigdefàbregas[1], J.Tomàs-Ferrer[1], A.Font[1], J.Soto-Navarro[3], D.Gomis[1], J.Villalonga[1], J.Ramos[1], C.Melo[2] and G.Jordà[2]